

NOVEL CORNEAL ENDOTHELIAL RESPONSES TO GENOTOXIC STRESS

by

Daniel Sam Roh

B.S., B.A., Duke University, 2002

Submitted to the Graduate Faculty of
University of Pittsburgh School of Medicine in partial fulfillment
of the requirements for the degree of
Doctor of Philosophy in Cell Biology & Molecular Physiology

University of Pittsburgh

2011

UNIVERSITY OF PITTSBURGH
SCHOOL OF MEDICINE

This dissertation was presented

by

Daniel Sam Roh

It was defended on

July 15, 2011

and approved by

Committee Chair:

Sandra A. Murray, Ph.D., Professor

Department of Cell Biology & Molecular Physiology

Committee Members (Primary¹, Secondary² Appointments):

Charleen T. Chu, M.D., Ph.D., Professor

Departments of Pathology¹, Ophthalmology¹

Laura J. Niedernhofer, M.D., Ph.D., Associate Professor

Departments of Microbiology & Molecular Genetics¹, Cell Biology & Molecular Physiology²

Carolyn B. Coyne, Ph.D., Assistant Professor

Departments of Microbiology & Molecular Genetics¹, Cell Biology & Molecular Physiology²

Dissertation Advisor:

James L. Funderburgh, Ph.D., Professor

Departments of Ophthalmology¹, Cell Biology & Molecular Physiology²

Copyright © by Daniel Sam Roh
2011

NOVEL CORNEAL ENDOTHELIAL RESPONSES TO GENOTOXIC STRESS

Daniel Sam Roh, Ph.D.

University of Pittsburgh, 2011

Most cells throughout their existence are constantly subjected to enormous amounts of endogenous and exogenous DNA damage. The cellular response to genotoxic stressors ultimately either leads to adaptive processes that mediate cellular repair and allow for continuous cellular function or leads to cell malfunction and death. In some theories of aging this cellular malfunction is due to accumulation of unrepaired DNA damage which over time leads to progressive deterioration of tissue/organ homeostasis and function resulting in organismal aging. The overall goal of my studies is to understand the responses to DNA damage in corneal endothelial (CE) cells whose pump and barrier functions are essential for corneal transparency and which *in vivo* display age-related degeneration and accumulation of DNA damage. In three complementary and related studies I have focused on how the CE is affected by genotoxic stress. In the first study I have examined the clinical application of the DNA crosslinking agent mitomycin C during photorefractive keratectomy and documented its effects on the CE such as significant accumulation of DNA lesions and elevated levels of apoptosis. In the second study I have examined the long term consequences resulting from failure to repair endogenous DNA damage *in vivo*. Using a DNA repair-deficient mouse strain I have observed significant premature age-related dystrophic changes in the CE that only occur in very old mice. This suggests that the CE is sensitive and vulnerable to the effects of accumulating endogenous genotoxic stress and that DNA damage may drive CE aging. In the third study I have examined how CE cell-cell communication mediated by gap junctions is affected by acute genotoxic stress. Given that gap junction intercellular communication is essential for homeostasis and associated with cell proliferation, death and survival, alterations in the gap junction protein connexin-43 may be crucial for CE cell function and viability during genotoxic stress. The key findings of all my studies elucidate the role of genotoxic stress in CE aging and identify novel responses to stresses from DNA damage. Through a greater understanding of the responses to these stressors, efforts to preserve and improve CE viability and function can be achieved.

TABLE OF CONTENTS

PREFACE	9
1.0 INTRODUCTION	11
1.1 THE CORNEAL ENDOTHELIUM	11
1.1.1 CE functions in the cornea	12
1.1.2 Age-related changes in CE	13
1.1.3 Exposures and responses to cellular stressors	13
1.1.3.1 Special focus on mitomycin C	15
1.1.4 Efforts for CE protection and enhancement	20
1.2 CELLULAR RESPONSES TO GENOTOXIC STRESS	22
1.2.1 The DNA Damage Response (DDR)	22
1.2.2 Alternative (non-DDR) stress responses to DNA damage	23
1.2.3 Genotoxic stress and aging	24
1.2.3.1 The <i>Ercc1</i>^{-Δ} mouse model of accelerated aging	26
1.3 CONNEXINS AND GAP JUNCTIONS	27
1.3.1 Structure and organization	27
1.3.2 Trafficking	27
1.3.3 Regulation by phosphorylation	29
1.3.3.1 Casein kinase 1 delta and its proposed role in Cx43 regulation	30
1.3.4 Gap junction-related functions of Cx43	31
1.3.5 Non gap junction-related functions of Cx43	32
1.3.6 Role of Cx43 in tissue homeostasis and function	32
1.3.6.1 Role of Cx43 and GJIC in corneal endothelial homeostasis and function	33
1.3.7 Role of connexins and gap junctions during genotoxic stress	34

1.4	SUMMARY & GOALS.....	35
2.0	DNA CROSS-LINKING, DOUBLE-STRAND BREAKS, AND APOPTOSIS IN CORNEAL ENDOTHELIAL CELLS AFTER A SINGLE EXPOSURE TO MITOMYCIN-C.....	36
2.1	INTRODUCTION	36
2.2	MATERIALS AND METHODS.....	38
2.3	RESULTS	42
2.3.1	MMC in the cornea after a single topical treatment.....	42
2.3.2	Induction of DNA Cross-Linking in the CE.....	43
2.3.3	Persistent and Elevated γ -H2AX Staining after MMC Treatment.....	45
2.3.4	Effect of MMC on the Proportion of Apoptotic Cells	46
2.4	DISCUSSION.....	47
3.0	AGE-RELATED DYSTROPHIC CHANGES IN CORNEAL ENDOTHELIUM FROM DNA REPAIR DEFICIENT MICE.....	51
3.1	INTRODUCTION	51
3.2	MATERIALS AND METHODS.....	53
3.3	RESULTS	56
3.3.1	<i>Ercc1</i> ^{-Δ} mice have normal eye development	56
3.3.2	Dystrophic changes in CE from <i>Ercc1</i> ^{-Δ} and naturally old WT mice.	58
3.3.3	Decreased cell density with normal overall corneal thickness in <i>Ercc1</i> ^{-Δ} and naturally old WT mice	59
3.3.4	Increased Descemet's membrane thickness and abnormal posterior banded collagen in <i>Ercc1</i> ^{-Δ} mice.....	60
3.3.5	Presence of posterior projections from CE of <i>Ercc1</i> ^{-Δ} mice.....	62
3.3.6	Presence of CD45 ⁺ cells on <i>Ercc1</i> ^{-Δ} mice CE.	64
3.3.7	CE cells are lost by apoptosis in <i>Ercc1</i> ^{-Δ} mice.	65
3.4	DISCUSSION.....	66
4.0	RAPID CHANGES IN CONNEXIN-43 IN RESPONSE TO GENOTOXIC STRESS STABILIZE CELL-CELL COMMUNICATION IN CORNEAL ENDOTHELIUM.....	69
4.1	INTRODUCTION	69

4.2	MATERIALS AND METHODS	71
4.3	RESULTS	75
4.3.1	Genotoxic stress to CE generates rapid changes in the Cx43 abundance and localization	75
4.3.2	MMC treatment increases Cx43 stability	79
4.3.3	Gap junction internalization is decreased after MMC treatment.	81
4.3.4	Genotoxic stress increases forward trafficking of Cx43 into gap junctions. 82	
4.3.5	Gap junction communication is stabilized by MMC treatment	84
4.3.6	GJIC protects against genotoxic stress-induced apoptosis	87
4.4	DISCUSSION	88
5.0	CASEIN KINASE 1 DELTA AS A REGULATOR OF CONNEXIN-43 AND GAP JUNCTION INTERCELLULAR COMMUNICATION DURING GENOTOXIC STRESS	92
5.1	INTRODUCTION	92
5.2	MATERIALS AND METHODS	93
5.3	RESULTS	99
5.3.1	CK1δ expression in CE	99
5.3.2	Increases in CK1δ after genotoxic stress	100
5.3.3	Cx43: CK1δ localization in homeostatic and genotoxic stressed CE	101
5.3.4	Antibody against Cx43 phosphorylated on serines 325, 328, 330	102
5.3.5	CK1δ phosphorylates Cx43-CT on serines 325, 328, 330	105
5.3.6	CK1δ inhibitors reduce gap junction formation and Cx43 stability in CE	106
5.3.7	shRNAs against CK1δ decreases pCx43 s325, 328, 330 in human corneal fibroblasts	108
5.3.8	Genotoxic stress increases levels of pCx43 s325, 328, 330	109
5.4	DISCUSSION	112
6.0	OVERALL CONCLUSIONS & SIGNIFICANCE	116
	APPENDIX A	118
	BIBLIOGRAPHY	121

LIST OF FIGURES

Figure 1.1: The cornea.

Figure 1.2: Functions of the CE.

Figure 1.3: Structure and membrane topology of Cx43.

Figure 1.4: Life cycle of Cx43.

Figure 2.1: Corneal concentration of MMC 2 minutes after a single topical administration of 0.02% MMC on a whole globe, as determined by growth inhibition assay.

Figure 2.2: Single cell gel electrophoresis (modified alkaline comet assay) of CE cell DNA.

Figure 2.3: CE DNA cross-linking induced by MMC treatment of whole globes.

Figure 2.4: Sensitivity of CE cells to DNA cross-linking by MMC.

Figure 2.5: H2AX phosphorylation (γ -H2AX) induced by MMC treatment.

Figure 2.6: MMC exposure initiates endothelial apoptosis.

Figure 3.1: Ocular developmental and eye structure is normal in progeroid *Ercc1*^{-Δ} mice.

Figure 3.2: Premature onset of aging-related dystrophic changes in *Ercc1*^{-Δ} mouse CE.

Figure 3.3: Loss of cell density in *Ercc1*^{-Δ} mouse CE.

Figure 3.4: Premature thickening and abnormal deposition of Descemet's membrane in *Ercc1*^{-Δ} mice.

Figure 3.5: Premature onset of posterior projections originating from *Ercc1*^{-Δ} CE.

Figure 3.6: Inflammatory cells interact with *Ercc1*^{-Δ} mouse CE.

Figure 3.7: Apoptosis of CE in *Ercc1*^{-Δ} mice.

Figure 4.1: Rapid accumulation of Cx43 protein in response to genotoxic stress with mitomycin C.

Figure 4.2: Changes in Cx43 gap junction plaque size and intensity after genotoxic stress.

Figure 4.3: MMC induces alteration in Cx43 association with ZO-1

Figure 4.4: The stability of preexisting Cx43 is altered after MMC treatment.

Figure 4.5: Genotoxic stress results in reduced internalization of Cx43 plaques.

Figure 4.6: MMC induces increased assembly of gap junction plaques.

Figure 4.7: MMC and forskolin do not significantly increase GJIC.

Figure 4.8: MMC treatment generates GJIC resistant to EGF-mediated downregulation.

Figure 4.9: GJIC effect on acute genotoxic stress-induced apoptosis.

Figure 5.1: Expression of CK1 δ in bovine CE.

Figure 5.2: MMC and UVC treatment increases levels of CK1 δ .

Figure 5.3: Dynamic interaction of Cx43 and CK1 δ in CE cells.

Figure 5.4: pCx43 antibody.

Figure 5.5: Recombinant CK1 δ phosphorylates Cx43 on specific residues in vitro.

Figure 5.6: CK1 δ controls Cx43 stability and gap junction formation.

Figure 5.7: Effect of CK1 δ shRNA on pCx43.

Figure 5.8: Genotoxic stress increases pCx43.

Figure 5.9: Potential model of events.

Figure S.1: PAS staining of mouse cornea.

Figure S.2: Cx43 accumulation after genotoxic stress.

Figure S.3: Cell-cell junctions after MMC.

Figure S.4: Cx43 expression after MMC.

PREFACE

I would like to thank and acknowledge my thesis advisor and mentor Professor James Funderburgh for guiding me through my dissertation research. Without his support on every level none of this would be possible. I have learned more than I ever imagined about research, science, and life during my time with him. I hope to be able to approach my future scientific endeavors with as much open mindedness, grace, and fearlessness as he has. Thank you to the past and present Funderburgh laboratory members who have made the experience enjoyable and memorable.

The Department of Ophthalmology has been the perfect environment for my studies and I would like to thank the chair of research, Professor Robert Hendricks for establishing a remarkable research center. The administrative support, CORE facilities, and faculty have contributed so much help and expertise to my development. I always felt, that in my research, anything was possible.

The following individuals contributed to my studies. Amar Joshi, MD, Amanda Cook, MD, Stephen Rhee, MD, Regis Kowalski, Deepinder Dhaliwal, MD contributed to the study in Chapter 2. Yiqin Du, MD/PhD, Michele Gabriele, PhD, Andria Robinson, and Laura Niedernhofer, MD/PhD contributed to the study in Chapter 3. Thank you for your help and collaboration.

Thank you to my family and friends for your support. It is reassuring to know that you are behind me in everything I do.

This work was financially supported by the Research to Prevent Blindness Medical Student Fellowship, a T32 training grant from the National Eye Institute, and an F30 NRSA pre-doctoral fellowship from the National Institute on Aging.

1.0 INTRODUCTION

1.1 THE CORNEAL ENDOTHELIUM

The cornea is the anterior most part of the eye which functions to provide refractive power and protection of more interior structures from environmental insults such as ultraviolet (UV) radiation, pathogens, and noxious particles (Fig. 1.1.A). Composed of three distinct layers (Fig. 1.1B) - a stratified epithelium, the stroma of primarily extracellular matrix and interspersed cells called keratocytes, the corneal endothelium- each with distinct physiology and function, maintenance of corneal transparency is largely dependent upon a well-functioning corneal endothelium (CE). Accelerated CE cell loss through disease or damage leads to irreversible corneal edema and blindness with transplantation presently the only therapeutic option (Bourne and McLaren 2004). As important as the CE monolayer is considered for corneal transparency, it is considered equally fragile and vulnerable to injury and insult for reasons not fully understood.

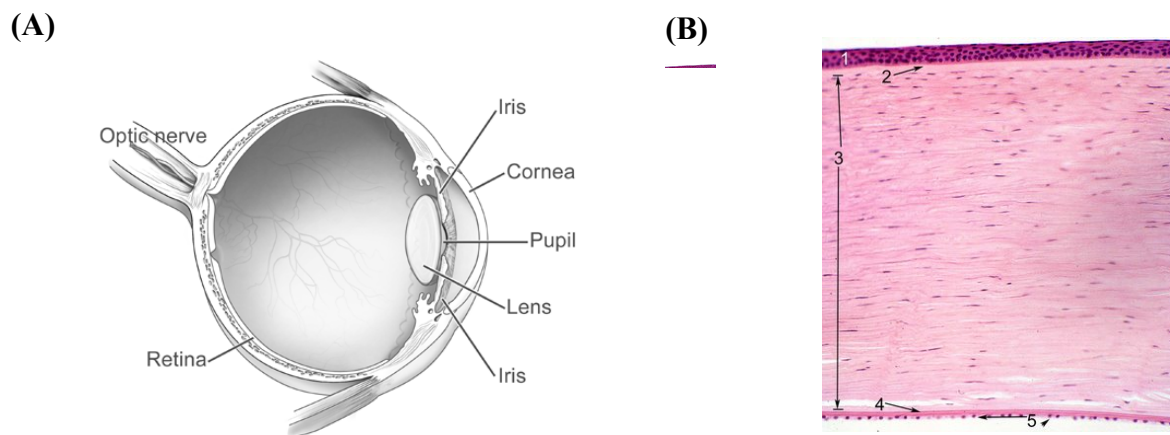


Figure 1.1: The cornea. (A) The cornea is the front most part of the eye that provides protection and refraction. Image adapted from NEI. www.nei.nih.gov. (B) Distinct cellular layers of the cornea include 1) epithelium, 3) stroma, 5) endothelium. 2) Bowman's and 4) Descemet's membranes are extracellular matrix. Image adapted from Mission for Vision. www.missionforvisionusa.org.

1.1.1 CE functions in the cornea

The CE monolayer provides essential barrier and pump functions that allow nutrients and metabolites to enter/leave the avascular cornea from the nutrient-rich aqueous humor while constantly maintaining optimal deturgescence of the stroma. The barrier established by the CE is created by tight junction complex proteins such as zonula occludens-1 (ZO-1), claudins, junctional adhesion molecules (JAM), and occludins (Srinivas 2010). What is unique about the barrier formed by the CE is its “leakiness”, characterized by a very small trans-endothelial resistance (TER) of 15–25 $\Omega\cdot\text{cm}^2$ (Edelhauser 2006) and permeability to macromolecules of molecular weight greater than 150 kilodaltons. The “leaky” CE barrier and hydrophilic properties of the corneal stromal proteoglycans are countered by the action of the CE fluid pump. High metabolic activity of the CE is necessary to fuel abundant Na^+/K^+ ATPase pumps, estimated at $2.1 \times 10^6/\text{cell}$, located on basolateral cell surfaces (Geroski, Matsuda et al. 1985). The Na^+/K^+ ATPase pumps establish the ionic gradients for numerous channels and exchangers resulting in a net movement of fluid from the corneal stroma into the aqueous humor. In addition, bicarbonate (HCO_3^-) and chloride (Cl^-) ion transporters help to drive Na^+ to the apical surface with carbonic anhydrases facilitating the conversion of CO_2 to/from bicarbonate (Bonanno 2003; Bonanno 2011).

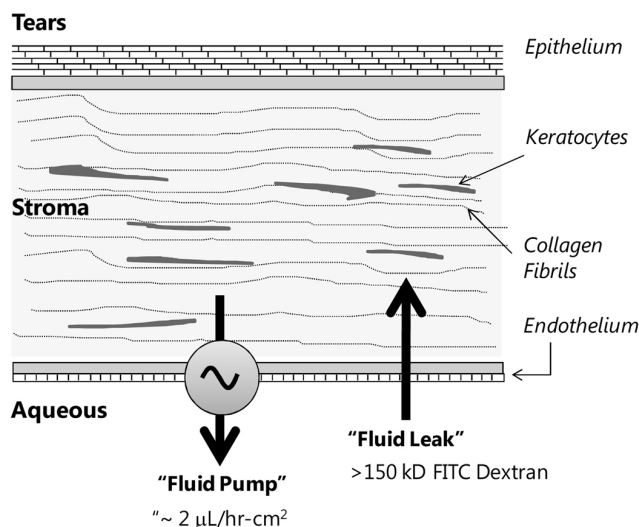


Figure 1.2: Functions of the CE. The CE has two major functions in the cornea including providing a barrier from the aqueous humor and pumping out fluid from the hydrophilic stroma. Image adapted from Srinivas 2010.

Corneal transparency is contingent on the fine-tuned balance of “fluid pump” and “fluid leak” established by the CE (Fig. 1.2). When either of these functions fails, the corneal stroma absorbs fluid and the lattice-like organization of stromal collagen fibrils is disrupted resulting in

altered transmission of light (Hassell and Birk 2010). A permanently damaged or diseased CE therefore leads to irreversible corneal edema and blindness.

1.1.2 Age-related changes in CE

CE cells *in vivo* do not replicate and normal aging is associated with a cell density loss at a rate of 0.6% per year, increasing polymegathism and pleomorphism, and decreased pump function and permeability (Bourne and McLaren 2004). *In vitro*, human CE cells have limited proliferative potential and display features of age-related senescence that is not related to replicative-induced telomere attrition (Konomi and Joyce 2007). Age-related differences between CE cells from older (>50 years) and younger (<30) corneal donors include decreased proliferative capacity in CE cells from older donors (Senoo and Joyce 2000), increased expression of cyclin-dependent kinase inhibitors (Enomoto, Mimura et al. 2006), increased senescence-associated β -galactosidase staining (Mimura and Joyce 2006; Song, Wang et al. 2008), and decreased sensitivity to mitogenic stimulation (Joyce 2005). The causes for these age-related changes remain unknown as well as why the CE fails to regenerate *in vivo*.

1.1.3 Exposures and responses to cellular stressors

The CE is vulnerable to metabolic stress, systemic and ocular drugs including their preservatives, alterations in pH or osmolarity, intraocular pressure, and mechanical stress during surgery (Parikh and Edelhauser 2003; Bourne and McLaren 2004; Fraunfelder 2006; DelMonte and Kim 2011). For example, hyperglycemic stress from diabetes (Roszkowska, Tringali et al. 1999) and high intraocular pressure from glaucoma (Setala 1980; Gagnon, Boisjoly et al. 1997) results in decreased CE cell density compared to age-matched controls. The rate of CE cell loss is accelerated to 10% at 1 year after cataract surgery (Bourne, Nelson et al. 1997) and 34% at 1 year after penetrating keratoplasty (Ing, Ing et al. 1998). Endothelial cell loss one year after Descemet's Stripping Endothelial Keratoplasty, the most advanced procedure for CE transplantation, averaged 41% at 1 year even with experienced surgeons (Lee, Jacobs et al. 2009). Accelerated CE cell loss can lead to bullous keratopathy (BK), a condition resulting from

CE dysfunction or damage which leads to corneal edema, subepithelial corneal scarring, and painful epithelial blistering (Smolin, Foster et al. 2005). Common ocular procedures and conditions associated with CE loss in BK are cataract extraction, primary or secondary (immune rejection) corneal graft failure, glaucoma surgery, and endothelial dystrophies (Smolin, Foster et al. 2005). BK is consistently the leading cause for corneal transplantation in the United States (Ghosheh, Cremona et al. 2008).

A more recent consideration of the aging and non-proliferative nature of the CE is the exposure of the CE to genotoxic stress (Joyce, Zhu et al. 2008; Joyce, Harris et al. 2010). In one's lifetime, the sources of potential DNA damage to the CE are numerous and may include the production of reactive oxygen species from high metabolic activity required for continuous pump function, UV absorbance (Kolozsvari, Nogradi et al. 2002), exposure to DNA-damaging drugs during ocular procedures such as mitomycin C (MMC) (Roh, Cook et al. 2008), and free radicals generated during cataract surgery (Takahashi 2005). The accumulation of DNA damage with age has recently been proposed based on increased endogenous presence of the oxidative DNA lesion, 8-hydroxy-2'-deoxyguanosine (8-OHdG) (Joyce, Zhu et al. 2009) as well as increased γ -H2AX foci representing DNA double strand breaks (Joyce, Harris et al. 2010) in older donor tissue. In Fuchs' dystrophy, characterized by premature loss of CE cells and considered an accelerated aging disease (Bergmanson, Sheldon et al. 1999), there is growing evidence that oxidative DNA damage plays a role in accelerated CE loss (Jurkunas, Bitar et al. 2010). With no identified source of stem cells renewing this monolayer, aging CE cells must maintain pump and barrier functions throughout their lifetime despite being subjected to many potential DNA damaging agents. In spite of this, little is known about how the CE responds to genotoxic stressors through stress responses, adaptation, and/or DNA repair mechanisms.

Studies of the CE response to cellular stressors have mostly focused on the resulting accommodation (including cell migration and spreading of existing cells) rather than how CE cells actually respond during exposure to various stressors. Only more recent studies have suggested that the unfolded protein response is a central CE response to disease states such as Fuchs' dystrophy (Engler, Kelliher et al. 2010) as well as in *ex vivo* storage conditions (Corwin, Baust et al. 2011). Proteomic approaches have revealed decreased peroxiredoxin expression (Jurkunas, Rawe et al. 2008) and increased clusterin expression (Jurkunas, Bitar et al. 2008) in CE affected by Fuchs' dystrophy. Donor CE in storage has been found to release ciliary

neurotrophic factor through a vasoactive intestinal peptide-induced autocrine loop resulting in increased integrity and upregulation of Cx43 mRNA (Koh 2002; Koh, Celeste et al. 2008). Because the CE is a unique and fragile layer critical to corneal transparency, understanding the pathways that are integrated in the response to stress before cell death may prove beneficial for preservation efforts.

1.1.3.1 Special focus on mitomycin C

The following section focuses on the clinical use of mitomycin C during photorefractive keratectomy and as is adapted, with copyright permission from SLACK Incorporated, from a published review. **Roh, D.S., & Funderburgh, J.L. (2009). Impact on the corneal endothelium of mitomycin C during photorefractive keratectomy. *Journal of Refractive Surgery*, (25)10, 894-898.**

Introduction

Mitomycin C (MMC) was proposed to be an effective modulator of the wound healing response after corneal stromal ablation as early as 1991 (Talamo, Gollamudi et al. 1991). Since then, MMC usage has expanded significantly within the field of refractive surgery, especially during photorefractive keratectomy (PRK), for prevention of recurrence of corneal haze and as prophylaxis to prevent initial haze development (Lacayo and Majmudar 2005). Despite the growing popularity of MMC usage during refractive procedures, there has been inconsistency in the conclusions of studies regarding the impact of MMC on the corneal endothelium. Because of the non-regenerative nature of the human corneal endothelium, it is imperative to understand how this vital cell layer responds to potential stressors at both the cellular and clinical levels. This brief review will examine both basic science and clinical studies to evaluate the potential impact of MMC usage during PRK on the health of the corneal endothelium.

Mechanism of Action of Mitomycin C

MMC is an antibiotic derived from *Streptomyces caespitosus* and is generally classified as a DNA alkylating agent. Cellular toxicity after MMC exposure can occur from MMC-induced

insults such as the generation of free radicals or DNA monoadducts; however, the most significant effects are due to the accumulation of covalent DNA interstrand cross-links (Tomasz 1995). A brief explanation of the mechanism of action of MMC is essential to understand the potential impact of MMC used during PRK on the corneal endothelium.

MMC Activation by Enzymatic Reduction

MMC by itself is non-reactive with DNA and after entering the cell must undergo bioreductive enzymatic activation. Numerous intracellular enzymes can activate MMC such as NAD(P)H:quinone oxidoreductase 1 (NQO1) which is present throughout all layers of the cornea (Schelonka, Siegel et al. 2000). Intracellular bioreductive activation results in the production of an unstable intermediate with high alkylating activity and formation of a covalent monoadduct with DNA. Subsequently, this activated MMC will form a second alkylating center which completes the DNA cross-link. The result is a covalent bond between two complementary strands of DNA which if not removed prevents DNA replication and transcription. These MMC-DNA cross-links occur within the minor groove of DNA causing relatively little DNA duplex distortion. The location of adducts is guanine specific and cross-links are located at opposing sequences of 5'-CpG-3' (CpG) (Tomasz 1995).

Processing and Repair of DNA Interstrand Cross-links

Specific recognition factors of the MMC-induced interstrand cross-link are not well defined, but may occur when DNA replication and/or transcription is blocked within the cell. Importantly, the MMC-induced interstrand cross-link may not be easily repaired in non-replicating mammalian cells because a stalled replication fork typically serves as the signal for initiating DNA repair. Although detailed repair mechanisms in mammalian cells have not been fully elucidated, interstrand cross-link repair is believed to involve a complex combination of nucleotide excision repair, DNA double strand break repair via homologous recombination or non-homologous end joining, and/or translesion DNA synthesis (Dronkert and Kanaar 2001; McHugh, Spanswick et al. 2001; Noll, Mason et al. 2006). One of the intermediates in interstrand cross-link repair, the DNA double-strand break, is known to be a potentially lethal lesion. Such breaks can be visualized as γ -H2AX nuclear foci (De Silva, McHugh et al. 2000; Niedernhofer, Odijk et al. 2004).

Consequences of MMC-induced DNA Interstrand Cross-links

Cytotoxicity of MMC-induced interstrand cross-links is most severe in cells undergoing active proliferation, although the details of the responses are specific to the cell type. The presence of a DNA interstrand cross-link during replication induces a stalled replication fork triggering multiple signaling pathways for cell cycle arrest, repair, or apoptosis. Initial responses to MMC induced interstrand cross-links include a strong activation of p53 and genes downstream (Abbas, Olivier et al. 2002; Boamah, White et al. 2007). Longer term consequences of such interstrand cross-links include increased apoptosis, cellular senescence and premature aging (Grillari, Katinger et al. 2007).

Review of Basic Science and Animal Studies

The effects of MMC exposure on corneal endothelium have been studied in both *in vitro* and animal models and have generated informative data about MMC corneal penetration and endothelial toxicity. In three separate studies the corneal penetration of a single topical application of MMC has been observed during protocols emulating PRK. Using high-performance liquid chromatography (HPLC), Torres et al. demonstrated the presence of MMC in hen aqueous humor after a single 0.02% intraoperative application during PRK (Torres, Merayo-Lloves et al. 2006). Song et al. also used HPLC to demonstrate the presence of MMC in both cornea and aqueous humor after a single 0.02% MMC application in a rabbit model of epithelial debridement (Song, Kim et al. 2006). Our recent study used a bioassay to demonstrate significant MMC concentrations at the depth of the corneal endothelium after a single topical 0.02% application in *ex vivo* goat corneas (Roh, Cook et al. 2008). It is clear from these studies that refractive surgery procedures such as photorefractive keratectomy (PRK) that involve the mechanical removal of the corneal epithelial barrier, excimer laser stromal ablation, and subsequent MMC treatment, expose the corneal endothelium to biologically substantial levels of MMC. Length of exposure and MMC concentration in the endothelium and aqueous are directly related to the amount of MMC applied to the anterior surface (Song, Kim et al. 2006; Torres, Merayo-Lloves et al. 2006).

Surprisingly, despite the widespread use of MMC during refractive surgery, only a few studies that have specifically focused on the effects of MMC on the corneal endothelium at the

cellular level. Although many more studies describe the keratocyte response to MMC, the response of the corneal endothelium should not be inferred from those results. An early 1991 study by McDermott et al. (McDermott, Wang et al. 1994) using four pairs of *ex vivo* human corneas found few changes in mean swelling rate or corneal endothelial ultrastructure after perfusion with 20 µg/ml MMC but found significant irreversible changes at 200 µg/ml. Later *in vitro* studies have shown dose-dependent toxic effects of MMC on corneal endothelial proliferation (Wu, Hong et al. 1999; Garweg, Wegmann-Burns et al. 2006). Perhaps the most cited study demonstrating MMC toxicity to corneal endothelium was by Chang (Chang 2004) in 2004, using a rabbit model of mechanical epithelial debridement followed by 0.02% MMC treatments. Over a 2-week period, MMC resulted in dose-dependent apoptosis of the endothelium resulting in increased corneal thickness and decreased corneal clarity. Our recent study (Roh, Cook et al. 2008) demonstrated that even a small and brief dose of MMC significantly alters corneal endothelial DNA producing significant potential downstream effects. Using MMC concentrations and exposure times that the corneal endothelium is most likely to encounter during intraoperative treatment, we found significant DNA cross-linking and persistent DNA double-strand breaks in goat corneas *ex vivo* (Roh, Cook et al. 2008). The proportion of apoptotic cells significantly increased in MMC treated cells; however, this number was smaller than the proportion of cells that had DNA double-strand breaks. Thus, MMC appears to generate living cells with an accumulation of unrepaired DNA damage. Most important we found that very brief exposures and low concentrations of MMC consistently induced changes in the corneal endothelial monolayer (Roh, Cook et al. 2008). Thus, it is highly likely that a single topical application of MMC alters corneal endothelial DNA generating downstream effects on cell viability. It remains to be determined what the long-term fate of these DNA cross-links and double strand breaks is and if the same phenomenon occurs in the *in vivo* setting.

Review of Clinical Studies

In contrast to the relatively small number of laboratory studies described above, a larger number of clinical reports have focused on the effects of a single intraoperative dose of MMC during refractive surgery on the corneal endothelium. Whereas a majority of the basic science studies

reported significant corneal endothelial toxicity after MMC exposure, the clinical studies have been less conclusive in their evaluation of corneal endothelial effects. Corneal endothelial cell loss has been the major endpoint of these studies carried out by statistical comparisons of pre- and post-operative endothelial central density measurements with occasional use of pachymetry.

The initial studies investigating this phenomenon generally reported that MMC treatment during PRK has no measurable effect on corneal endothelial central density. These include a few retrospective (Lee, Chung et al. 2005) and prospective studies (Diakonis, Pallikaris et al. 2007; Goldsberry, Epstein et al. 2007). Lee et al. (Lee, Chung et al. 2005) examined 1011 eyes in a noncomparative retrospective study and determined that endothelial density was not affected by 0.02% MMC treatments ranging from 30 seconds to 2 minutes during PRK after 3, 6, and 16 months. Goldsberry et al. (Goldsberry, Epstein et al. 2007) found no changes in density or morphology after 1 year in 16 eyes treated with 0.02% MMC for 12 seconds. Diakonis et al. (Diakonis, Pallikaris et al. 2007) followed 15 eyes after PRK with 0.02% MMC for 15 seconds and compared this to epi-LASIK in the fellow eyes. They found a decrease in endothelial density at 1 and 3 months after surgery, however, it was not statistically significant (Diakonis, Pallikaris et al. 2007).

In contrast, clinical studies associating MMC usage with significant corneal endothelial loss are fewer in number and more recent than those reporting no effect. Two recent studies found significant decreases in endothelial central density after PRK with MMC (Morales, Zadok et al. 2006; Nassiri, Farahangiz et al. 2008). Nassiri et al. (Nassiri, Farahangiz et al. 2008), in a nonrandomized prospective study of 162 eyes, determined that intraoperative 0.02% MMC caused significant corneal endothelial cell loss over a 6-month period that was correlated with the duration of MMC exposure during PRK. In a prospective study of 18 eyes Morales et al. (Morales, Zadok et al. 2006) found that 0.02% MMC exposure of 30 seconds caused significant cell loss at 1 and 3 months.

Although the results from PRK studies do not agree as to a detrimental effect of MMC treatment on corneal endothelial density, the potential for significant MMC toxicity on the corneal endothelium has been well documented in other ocular procedures. Avisar et al. (Avisar, Avisar et al. 2008) found that a 5-minute 0.02% MMC treatment on bare sclera after pterygium resection lead to significant postoperative endothelial cell loss up to 3 months postoperatively. A case report by Mohammadpour et al. (Mohammadpour, Jabbarvand et al.

2007) described irreversible focal corneal decompensation after filtering surgery with MMC. Mietz et al. (Mietz, Roters et al. 2005) reported two cases of bullous keratopathy after trabeculectomy with MMC. Continued MMC treatment in the form of repeated drops after phototherapeutic keratectomy resulted in permanent corneal edema as reported by Pfister (Pfister 2004). These case reports validate the potential for MMC induced corneal endothelial damage across various settings.

Explanation of Possible Differences and Future Research

Based on the established mechanism of MMC action, *in vitro* and animal studies, and reports of endothelial cells loss after MMC treatment in non-PRK treatments, it is apparent that MMC has the intrinsic potential to damage the corneal endothelial DNA under conditions of current clinical use. How can this vulnerability be consistent with the number of clinical reports that describe little or no loss of endothelial central density? Our recent study showed that in goat corneas, the number of cells exhibiting long-term DNA damage by MMC greatly outnumbered the cells undergoing apoptosis in response to clinical concentrations of MMC (Roh, Cook et al. 2008). If similar DNA cross-linking is occurring in human eyes we might expect, ultimately, to see increased apoptosis in the monolayer of those cells that are unable to tolerate further DNA damage. However, the profoundly quiescent nature of the human endothelium may lead to less cell death in the short-term as a result of these insults. Thus, the corneal endothelium may simply ‘silently’ accumulate this DNA damage without an immediate pathological response. It remains to be determined how the corneal endothelium will eventually respond to such MMC-induced DNA damage over a period of years or decades. Considering unequivocal data demonstrating irreversible DNA damage in endothelium at MMC concentrations now employed clinically, it will be important to initiate follow-up studies of treated individuals to identify any potential long-term effects.

1.1.4 Efforts for CE protection and enhancement

The importance of the CE for corneal transparency has led to significant efforts aimed at protecting the CE *in vivo* during intraocular procedures and *ex vivo* during donor cornea storage for future corneal transplants.

The advent of ophthalmic viscosurgical devices (OVD) and viscoelastic materials for use during intraocular surgery has greatly enhanced CE survival (Bissen-Miyajima 2008). These OVDs protect the CE by coating it during intraocular procedures such as vitrectomy (for retinal detachments), trabeculectomy (for glaucoma), corneal lamellar surgery, and cataract phacoemulsification. The coating provides a physical barrier to toxic substances, dry air exposure, and mechanical stressors encountered during these procedures (Tognetto, Cecchini et al. 2004). There may also be some protection against free radicals formed during cataract phacoemulsification (Takahashi 2005).

Descemet's Stripping Endothelial Keratoplasty (DSEK) is a new surgical technique designed to replace diseased CE with donor grafts that contain healthy CE and a small portion of the posterior stroma. This allows for preservation of the corneal surface topography or refractive power and rapid visual recovery compared to full penetrating keratoplasty (Price and Price 2007). Due to the complex surgical technique and handling of donor tissue, there is a high rate of post-operative CE cell loss (Lee, Jacobs et al. 2009). To combat this rapid loss of CE cells significant efforts have been focused on optimization of donor graft handling and delivery, surgical techniques, and donor tissue preparation and storage (Price and Price 2007; Price and Price 2008).

A variety of storage solutions have been formulated to try to preserve CE cell viability during donor cornea storage. Some examples include the addition of salubrinal, which dephosphorylates eIF2 α and protects cells from ER stress-induced apoptosis, to decrease the unfolded protein response resulting in enhanced survival (Corwin, Baust et al. 2011). Treatment with aspirin-triggered lipoxin A4 (15-epi-LXA4), which is a lipid mediator involved in resolution of inflammation, prior to storage resulted in increased viability (He, Kakazu et al. 2011). The addition of vasoactive intestinal peptide (VIP), a neuropeptide with anti-inflammatory properties, decreased inflammatory potential and enhanced CE survival in organ culture (Koh, Cheng et al. 2009). These studies provide examples of how understanding stress responses can be used to promote CE viability and protection from injury.

Enhancement of CE cell viability and proliferation using gene targeting approaches has been attempted, however, with limited applicability in the clinical setting due to the use of viral vectors. Lentiviral vectors expressing p35 or Bcl-xl, anti-apoptotic proteins, were able to extend donor storage times by prolonging CE survival (Fuchsluger, Jurkunas et al. 2011). Adenoviral

delivery of catalase, an antioxidant enzyme, was able to protect rabbit CE from oxidative stress in *ex vivo* storage conditions (Hudde, Comer et al. 2002). Despite the promise of enhanced survival, the limitations of viral delivery are the optimization of viral titer for adequate expression versus cell toxicity and the difficulty of targeting *in vivo* expression to CE cells exclusively and not other cells within the anatomical vicinity. Determining the long term effects of viral transduction of exogenous genes will need to be performed prior to clinical usage.

1.2 CELLULAR RESPONSES TO GENOTOXIC STRESS

Most cells throughout their existence are constantly subjected to enormous amounts of endogenous and exogenous DNA damage. It is estimated that in any given cells, there are up to 100,000 lesions in the nuclear DNA per cell per day (Garinis, van der Horst et al. 2008). . In cells with greater exposure to environmental stressors such as the skin and eye, these estimates are even higher. Thus it is not surprising to find many ocular manifestations including corneal dysfunction in inherited DNA repair disorders (Yamaguchi, Okabe et al. 1991; Goyal, Rao et al. 1994; Jalali, Boghani et al. 1994; McElvanney, Wooldridge et al. 1996; Dollfus, Porto et al. 2003). The cellular response to genotoxic stressors ultimately either leads to adaptive processes that mediate cellular repair and allow for continuous cellular function or leads to cell malfunction and death.

1.2.1 The DNA Damage Response (DDR)

A generalized response to DNA damage involves 1) DNA damage-sensing and signal initiating events, 2) signal transduction, and 3) a biological consequence or attenuation of the response (Yang, Yu et al. 2003). There are numerous DNA repair pathways that focus on specific DNA lesions such as mismatch repair (MMR), base excision repair (BER), nucleotide excision repair (NER), double-strand break repair (DSB), and interstrand crosslink (ICL) repair; each with sensors and effectors that can overlap (Jackson and Bartek 2009).

The DNA damage response can vary according to the extent and type of DNA damage, cell cycle status, and the cell type. Cells may repair DNA damage, undergo senescence, or apoptosis in different conditions. For example, DNA repair in post-mitotic, terminally differentiated, or non-dividing cells is different from and not as well understood as repair in dividing cells. A number of DNA damage response proteins are downregulated during terminal differentiation and these cells shift the focus of DNA repair to more important transcribed genes, via transcription-coupled NER, rather than the entire genome (Nospikel and Hanawalt 2002; Nospikel 2007). As a result of this change in DNA repair, accumulation of DNA damage in non-transcribed regions has been predicted to occur with any re-entry into the cell cycle potentially leading to “mitotic catastrophe” due to the overwhelming amount of DNA damage encountered in these regions during replication (Nospikel and Hanawalt 2002).

One example of the variation in DNA repair between cycling and non-cycling cells is the complex process of ICL repair. Covalent ICLs prevent both replication and transcription, thus are highly cytotoxic and are believed to contribute to aging (Grillari, Katinger et al. 2007). A single ICL has been shown to induce checkpoint activation in mammalian cells (Ben-Yehoyada, Wang et al. 2009). ICL repair in cycling cells occurs during the S-phase of DNA synthesis. After a replication fork encounters the ICL, a double strand break intermediate is formed which is subsequently repaired through homologous recombination or the more error-prone nonhomologous end joining or translesion bypass (Legerski 2010). As most of the body’s cells are nondividing and because there are endogenous sources of ICLs (Grillari, Katinger et al. 2007), there must be other ways to deal with ICLs that does not involve replication. In contrast to ICL repair in S-phase, ICL repair in the G1 phase is much less understood but involves both global genome-, but mostly transcription-coupled NER (Hlavin, Smeaton et al. 2010). The error-prone translesion polymerase ζ appears to be critical to ICL resolution in non-dividing cells (Sarkar, Davies et al. 2006).

1.2.2 Alternative (non-DDR) stress responses to DNA damage

Genome-wide studies of gene expression have shown that cells exposed to DNA-damaging agents mount a robust and multifaceted response that involves many different cellular functions beyond just DNA repair (Workman, Mak et al. 2006; Matsuoka, Ballif et al. 2007).

Cellular protection from DNA damage appears to involve an intricate network of proteins involved in a multitude of cellular processes including protein turnover, cytoskeletal changes, and general stress pathways (Fry, Begley et al. 2005). Therefore, it is not surprising that thousands of protein kinases respond rapidly to genotoxic stress in a manner that extends to multiple functions of the cell making the DNA damage response one of the most extensive signaling responses to cellular stimuli (Matsuoka, Ballif et al. 2007; Bensimon, Aebersold et al. 2011).

DNA damage can trigger signaling pathways related to inflammation, growth signaling, and survival (Niedernhofer and Robbins 2008). NF- κ B is a family of transcription factors that can control proliferation and survival in response to stress and inflammatory cytokines. NF- κ B is linked to the DDR and activated through ATM-dependent pathways promoting apoptotic-related signaling (Janssens and Tschopp 2006). Persistent DNA damage signaling has been shown to also promote inflammatory cytokine secretion related to senescence (Rodier, Coppe et al. 2009). Genotoxic stress promotes transition of cellular resources from growth to conservation of energy for maintenance after DNA damage through reduced IGF-1 (insulin-like growth factor-1) (Niedernhofer, Garinis et al. 2006; van der Pluijm, Garinis et al. 2007; Garinis, Uittenboogaard et al. 2009) and mTOR (mammalian target of rapamycin) (Reiling and Sabatini 2006) signaling pathways.

In multicellular organisms, the physiological response to stressors typically involves the coordinated action of many cells, thus many of the genes induced by multiple diverse stresses have been consistently found to be involved in intercellular communication (Murray, Whitfield et al. 2004). Understanding how cell-cell communication is affected by DNA damage may provide insights into how aging cells tolerate or succumb to genotoxic stress which ultimately effects tissue function and viability.

1.2.3 Genotoxic stress and aging

In some theories of aging cellular malfunction is due to accumulation of unrepaired DNA damage which over time leads to progressive deterioration of tissue/organ homeostasis and function resulting in organismal aging (Niedernhofer, Garinis et al. 2006; Garinis, van der Horst et al. 2008; Niedernhofer 2008; Schumacher, van der Pluijm et al. 2008). Included in these

theories is the free radical theory of aging originally proposed in 1956 by Denham Harman, which postulated that reactive oxygen species (ROS) were the main cause of aging (Harman 1956). ROS, including hydrogen peroxide (H_2O_2), superoxide (O_2^-), hydroxyl radicals (OH^\cdot), could potentially damage macromolecules including DNA. It is common for aging studies to detect elevated levels of oxidatively damaged DNA in older human and animal tissues and organs (Moller, Lohr et al. 2010; Sedelnikova, Redon et al. 2010). Interestingly, in a meta-analysis of 69 animal studies by Moller et al., organs containing more terminally differentiated cells such as the brain, heart, liver, lung, and pancreas had higher age-related accumulation of oxidatively damaged DNA than organs with higher proliferative capacity such as the intestine, spleen, and testis (Moller, Lohr et al. 2010).

In addition to oxidative DNA damage, other DNA lesions have been linked to aging such as DSBs and ICLs. Senescent human cells and aging mice were found to accumulate γ H2AX foci which indicated DSBs (Sedelnikova, Horikawa et al. 2004). Numerous other studies have also demonstrated increased γ H2AX in aging cells, tissues and organs (Li, Mitchell et al. 2008; Wang, Jurk et al. 2009). Chemotherapy treatments with ICL agents have been associated with accelerated aging seen in acquired premature progeroid syndrome and endogenously formed ICLs are thought to increase with age (Grillari, Katinger et al. 2007). As many DNA repair pathways also are decreased or altered with aging, it is postulated that this creates a cycle of DNA damage driving aging and aging driving accumulation of DNA damage (Gorbunova, Seluanov et al. 2007).

Progeria, or premature and accelerated aging, has been consistently linked to some conditions of genomic instability. Some examples of progeria resulting from failure to repair DNA damage include Cockayne syndrome and trichothiodystrophy which results from defects in NER, Werner syndrome which results from defects in the WRN helicase, a subset of xeroderma pigmentosa (XPE) which results from defects in ERCC1-XPF, and Hutchinson-Gilford syndrome which results from defects in nuclear lamin A (Burtner and Kennedy 2010; Gregg, Robinson et al. 2011). The DNA repair deficiency drives tissue-specific degeneration and accelerated aging of tissues such as the skin, eye, bone marrow, nervous system, and endocrine axis (Niedernhofer 2008). Fortunately, some of these diseases can be recapitulated in animal models which has allowed for a greater understanding of their pathogenesis as well as opportunities to study the impact of genotoxic stress on aging at the organism, organ, tissue, and

cellular levels (Niedernhofer, Garinis et al. 2006; Niedernhofer 2008; Vo, Seo et al. 2010; Goss, Beer Stolz et al. 2011; Gregg, Robinson et al. 2011; Wang, Vo et al. 2011).

1.2.3.1 The *Ercc1*^{-Δ} mouse model of accelerated aging

ERCC1-XPF is a heterodimeric complex involved in structure-specific endonuclease repair of DNA damage. It functions in nucleotide excision repair especially for bulky UV – induced lesions, interstrand crosslink repair, and double-strand break repair (Niedernhofer, Odijk et al. 2004; Ahmad, Robinson et al. 2008). Humans that have XPF or ERCC1 mutations suffer from symptoms related to deficient DNA repair. Remarkably, some of these mutations result in an accelerated aging phenotype. An XPF patient was found to have accelerated aging of the brain, liver, musculoskeletal and hematopoietic systems (Niedernhofer, Garinis et al. 2006). Mutations in ERCC1 resulted in a patient with severe developmental failure and cerebro-oculo-facio-skeletal syndrome (Jaspers, Raams et al. 2007).

ERCC1 knockout mice were reported in 1993 (McWhir, Selfridge et al. 1993) and 1997 (Weeda, Donker et al. 1997) and display severe growth retardation with spontaneous development of neurodegeneration, hematopoietic deficiency, liver abnormalities, and musculoskeletal defects (Niedernhofer, Garinis et al. 2006) similar to the patients with ERCC1-XPF mutations. Although the age-related changes in these mice significantly overlap with naturally old wild-type mice, they only live 21 to 28 days and are exceptionally frail (Niedernhofer, Garinis et al. 2006). Generation of hypomorphic *Ercc1*^{-Δ} mice (null and mutant *Ercc1* allele combination) increases maximum lifespan to 6 to 7 months and have been used as a model of accelerated aging in numerous tissues (Vo, Seo et al. 2010; Goss, Stolz et al. 2011; Gregg, Robinson et al. 2011). The notable difference with these mice and the full knockout mice is that the hypomorphs grow and develop similarly to their wild type littermates until approximately 16 weeks at which point they rapidly deteriorate and display degenerative signs of aging (Gregg, Robinson et al. 2011). This suggests that DNA damage accumulates in the *Ercc1*^{-Δ} mice until an undefined threshold for damage is crossed at which point the overwhelming damage drives the progression of aging-related degenerative changes in vulnerable cells, tissues and organs.

1.3 CONNEXINS AND GAP JUNCTIONS

1.3.1 Structure and organization

The connexins are a multigene family of 21 isoforms of non-glycosylated polytopic integral membrane proteins. Their common protein structure includes four conserved α -helical transmembrane domains, two conserved extracellular loops interconnected by three disulfide bridges, a cytoplasmic loop, and cytoplasmic N- and C-termini (Fig. 1.3) (Laird 2006). Members of the connexin family have a diverse C-terminal which can contain multiple serine and tyrosine residues subject to kinase phosphorylation (Lampe and Lau 2004). Many cells and tissues express one or more members of the connexin family; however, connexin-43 (Cx43) is the most ubiquitous and hence most well-studied member. Connexins are the protein building blocks of gap junctions which permit the intercellular exchange of electrical signals, ions, small metabolites, second messengers, and molecules less than 1kDa in size (Laird 2006).

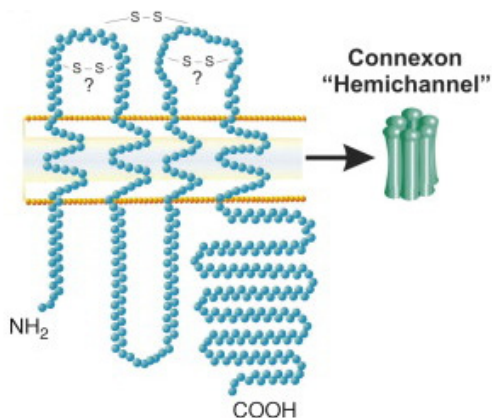


Figure 1.3: Structure and membrane topology of Cx43. Cx43 has an intracellular N-terminus, four transmembrane domains, two extracellular loops, a cytoplasmic loop, and a long and disordered intracellular C-terminus. Six connexins oligomerize to form a connexon or hemichannel. Image adapted from Laird 2010.

1.3.2 Trafficking

Cx43 is co-translationally inserted into the endoplasmic reticulum (ER) and follows the general secretory pathway for membrane proteins (Segretain and Falk 2004). Upon completion of proper folding, Cx43 exits the ER and passes through the Golgi apparatus, where oligomerization into connexon hemichannels (six connexin proteins) occurs in the *trans* compartment (Koval 2006). Vesicles containing Cx43 hemichannels, which can bind tubulin, are then transported along microtubules to the plasma membrane (Giepman, Verlaan et al.

2001). Directed delivery to adherens junctions next to pre-existing GJs has been demonstrated (Shaw, Fay et al. 2007) although Cx43 may also be found at non-GJ regions and have lateral mobility within the membrane (Lauf, Giepmans et al. 2002). These hemichannels are believed to remain closed until they reach the plasma membrane at which they may transiently open after stimulation (Goodenough and Paul 2003).

At the plasma membrane, Cx43 has been shown to have distinct mobility at all cell-surface membranes and progressively forms into gap junctions (Simek, Churko et al. 2009). Hemichannels on apposing cells dock with one another through interactions between the extracellular loops forming gap junctions which permit intercellular exchange (Laird 2006). Clustering of individual hemichannels into gap junctions is a dynamic and continuous process in which new channels are added at the periphery and old channels are in the center of gap junction plaques (Gaietta, Deerinck et al. 2002). Gap junction plaques are composed of Cx43 that is primarily in the P2 form on SDS-PAGE and increasingly Triton X-100 insoluble (Musil and Goodenough 1991). Altered gap junction stability through interactions with Cx43-binding partners such as ZO-1 (Hunter, Barker et al. 2005) and caveolin-1 (Langlois, Cowan et al. 2008) have been observed.

The mechanisms of internalization of gap junctions and degradation of connexins are still being defined. Internalization by formation of annular gap junctions, which are large double-membrane vesicular structures, is believed to be one mechanism of gap junction removal (Laird 2006), while a more recent study demonstrated that there is also internalization of small endocytic double-membrane vesicles (Falk, Baker et al. 2009). Both of these processes involve a clathrin-mediated mechanism (Piehl, Lehmann et al. 2007; Nickel, DeFranco et al. 2008). Ubiquitin and the associated cellular machinery are believed to “tag” connexin for internalization and help guide it to lysosomes (Leykauf, Salek et al. 2006; Leithe, Kjenseth et al. 2009; Kjenseth, Fykerud et al. 2010; Catarino, Ramalho et al. 2011).

With a short protein half-life of 1.5-5 hours, connexins are actively being synthesized and degraded. Newly synthesized misfolded Cx43 may be degraded by ER-associated degradation (ERAD), while degradation of Cx43 at the plasma membrane appears to involve both lysosomes and proteosomes (Berthoud, Minogue et al. 2004). Steady-state mechanism of degradation are unknown however many phosphorylation events are involved in targeting membrane Cx43 for degradation (Berthoud, Minogue et al. 2004). It is believed that the short half-life of connexins

is indicative of their ability to respond to physiological changes rapidly by either up or downregulating gap junction coupling.

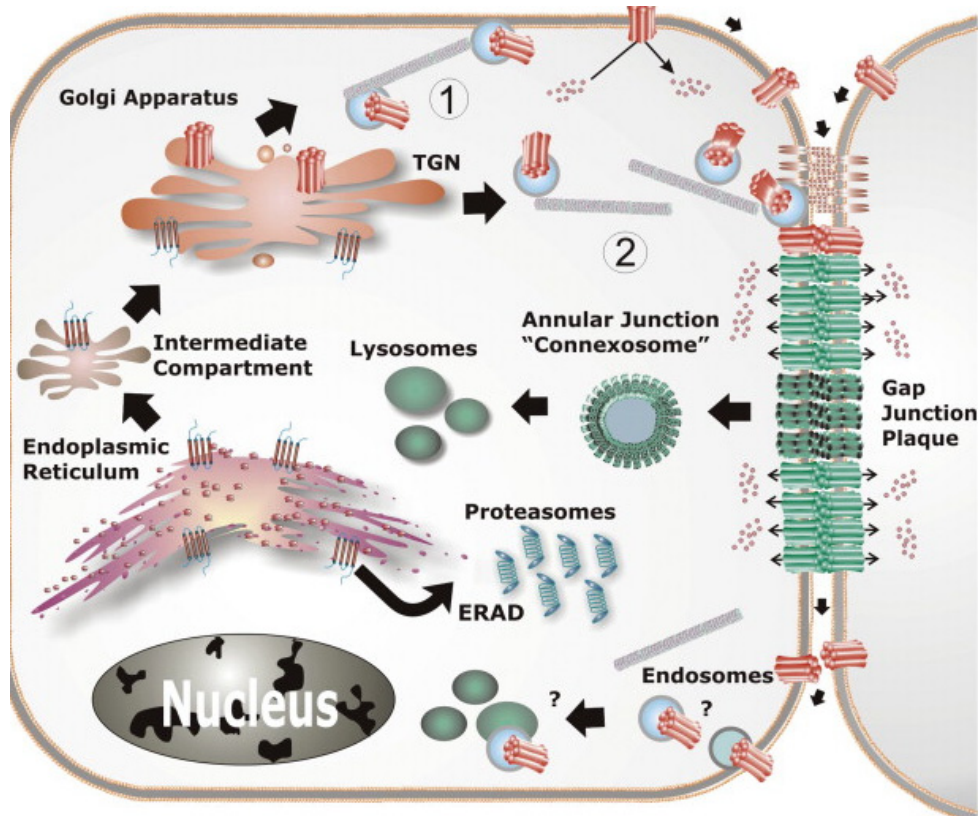


Figure 1.4: Life cycle of Cx43. Key events related to gap junction assembly and turnover. Cx43 is co-translationally inserted into the ER and oligomerized into connexons at the trans-Golgi network. Pathway 1 shows delivery of Cx43 hemichannel-containing vesicles via microtubules to the cell surface where they proceed to coalesce at sites of gap junction assembly. Pathway 2 shows microtubule-dependent direct delivery of Cx43-containing vesicles to adherens junctions in proximity to gap junctions. Internalization of gap junctions occurs via endocytotic processes from either the central regions of gap junction plaques or other regions. Internalization results in large double membrane annular junctions or small endocytic vesicles. The resulting vesicles fuse with the lysosome for degradation. Some unfolded or misfolded connexins are degraded via ERAD and the proteasomal system. Image adapted from Laird 2010.

1.3.3 Regulation by phosphorylation

The Cx43 C-terminal contains over 14 known phosphorylation sites, mostly on serine residues (Lampe and Lau 2004). These phosphorylation events are often associated with rapid and dramatic changes in migration patterns on SDS-PAGE, gap junction assembly, detergent solubility, degradation, and GJIC.

Cx43 migrates at different speeds in SDS-PAGE which include the fastest-migrating form called “P0” and typically two slower migrating forms, “P1” and “P2” (Musil and

Goodenough 1991). These general forms reflect sequential phosphorylation states in the maturation of Cx43 from synthesis to incorporation into gap junctions. P0 is considered nascent and non-phosphorylated progressing to P1 then P2 (Musil, Cunningham et al. 1990; Musil and Goodenough 1991). Although phosphorylation of the C-terminus drives electrophoretic migration changes, it is not achieved through changes in molecular weight but instead structural and conformational changes in the Cx43 (Sosinsky, Solan et al. 2007; Solan and Lampe 2009). The development of phosphospecific antibodies have further distinguished specific residues that are phosphorylated on Cx43 that make up the P0, P1, and P2 forms (Solan and Lampe 2007).

Known kinases that phosphorylate Cx43 include the tyrosine kinase src, and the serine/threonine kinases PKC, MAPK (ERK1/2), cdc2, PKA, and casein kinase 1 (Lampe and Lau 2004). Most of these phosphorylation events result in decreased Cx43 and GJIC, however, PKA and casein kinase 1 are involved in promoting gap junction formation and GJIC through direct and/or indirect Cx43 phosphorylation on serine 364/365 and 325,328,330 respectively (Cooper and Lampe 2002; Lampe and Lau 2004). While connexin phosphorylation is well-studied, substantially less is known about dephosphorylation of Cx43 by cellular phosphatases.

1.3.3.1 Casein kinase 1 delta and its proposed role in Cx43 regulation

CK1 δ is a member of the ubiquitously expressed CK1 family of conserved serine/threonine specific protein kinases (Knippschild, Gocht et al. 2005; Lohler, Hirner et al. 2009). The seven CK1 members are monomeric, constitutively active enzymes that use ATP as their phosphate donor and have a wide array of functions dictated by their localization (Knippschild, Gocht et al. 2005). The CK1 δ isoform is localized throughout the cell including the membrane, cytoplasm, and nucleus, indicative of many of its described functions including regulation of membrane transport, circadian rhythm, cell division, apoptosis, Wnt signaling, and DNA repair (Knippschild, Wolff et al. 2005). The known roles of CK1 δ in DNA damage and repair include phosphorylation of p53 on Thr18 which prevents its degradation by MDM2 (Sakaguchi, Saito et al. 2000) and binding to the spindle apparatus and centrosomes to prevent mitosis (Behrend, Stoter et al. 2000). The activity and expression levels of CK1 δ have also been shown to be induced by many DNA damaging agents (Knippschild, Milne et al. 1997; Behrend, Stoter et al. 2000; Alsheich-Bartok, Haupt et al. 2008) through unknown mechanisms.

The subcellular localization of CK1 δ within the *trans*-Golgi apparatus, on microtubules, and transport vesicles on microtubules confirm CK1 δ 's role in regulating protein trafficking (Behrend, Stoter et al. 2000; Milne, Looby et al. 2001). CK1 δ t was also recently identified as a binding partner of Cx43 (Cooper and Lampe 2002), however, where and how this interaction occurs has not been determined. It may take place at the plasma membrane where other members of the CK1 family have been shown to interact and phosphorylate E-cadherin (Dupre-Crochet, Figueroa et al. 2007) and occludins (McKenzie, Riento et al. 2006) at the cell-surface. Cx43 phosphorylation by CK1 δ on serines 325,328,330 is proposed to be crucial for the assembly of gap junctions resulting in increased gap junction stability and GJIC (Cooper and Lampe 2002). The importance of phosphorylation of Cx43 on these residues is demonstrated in ischemic cardiomyocytes where the loss of serine 325,328,330 phosphorylation is associated with decreased gap junction stability, downregulation of intercellular communication, and dysfunctional electrical coupling (Lampe, Cooper et al. 2006).

1.3.4 Gap junction-related functions of Cx43

The gap junction channel connects the cytoplasm of adjacent cells leaving a very narrow 2-3 nanometer gap (Goodenough and Paul 2009). The channel created by Cx43 has a pore size roughly estimated at 40 Å, the widest of all connexin channels, and allows for gap junction intercellular communication (GJIC) and the establishment of interconnectivity between cells (Saez, Berthoud et al. 2003; Harris 2007). A principal function of GJIC is to share metabolic demands across groups of cells and buffer gradients of nutrients or signaling molecules. Using metabolic labeling, endogenous metabolites such as glucose, ATP, ADP, AMP, adenosine, glutathione, and glutamate have been shown to transfer via Cx43 channels (Goldberg, Lampe et al. 1999; Goldberg, Moreno et al. 2002). GJIC also allows for electrical transmission between adjacent cells through a relatively low-resistance pathway for ions such as K⁺ (Mese, Richard et al. 2007). Imaging of fluorescent sensors to secondary messengers such as cAMP, inositol trisphosphate (IP₃) and Ca²⁺ demonstrated that they are all transmitted via gap junctions and can regulate intercellular calcium levels and downstream signaling (Hernandez, Bortolozzi et al. 2007).

1.3.5 Non gap junction-related functions of Cx43

Cx43 has other functions that extend beyond cell-cell communication via gap junctions. With numerous direct and indirect protein-protein interactions, Cx43 belongs to part of a larger junctional and signaling complex within cells that controls diverse cellular processes such as cell signaling, migration, growth and proliferation, tumorigenicity, differentiation, injury and apoptosis (Jiang and Gu 2005). Cx43 exists as hemichannels prior to docking with apposing cells forming a gap junction. Some of these hemichannels have unitary conductance and participate in intercellular propagation of Ca^{2+} waves or NAD^+ and ATP release which have roles in paracrine signaling (Goodenough and Paul 2003). Cx43 has a proposed channel-independent role in cytoskeletal regulation that appears related to cell injury and survival. Exogenous expression of Cx43 led to cytoskeletal reorganization and morphological changes even in the presence of gap junction inhibitors (Lin, Yang et al. 2003). Connexin expression also influences reorganization of actin resulting in stress fiber formation, flattening, and adhesiveness of transfected cells (Cotrina, Lin et al. 2008). This adhesiveness can play a role in migration that is independent of GJIC (Elias, Wang et al. 2007). Finally, an inverse relationship between connexin expression and proliferative capacity has generally been accepted as exogenous expression of Cx43 in cancer cell lines can reduce their proliferative and invasive capacity in a non-GJIC manner (Huang, Fan et al. 1998; Qin, Shao et al. 2002; Olbina and Eckhart 2003).

1.3.6 Role of Cx43 in tissue homeostasis and function

The fundamental importance of Cx43 in life is evident by the fact that global Cx43 knockout in mice is embryonic lethal (Reaume, de Sousa et al. 1995). Mutations of Cx43 in the autosomal dominant developmental disorder oculodentodigital dysplasia (ODDD) demonstrate the wide array of tissues disturbed by decreased functional Cx43 such as various craniofacial abnormalities, limb defects, neurodegeneration, and cardiac abnormalities (Paznekas, Boyadjev et al. 2003). Expression of the known mutant forms of Cx43 from ODDD in cell models have demonstrated loss-of-function properties with a majority of mutant forms trafficked to the cell surface and incorporated into gap junction plaques but unable to transmit dye between cells

(Laird 2006). The importance of Cx43 in ocular development and physiology is evident by the specific ocular defects in ODDD including micro-ophthalmia, microcornea, cataracts, iris defects, and glaucoma (Musa, Ratajczak et al. 2008). One mouse model of ODDD also demonstrated significant corneal opacities (Flenniken, Osborne et al. 2005).

Due to the lethality of total Cx43 knockout, conditional Cx43 knockouts have also provided valuable insight into the function of Cx43 in many other tissues and cell types. Specific conditional Cx43 knockout in cells/phenotypes include: sertoli cells/reduced spermatogenesis (Sridharan, Brehm et al. 2007), vascular smooth muscle cells/pathological hyperproliferation and neointima formation after injury (Liao, Regan et al. 2007), vascular endothelial cells/hypotension and bradycardia (Liao, Day et al. 2001), and osteoblasts/reduced bone formation and osteopenia (Chung, Castro et al. 2006). Within the eye, Cx43 knockout in ciliary epithelium resulted in loss of aqueous humor production and abnormalities associated with loss of intraocular pressure (Calera, Topley et al. 2006). Assessing the role of Cx43 and GJIC at the cellular level demonstrates that intrinsic functions and properties such as transepithelial resistance (Langlois, Maher et al. 2007), Na⁺/K⁺ ATPase pump function (Matchkov, Gustafsson et al. 2007), and fluid transport (Calera, Topley et al. 2006; Law, Candia et al. 2009) are intimately related to Cx43 and GJIC. Thus, in cell types with high endogenous levels of connexins and GJIC, tight regulation of connexin expression and GJIC is imperative to maintenance of normal physiological function. Downregulation of Cx43 and GJIC in these cells consistently leads to disruption of function and pathology.

1.3.6.1 Role of Cx43 and GJIC in corneal endothelial homeostasis and function

Changes in Cx43 expression and GJIC in CE cells have previously been observed after treatments that disrupted tissue homeostasis. One example is the CE release of ciliary neurotrophic factor (CNTF) and its receptor complex upon exposure to low levels of hydrogen peroxide (Koh 2002). The signaling events leading to the upregulation of Cx43 mRNA and protein (Koh, Celeste et al. 2008) have recently been proposed to be involved in promoting survival of dying CE cells (Koh, Cheng et al. 2009). Studies employing point mechanical stimulation of CE cells have shown that upon disruption there is a Cx43-dependent increase in ATP release and calcium-wave propagation between cells through both GJIC and paracrine

communication (Gomes, Srinivas et al. 2006). Cx43 and GJIC appear to also have a reciprocal role in CE pump function as inhibition of the Na⁺/K⁺ ATPase pump with ouabain resulted in reduction in gap junctions plaques (Watsky, McCartney et al. 1990) and bicarbonate treatment, which stimulates CE pump function, resulted in increased dye diffusion between CE cells (Williams and Watsky 2004). Thus, it is apparent that CE relies on Cx43 and GJIC changes during stress which is potentially coupled with the barrier and pump function of CE.

1.3.7 Role of connexins and gap junctions during genotoxic stress

Rapid increases in expression and phosphorylation of Cx43 have been observed after DNA damage with ionizing radiation, oxidative stress, and UV light and other stressors including hyperthermia and ER stress (Liu, Kasper et al. 1997; Azzam, de Toledo et al. 2003; Glover, Little et al. 2003; Gambichler, Rotterdam et al. 2008). One of the most well studied phenomena is the “radiation bystander effect” in which DNA damage with ionizing or α -particle radiation to a few cells results in gene expression changes, genomic instability, mutations, and death in neighboring non-irradiated cells (Little 2006). Consistently, increased expression of Cx43 at the mRNA and/or protein levels is observed rapidly after exposure to irradiation and GJIC has been thought to mediate the changes observed in non-irradiated cells (Azzam, de Toledo et al. 2003; Glover, Little et al. 2003; Banaz-Yasar, Tischka et al. 2005). Examination of the Cx43 promoter after ionizing irradiation suggests that the activator protein (AP)-1 binding site is involved in the upregulation of Cx43 mRNA (Liu, Kasper et al. 1997; Glover, Little et al. 2003). However, beyond ionizing radiation, the mechanisms of increased Cx43 expression after DNA damage have not been further explored and may be cell-type specific based on the function and necessity of Cx43 and GJIC in that cell.

1.4 SUMMARY & GOALS

The eye is an ideal organ to study age-related changes and the effects of DNA damage due to its continuous exposure to environmental and endogenous stressors. Almost every specialized tissue in the eye including the cornea, trabecular meshwork, ciliary body, lens, and retina undergoes age-related degeneration that results in deterioration of vision (Salvi, Akhtar et al. 2006). Many of the tissues in the visual axis are non-proliferative which is believed to be important for maintenance of clear vision; however, these quiescent states also may permit the accumulation of DNA damage with time which may be especially detrimental to non-regenerative tissues such as the corneal endothelium and retinal pigment epithelium. With age comes exposure to increasing amounts of potential DNA damage which may accumulate in time. As those suffering from corneal endothelial dysfunction are typically older and the source of corneal tissue for transplantation is generally from older donors, it is becoming increasingly evident that age affects the corneal endothelium and those that receive corneal transplantations. Whether DNA damage is a cause of the non-regenerative nature of the corneal endothelium or in fact a by-product of lack of proliferation remains to be determined. Regardless, the transparency of the cornea, which controls the very first entry of light on our visual system, depends upon the proper function of the corneal endothelium.

The goals of this body of work are to establish a role for genotoxic stress and identify novel responses in corneal endothelium. Specifically, I sought to determine and characterize: (1) novel exposures to genotoxic stress (Chapter 2), (2) the effects of unrepaired DNA damage in aging and vulnerability of the corneal endothelium (Chapter 3), and (3) novel acute cellular responses to genotoxic stress that mediate corneal endothelial survival (Chapters 4 and 5). By studying the cellular and molecular mechanisms by which the corneal endothelium responds to DNA damage, we may begin to find ways to prevent its decline or protect it from future insults.

2.0 DNA CROSS-LINKING, DOUBLE-STRAND BREAKS, AND APOPTOSIS IN CORNEAL ENDOTHELIAL CELLS AFTER A SINGLE EXPOSURE TO MITOMYCIN-C

Chapter 2 is adapted, with copyright permission from the Association for Research in Vision and Ophthalmology, from a published article. **Roh DS, Cook AL, Rhee SS, Joshi AB, Kowalski R, Dhaliwal DK, Funderburgh JL. (2008) DNA Cross-linking, Double-Strand Breaks, and Apoptosis in Corneal Endothelial Cells after a Single Exposure to Mitomycin C. *Invest Ophthalmol Vis Sci* 49(11): 4837-4843.** Note that the figure numbers have changed.

2.1 INTRODUCTION

Mitomycin C (MMC), an antibiotic isolated from *Streptomyces caespitosus*, is classified as an alkylating agent capable of covalently binding DNA and inducing inter- and intrastrand cross-links. The presence of such cross-links results in inhibition of DNA synthesis primarily during late G₁ and S phases, although it is not cell-cycle specific. In addition, MMC inhibits RNA and protein synthesis and interacts with molecular oxygen, generating free radical damage to DNA and protein (Chabner, Amrein et al. 2006). MMC is predominantly used as a systemic chemotherapeutic agent; however, off-label usage of MMC is common during ophthalmic procedures, such as glaucoma filtering surgery, lacrimal surgery, treatment of ocular neoplasia, ocular cicatrization surgery, and corneal refractive surgery (Abraham, Selva et al. 2006).

Currently, the use of adjuvant MMC as an intraoperative prophylactic for reducing haze has become increasingly widespread in photorefractive keratectomy (PRK) (Majmudar, Forstot et al. 2000; Carones, Vigo et al. 2002; Lane, Swale et al. 2003; Gambato, Ghirlando et al. 2005; Lacayo and Majmudar 2005; Lee, Chung et al. 2005; Abraham, Selva et al. 2006; Bedei,

Marabotti et al. 2006; Nakano, Bains et al. 2007). As a topical adjunct during refractive surgery, MMC is exclusively used to modulate corneal wound healing and, through its effects on stromal keratocytes, to prevent active fibrosis, abnormal collagen deposition, and haze formation. The induction of apoptosis of keratocytes by MMC seems to play a central role in preventing the formation of clinically significant haze (Kim, Tchah et al. 2003; Kim, Pak et al. 2004; Chang 2005).

MMC applied topically has been shown to penetrate the cornea and can be detected in corneal tissue and the aqueous humor well after initial application (Song, Kim et al. 2006; Torres, Merayo-Llives et al. 2006; Song, Kim et al. 2007); thus, treatment with MMC during refractive surgery has the potential to impact ocular tissues other than the target keratocytes. Of particular interest is the corneal endothelium, a monolayer of nonregenerating cells essential to the clarity of the cornea. Initially, several clinical studies regarding corneal endothelial cell density and morphology indicate few short-term complications with the use of adjuvant MMC during refractive surgeries (de Benito-Llopis, Teus et al. 2007; Diakonis, Pallikaris et al. 2007; Goldsberry, Epstein et al. 2007); however, recent studies have suggested potential adverse effects of such treatments. The corneal endothelium appears to exhibit significant vulnerability to the toxicity of MMC. Single intraoperative MMC applications over a denuded stroma result in dose-dependent corneal edema and endothelial apoptosis (Chang 2004). Similarly, significant endothelial cell loss has been reported in MMC-treated eyes within a few months after photorefractive keratectomy (Morales, Zadok et al. 2006). In addition, numerous case reports have suggested that a single intraoperative application of MMC during other ocular procedures may be responsible for corneal endothelial damage and loss (Sihota, Sharma et al. 1998; Fukuchi, Hayakawa et al. 2002; Mietz, Roters et al. 2005; Mohammadpour, Jabbarvand et al. 2007). Thus, as the surgical use of MMC increases, the need to define its cellular effects at relevant clinical applications and dosages on corneal endothelial cells is of high importance.

In this study, we assessed the effects of a single MMC application on corneal endothelial cells, using concentrations and times relevant to current clinical practice. We used a modified version of the highly sensitive comet assay (single cell gel electrophoresis) to detect DNA cross-linking and examined the phosphorylated histone variant H2AX (γ -H2AX) to demonstrate DNA double-strand breaks. Finally, we assessed MMC-treated cells for annexin V staining to detect apoptosis. Our results clearly demonstrate that exposure to MMC at the times and concentrations

commonly used in refractive surgery produced cross-linking of corneal endothelial DNA, persistent DNA damage, and endothelial death via apoptosis.

2.2 MATERIALS AND METHODS

Animals and Cell Culture

Fresh whole goat eyes were obtained from a local butcher within a few hours of death. For indicated experiments, whole globes were used immediately as described below. To isolate corneal endothelial (CE) cells, we excised corneas with a scleral rim and placed them endothelium side up in plastic tube caps. The CE cells were enzymatically detached by direct application of 0.05% trypsin/0.5 mM EDTA (Sigma-Aldrich, St. Louis, MO) with incubation at 37°C and harvested by gentle scraping. The CE cells were separated from Descemet's membrane and cell suspensions were broken up by gentle pipetting and sieved through a 70- μ m nylon mesh. The suspended CE cells were centrifuged, and pelleted cells used for comet assay were directly resuspended in 1% low-melting-point (LMP) agarose and used as described below. CE cells for culture were resuspended in DMEM (no. 1569; Invitrogen, Carlsbad, CA) supplemented with 10% fetal bovine serum (Hyclone, Logan, UT), gentamicin, penicillin/streptomycin, and amphotericin B and cultured in 25 cm² cell culture flasks at 37°C in 5% CO₂ until 90% confluent. The cells were passaged on a cell dissociation enzyme (TrypLE Express; Invitrogen), centrifuged, resuspended, and plated on sterile glass coverslips for γ -H2AX detection or in six-well plates for annexin V detection. Cell culture pellets used for the comet assay were directly resuspended in 1% LMP agarose and used as described later. Confluent passage-one or -two cells were used in all cell culture experiments.

MMC Treatment

MMC (Sigma-Aldrich) was dissolved to desired concentrations in phosphate-buffered saline (PBS) for whole globe treatments and in DMEM with 10% FBS for cell culture studies. We referred to established MMC treatment protocols used in refractive surgery for the treatment of whole intact globes (Majmudar, Forstot et al. 2000; Carones, Vigo et al. 2002; Lane, Swale et al.

2003; Gambato, Ghirlando et al. 2005). First, the corneal epithelium was treated with 20% ethanol within an 8-mm trephine for 20 seconds followed by mechanical epithelium debridement of the 8-mm area with a beaver blade. Immediately after debridement, a corneal shield (Medtronic Solan, Jacksonville, FL) soaked with 200 $\mu\text{g}/\text{mL}$ (0.02%) MMC in PBS was placed over the denuded area for 6, 12, 30, 60, or 120 seconds. The control globes were not treated with MMC. After the MMC sponge was removed, the eyes were copiously washed with 30 mL of PBS and then placed in a humid chamber for 30 minutes before isolation of CE cells as described earlier. Laser ablation was performed on a subset of intact whole globes before MMC treatment (Visx Star S4 Excimer Laser System; Visx Technology, Santa Clara, CA) with a fluence of 160 mJ/cm^2 per pulse at 10.0 Hz. The laser was programmed for a 75- μm ablation depth with a 6.0-mm optical zone and a 0.3-mm transition zone. To allow for DNA repair in a subset of corneal buttons, we excised the corneas after MMC treatment, placed them in 35- mm^2 tissue culture plates, and immersed them in culture medium at 37°C in 5% CO_2 for 24 hours before CE cell isolation.

For comet assay of cultured CE cells, we treated confluent cultures with MMC concentrations ranging from 0.02 to 200 $\mu\text{g}/\text{mL}$ for 10, 30, or 60 minutes and isolated cells per the protocol above.

For treatment of cultured CE cells to detect $\gamma\text{-H2AX}$ and annexin V, we selected a MMC concentration of 0.4 $\mu\text{g}/\text{mL}$ (0.00004%) which we determined via growth inhibition bioassay to be present in the corneal endothelium after topical treatment of intact globes with 0.02% MMC. Furthermore, this concentration was similar to those found in the aqueous humor 30 minutes to 1 hour after MMC treatment in previous studies (Torres, Merayo-Llives et al. 2006; Song, Kim et al. 2007). We treated confluent monolayers of CE cells with 0.4 $\mu\text{g}/\text{ml}$ MMC in DMEM/10% FBS for 30 minutes at 37°C in 5% CO_2 then immediately removed the medium, washed with PBS, and replaced it with fresh culture medium. The cells were incubated 24, 48, or 72 hours before assaying for $\gamma\text{-H2AX}$ or annexin.

Determination of Radial and Posterior Diffusion of MMC

Determination of the extent of radial and posterior diffusion of MMC in whole globes after topical exposure to 0.02% MMC was assayed by sectioning the excised cornea into radial or anterior to posterior (coronal) portions and estimating concentrations of MMC in the tissue with

an *Escherichia coli* growth-inhibition bioassay. For radial sectioning, MMC-treated corneas were immediately cut into concentric rings with 8-, 6-, and 4-mm trephines; minced; and placed into tubes containing PBS. For coronal sections, groups of five 40- μ m-thick sections of treated corneas, cut with a sliding microtome, were combined, minced, and placed into tubes containing 1 mL of PBS. Fifty microliters of each extract was pipetted onto a minimum inhibitory concentration (MIC) disc, which was then placed onto an *E. coli* plate, and incubated overnight. The resulting zone of inhibition of growth of *E. coli* was measured manually and compared to a standard curve to determine the concentration of MMC present in the extracts. Radial measurements were made from duplicate assays and coronal measurements were obtained from a single assay.

Modified Alkaline Comet Assay and Analysis

The CE cell suspensions were pelleted and resuspended in 80 μ L of 1% LMP agarose. The resuspended cells were immediately transferred to microscope slides precoated with 1% normal melting-point agarose, covered with coverslips, and chilled over ice for 20 minutes. The coverslips were removed and the slides placed in lysis solution (10 mM Tris, 100 mM EDTA, 2.5 M NaCl [pH 10], 1% Triton-X) over ice for 60 minutes. Lysis solution was removed, and the slides were rinsed three times with distilled water. The slides were then irradiated with 5 Gy (Cs^{137} source) γ -irradiation to induce random double-strand DNA breaks. After irradiation, DNA was alkaline-denatured by immersion of slides in cold 3 M NaOH, 10 mM EDTA for 30 minutes. Electrophoresis was conducted in the same buffer at 25 V (0.8 V/cm) for 40 minutes at room temperature. The slides were incubated in neutralization buffer (0.4 mM Tris, pH 7.5) for 10 minutes and then stained with SYBR gold (Invitrogen) in TE (10 mM Tris-HCl, 1 mM EDTA [pH 8.0]). Coverslips were placed over the slides which were allowed to dry overnight protected from the light. DNA from individual cells was visualized using an epifluorescence microscope (TE2000; Nikon, Melville, NY) with a 10 \times objective (Pan Fluor; Nikon). Photography and analysis of the samples were performed in a masked fashion. Images were captured with a 12-bit digital camera (SPOT; Diagnostic Instruments, Sterling Heights, MI). All comet analysis was performed using software designed for this purpose (CometScore software; TriTek Corp., Sumerduck, VA) which measures a wide range of fluorescence parameters for selected comets. The primary measurement, %DNA-in-head, reflected the relative distribution of DNA in each

comet. In both the intact globe and cell culture studies, more than 1000 comets were analyzed in each of two independent experiments.

γ -H2AX Detection

Confluent CE cells grown on sterile glass coverslips were exposed to a single 30-minute treatment with 0.4 $\mu\text{g}/\text{mL}$ MMC, rinsed, and continued in culture for 24, 48, or 72 hours. MMC-treated CE cells were briefly rinsed in PBS and then fixed with 3% paraformaldehyde in PBS for 20 minutes at room temperature. After the cells were rinsed with PBS, they were permeabilized with 0.1% Triton-X in PBS for 1 minute, rinsed with PBS, and stored in 50% glycerol in PBS (vol/vol) at 4°C until staining. Nonspecific binding was blocked with 10% heat-inactivated goat serum for 1 hour at room temperature. After they were washed with PBS, the CE cells were incubated overnight at 4°C with anti- γ -H2AX polyclonal rabbit antibody (AF2288; R&D Systems, Minneapolis, MN) diluted 1:800 in 1% bovine serum albumin (BSA) in PBS. The cells were washed and incubated with DAPI nuclear stain, 0.5 $\mu\text{g}/\text{mL}$ and Alexa Fluor 488–conjugated goat anti-rabbit IgG, 1 $\mu\text{g}/\text{mL}$ (A-11094; Invitrogen) for 1 hour at room temperature. The coverslips were placed onto slides, and the nuclei were visualized with an inverted microscope (TE200-E Eclipse; Nikon) with a 40 \times oil objective (Nikon). A digital camera (CoolSnapHQ; Roper, Tucson, AZ) was used for image acquisition. Manual counting, processing, and analysis were performed (MetaMorph Software; Molecular Devices, Sunnyvale, CA). Fifteen images from each treatment group were analyzed in each of two independent experiments.

Annexin V Detection

Annexin V detection (TACS Annexin V-FITC Apoptosis Detection kit; R&D Systems) was performed on confluent CE cells grown in six-well culture plates 24 or 48 hours after a single 30-minute treatment with 0.4 $\mu\text{g}/\text{mL}$ MMC, according to the manufacturer's protocol. Nuclei were counterstained with Hoechst 33342 dye at 1 $\mu\text{g}/\text{mL}$ (Invitrogen). Cells were photographed and analyzed as for γ -H2AX detection. Ten images representing different locations throughout the culture were analyzed from each treatment group.

Statistics

Statistical analysis was performed with one-way analysis of variance (ANOVA) followed by the Dunnett multiple comparison test (GraphPad Prism 4 software; GraphPad Software, San Diego, CA). The Dunnett test was used to compare values for MMC treatment groups with those of the control cultures. $P < 0.05$ was considered significant for all tests.

2.3 RESULTS

2.3.1 MMC in the cornea after a single topical treatment

A single topical treatment of MMC (0.02%) for 2 minutes on a de-epithelialized cornea resulted in measurable MMC concentrations throughout the entire cornea (Fig 2.1). Radial sections of MMC-treated corneas revealed concentrations of MMC from 1.05 $\mu\text{g/mL}$ in the central area to 0.37 $\mu\text{g/mL}$ in the periphery (>8 mm), demonstrating the rapid diffusion of MMC from the central cornea to the periphery (Fig 2.1.A). Coronal sections of MMC-treated corneas revealed the presence of MMC in all layers of the cornea after treatment, ranging from 1.05 $\mu\text{g/mL}$ in the anterior stroma (1–200- μm section) to 0.37 $\mu\text{g/mL}$ in the CE (601–800- μm section) (Fig 2.1.B). This concentration was similar to those found in the aqueous humor 30 minutes to 1 hour after MMC treatment in previous studies (Torres, Merayo-Llodes et al. 2006; Song, Kim et al. 2007).

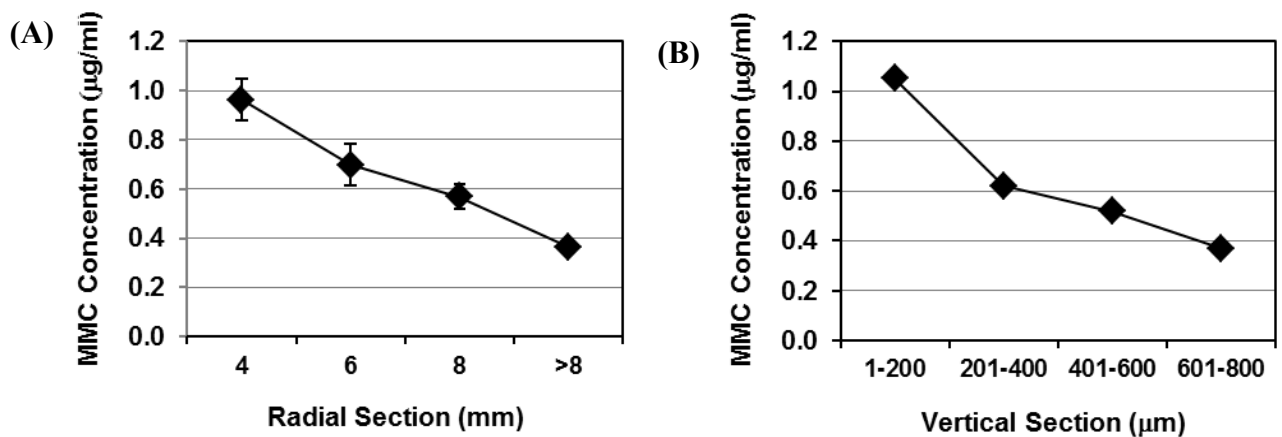


Figure 2.1: Corneal concentration of MMC 2 minutes after a single topical administration of 0.02% MMC on a whole globe, as determined by growth inhibition bioassay. The zone of inhibition of *E. coli* growth was compared to a standard curve to determine MMC concentrations. (A) MMC concentration decreases radially, away from the site of application. (B) CE concentration is approximately 0.37 $\mu\text{g/mL}$ at the depth of the endothelium (601–800 μm). Mean \pm SEM.

2.3.2 Induction of DNA Cross-Linking in the CE

Modified Comet Assay We investigated the cross-linking effects of MMC treatment on goat CE by using a modification of the comet assay previously developed by McKenna et al. (McKenna, Gallus et al. 2003) to evaluate MMC-induced DNA cross-linking damage in RT4 cells. Fig 2.2.A is a representative image of the results of the comet assay illustrating staining of DNA from individual CE cells after fragmentation and denaturation. Distinct head and tail regions are seen in the DNA from each cell, representing DNA fragments with differing electrophoretic mobility. DNA fragments without cross-links are smaller and migrate more rapidly (i.e., in the tail portion of the comet). In contrast, DNA fragments with MMC-induced cross-links resist full denaturation in alkaline conditions and exhibit decreased electrophoretic mobility, thereby forming the head of the comet. Fig 2.2.B provides a representative image illustrating the increasing percentage of DNA remaining in the head (%DNA-in-head) of the comet as MMC treatment time increased.

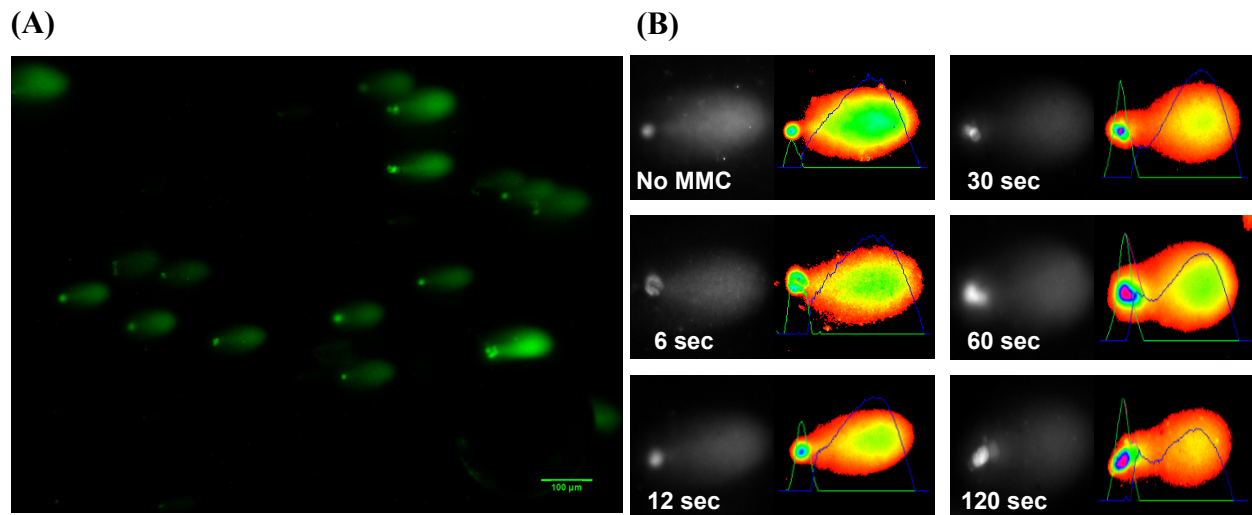


Figure 2.2: Single cell gel electrophoresis (modified alkaline comet assay) of CE cell DNA. (A) Representative images of individual CE cell DNA after electrophoresis show migration patterns with a comet-like appearance. (B) Individual comets are oriented with the head to the left. The image on the right of each shows a pseudocolor of the image with an overlaid graphic representation of staining intensity. This intensity is proportional to the amount of DNA at that location in the gel. Area under these curves was used to calculate %DNA-in-head. With increasing length of treatment of MMC, more DNA was observed in the head of comets.

MMC-Induced DNA Cross-Links in Intact Globes. Quantitative analysis of images similar to those in Fig 2.2, found that a single topical application of 0.02% MMC on intact whole globes caused DNA cross-linking in CE cells at all treatment times (Fig 2.3). More than 1000 individual comets were analyzed in each experiment. In experiment A, we used epithelial debridement followed by MMC treatments. The presence of the epithelial basement membrane did not prevent the cross-linking effects of MMC, as all treated groups had significantly more %DNA-in-head than did the untreated control (Fig 2.3.A, ANOVA $p < 0.05$, Dunnett's $p < 0.01$). In experiment B, we used epithelial debridement followed by laser ablation and MMC treatments. In these conditions, which emulate PRK protocols, all MMC treatment groups had significantly more %DNA-in-head when compared with the untreated control (Fig 2.3.B, ANOVA $p < 0.05$, Dunnett's $p < 0.01$). Experiment C was similar to experiment A, but MMC treatment was followed by a 24-hour incubation period to allow for repair. In this experiment, MMC-induced DNA cross-linking in the endothelium was not significantly reduced after 24 hours, as all MMC treatment groups had significantly more %DNA-in-head than did the control (Fig 2.3.C, ANOVA $p < 0.05$, Dunnett's $p < 0.01$). Across all trials, there was also an apparent time response between the length of MMC treatment and amount of DNA cross-linking evident as %DNA-in-head.

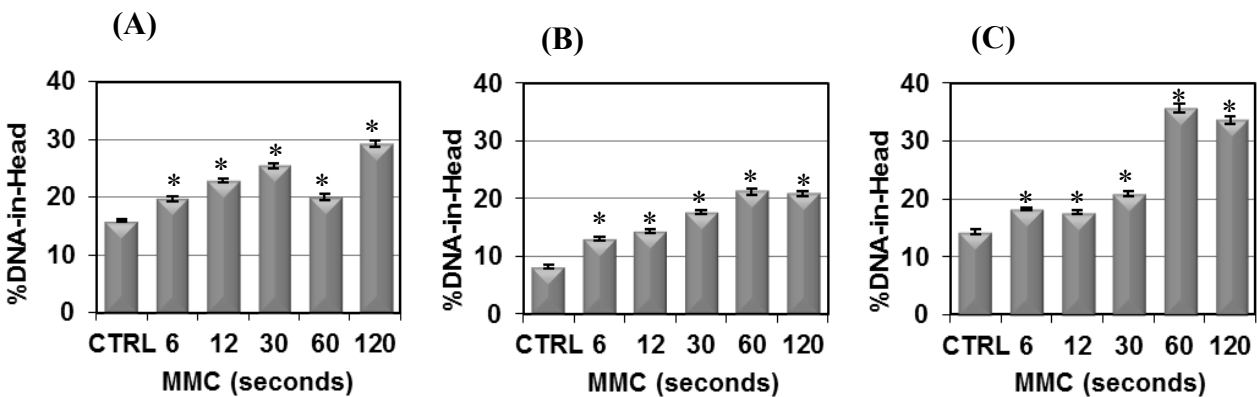


Figure 2.3: CE DNA cross-linking induced by MMC treatment of whole globes. %DNA-in-head was calculated for comets (as in Fig. 2.2) derived from CE cells after topical MMC treatment of intact goat eyes. (A) 0.02% MMC treatment followed epithelial debridement. (B) MMC treatment followed epithelial debridement and 75 μ m stromal ablation. (C) Eyes treated with MMC after epithelial debridement (as in A) were incubated 24 hours at 37°C, to allow DNA repair. *Significant difference from control; ANOVA $P < 0.0001$, Dunnett $P < 0.01$. Mean \pm SEM.

MMC-Induced DNA Cross-Links in Cultured CE cells. Confluent monolayers of goat CE cells also exhibited significant DNA cross-linking similar to that shown in Fig 2.3 in MMC-treated intact globes. MMC concentrations ranging from 0.02 to 200 $\mu\text{g/mL}$ all resulted in significant DNA cross-linking when compared with the untreated control (Fig 2.4, ANOVA $p < 0.05$, Dunnett's $p < 0.05$). Increasing the length of exposure to MMC at all concentrations, except 0.2 $\mu\text{g/mL}$, resulted in increased DNA cross-linking, similar to the results in intact globes.

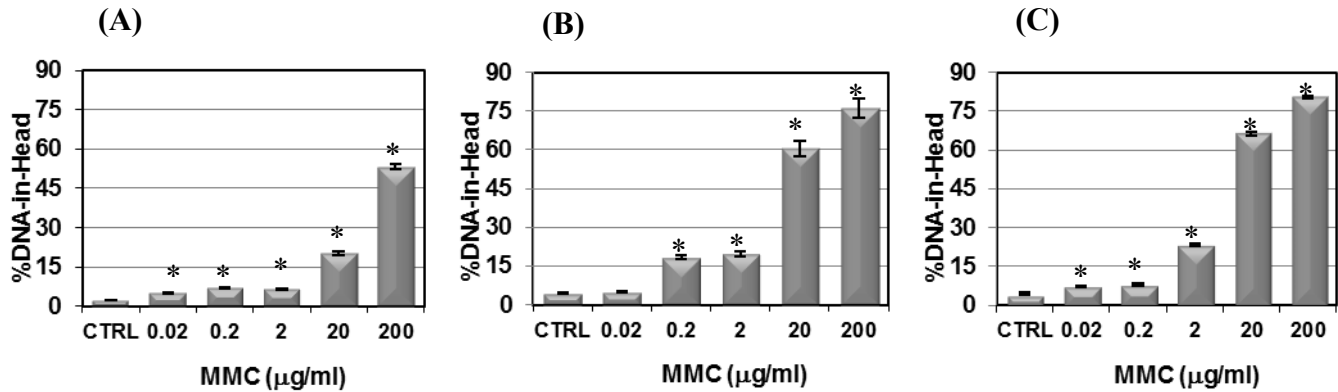


Figure 2.4: Sensitivity of CE cells to DNA cross-linking by MMC. Goat CE cells in culture were treated with a range of MMC concentrations, and DNA cross-linking was determined using the comet assay as described in Figure 2.2 at three exposure times. (A) Ten-minute exposure to MMC at all concentrations induced significant DNA cross-links compared to controls. (B) Thirty-minute exposure to MMC at all concentrations (except 0.02 $\mu\text{g/mL}$, Dunnett $P > 0.05$) induced significant DNA cross-links compared with controls. (C) Sixty-minute exposure to MMC at all concentrations induced significant DNA cross-links compared with the control. *Significant differences from control; ANOVA $P < 0.0001$, Dunnett $P < 0.01$. Mean \pm SEM.

2.3.3 Persistent and Elevated γ -H2AX Staining after MMC Treatment

γ -H2AX nuclear foci represent phosphorylation at Ser139 of histone variant H2AX and are sensitive markers for DNA double-strand breaks (Sedelnikova, Pilch et al. 2003). Dephosphorylation of histone H2AX accompanies subsequent effective repair of the DNA damage (Chowdhury, Keogh et al. 2005). As shown in Fig 2.5.A, CE cells treated with 0.4 $\mu\text{g/mL}$ MMC for 30 minutes developed γ -H2AX-positive nuclei, demonstrating the presence of DNA double-strand breaks. Recovery for 24, 48, and 72 hours after MMC treatment showed no decrease in the percentage of γ -H2AX-positive nuclei (Fig 2.5.B). MMC treatment therefore produces a long-term activation of γ -H2AX in CE cells, a phenomenon previously reported to be transient in cells undergoing DNA repair (Downey M 2006).

(A)

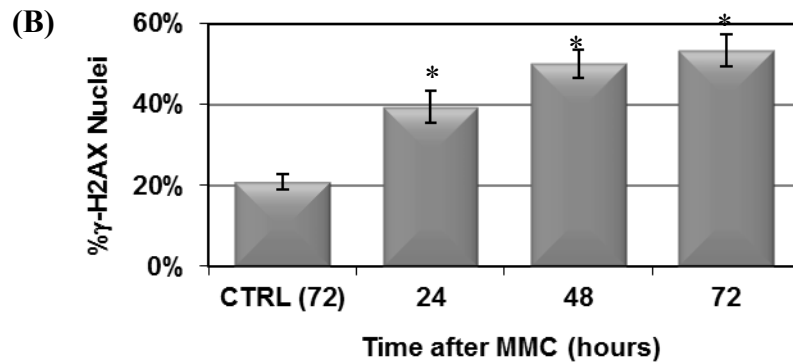
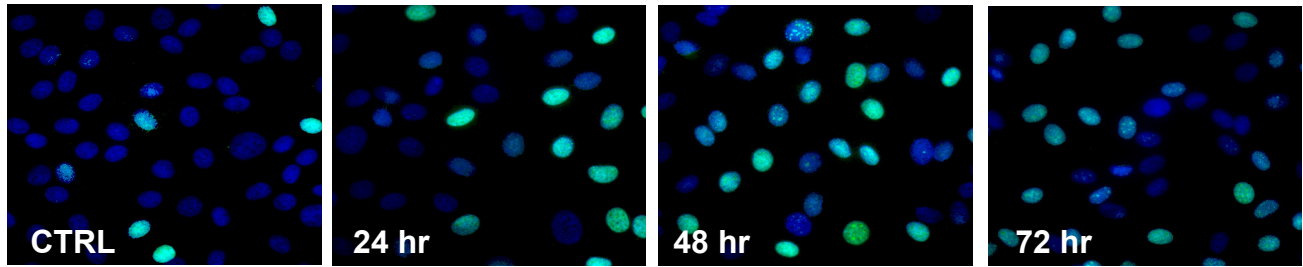


Figure 2.5: H2AX phosphorylation (γ -H2AX) induced by MMC treatment. (A) Confluent CE cells were treated with MMC at 0.4 $\mu\text{g}/\text{mL}$ for 30 minutes and nuclei were stained with DAPI (*blue*) and anti- γ -H2AX antibody (*green*) at 24, 48, and 72 hours after treatment. (B) The proportion of nuclei with γ -H2AX staining was similar to that in (A). *Significant differences from control; ANOVA $P < 0.0001$, Dunnett $P < 0.01$. The control cells were assayed at 72 hours. Mean \pm SEM.

2.3.4 Effect of MMC on the Proportion of Apoptotic Cells

To examine the potential irreversible effects of MMC-induced DNA damage, we examined confluent CE cells for annexin V binding to phosphatidylserine flipping, an early signal of apoptosis. CE cells briefly treated with 0.4 $\mu\text{g}/\text{mL}$ MMC for 30 minutes showed increased annexin V staining compared with the control (Fig 2.6.A). MMC treatment increased the proportion of annexin V cells, with the number labeled becoming significantly different from the control at 24 and 48 hours after treatment (Fig 2.6.B). Similar results were obtained after treating confluent CE cells with higher concentrations of MMC.

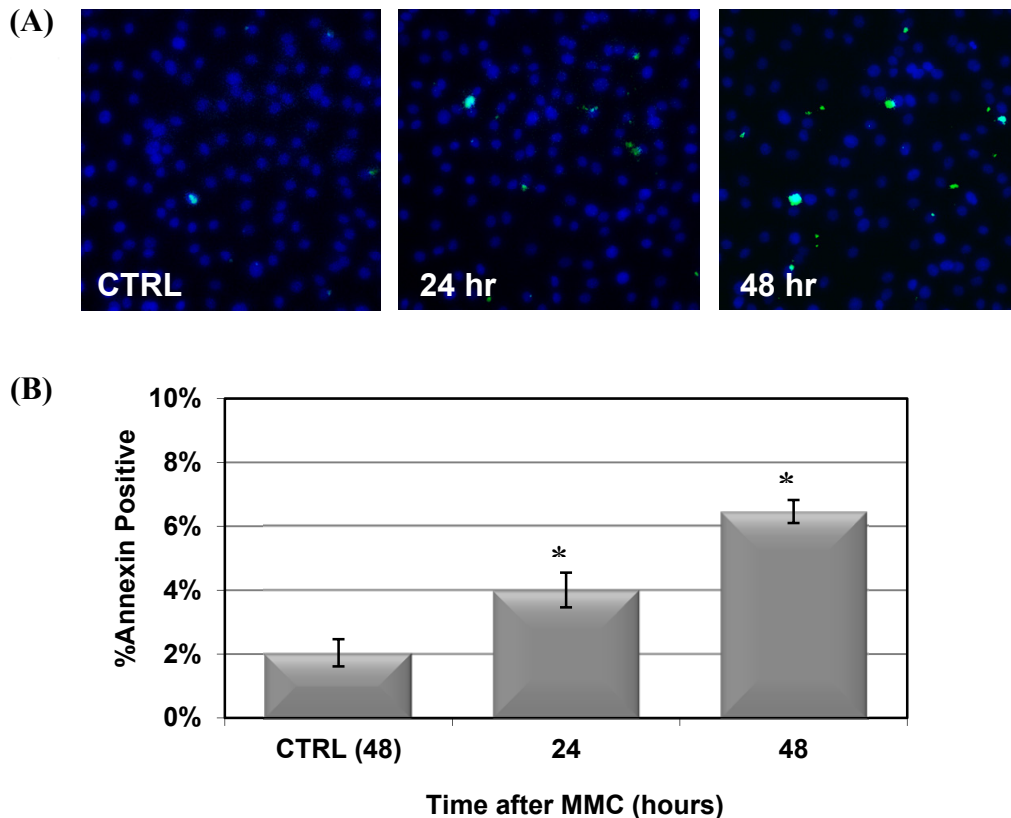


Figure 2.6: MMC exposure initiates endothelial apoptosis. (A) Confluent CE cells were treated with MMC 0.4 $\mu\text{g}/\text{mL}$ for 30 minutes and stained with Hoechst 33342 (*blue*) and annexin V-FITC (*green*) 24 and 48 hours later. Cells positive for annexin V-FITC are apoptotic. (B) The proportion of apoptotic cells after MMC treatment was significantly elevated above the untreated control. *Significant differences from control; ANOVA $P < 0.0001$, Dunnett $P < 0.01$. The control cells were assayed at 48 hours. Mean \pm SEM.

2.4 DISCUSSION

Recent studies have demonstrated the presence of MMC in the anterior chamber after photorefractive keratectomy (Song, Kim et al. 2006; Torres, Merayo-Llodes et al. 2006; Song, Kim et al. 2007), dose-dependent corneal edema after a single application of MMC on the corneal surface (Chang 2004), and significant endothelial cell loss occurring within a few months after PRK with MMC (Morales, Zadok et al. 2006). Our study has added new evidence of the effects of MMC on the CE, which DNA repair mechanisms did not appear to reverse. We confirmed both radial and coronal diffusion of MMC after a single topical treatment that extended to the CE. Using a sensitive, recognized measure of DNA cross-linking, the comet assay, we detected significant levels of cross-linked DNA in MMC-treated CE cells. In addition,

we observed persistent DNA double-strand breaks and an increase in the proportion of apoptotic cells after a brief exposure to MMC.

Our study design included three separate trials to examine the effects of MMC treatment on intact globes across a range of conditions while emulating a standard protocol of photorefractive keratectomy with intraoperative MMC treatment. It is important to emphasize that our MMC application times ranged from 6 to 120 seconds, including the range of currently recommended MMC application times. Our results showed that the presence or absence of the epithelial basement membrane and Bowman's layer did not affect the ability for MMC to induce cross-links in CE DNA. Ablation of 75 μm of the stroma was within the range of ablation for human PRK and has been thought to facilitate MMC access to the CE (Song, Kim et al. 2007). In the eyes that underwent laser ablation, we observed the greatest absolute difference between the control and the 6-second treatment; however, there was no other evidence of increased risk. Finally, allowing the excised corneas 24 hours to repair the MMC-induced DNA damage produced an observable difference between treatment times less than and greater than 60 seconds. However, even with time for repair of the DNA cross-links, all treatment groups had significantly more cross-linked DNA than the untreated controls.

The effects of MMC concentration and treatment times on DNA cross-linking in CE cells were better defined in the cell culture experiments (Fig 2.4). The cross-linking effects of MMC were evident across a wide range of concentrations and even 10-fold below the amounts we detected in the CE after a single topical treatment (Fig 2.1). Although there is continuous turnover of aqueous humor content and significant decrease in MMC concentration over time (Song, Kim et al. 2006; Torres, Merayo-Llodes et al. 2006; Song, Kim et al. 2007), we found that even the brief 10-minute exposure to 0.02 $\mu\text{g}/\text{mL}$ MMC was long enough to induce significant DNA cross-linking in cultured CE cells (Fig 2.4.A).

Despite evidence that human CE appears protected from UV irradiation damage the ability of these cells to repair other DNA damage such as MMC-induced cross-linking is essentially unknown. McKenna et al. (McKenna, Gallus et al. 2003) found in the bladder tumor cell line RT4 that almost all MMC-induced cross-links were repaired within 24 hours, reversing the characteristic changes in DNA migration in the modified comet assay. In contrast, we observed no reversal of the %DNA-in-head proportion after 24 hours in culture. In fact the proportion of cross-linked DNA in most treatment conditions actually increased 24 hours after

MMC treatment (compare Fig 2.3.A and 2.3.C). We also observed significant γ -H2AX positive nuclei in MMC-treated confluent cultures (Fig 2.5). This histone becomes phosphorylated at the site of double-strand DNA breaks and is dephosphorylated during repair. Our observation that MMC induces γ -H2AX phosphorylation is consistent with the comet data indicating DNA damage induced by MMC. The presence of phosphorylated γ -H2AX foci is believed to represent a signal for repair and to stimulate recruitment of DNA repair enzymes. Phosphorylation of γ -H2AX in most systems is transient, however, and dephosphorylation occurs after repair has been completed (Chowdhury, Keogh et al. 2005). The persistence of the activated γ -2HAX in CE cells is an unusual observation. It suggests that little or no DNA repair of the induced breaks occurs in these quiescent cells. The nonproliferative state of the CE may limit its ability to initiate and repair MMC-induced cross-links, leaving it increasingly vulnerable to DNA damage. Current models of DNA cross-linking repair suggest that the coordinated action of several DNA repair pathways, including nucleotide excision repair and double-strand break repair, may not be as efficient in nonreplicating cells, since they are initiated during active DNA replication (McHugh, Spanswick et al. 2001). In repair-deficient mammalian cells, only 40 DNA cross-links per cell have been estimated to be lethal (Lawley and Phillips 1996). Additional studies are needed to evaluate the capacity to repair MMC-induced DNA cross-links in the CE.

The presence of DNA cross-linking in the CE is likely to be associated with the decreased endothelial cell density, endothelial apoptosis, and potential corneal edema observed in previous studies (Sihota, Sharma et al. 1998; Fukuchi, Hayakawa et al. 2002; Chang 2004; Mietz, Roters et al. 2005; Morales, Zadok et al. 2006; Mohammadpour, Jabbarvand et al. 2007). Evidence of MMC-induced apoptosis was found in rabbit CE after epithelial debridement and MMC treatment for 2 minutes (Chang 2004). Given the ocular penetration profile of a single topical application of MMC as well as our evidence of MMC-induced DNA cross-links and apoptosis in cultured CE cells (Fig 2.6), it is probable that in vivo the CE layer is at risk to MMC-induced DNA damage and potential apoptosis. Because the human CE is nonproliferative in vivo, it is already considered fragile to insults and responds only through cell enlargement and migration as a means of repair (Joyce 2003). When CE cell density decreases below the level of 1000 cell/mm², the number of pump sites per cell progressively increases; however, pump function is eventually inadequate to maintain the balanced hydration of the stroma and corneal edema ensues (Crawford, Ernst et al. 1995). Disruption of the normal function of CE with a

genotoxic stressor such as MMC may eventually accelerate this pathologic process.

Recent acknowledgment of MMC toxicity has led to the development of methods to limit corneal exposure, mostly through reductions in concentration and exposure times. Efforts to reduce the initial recommendation of 120 seconds to shorter exposure times (de Benito-Llopis, Teus et al. 2007; Goldsberry, Epstein et al. 2007) as well as lower concentrations (Lane, Swale et al. 2003; Thornton, Puri et al. 2007) have since been in practice. Despite these efforts, it is noteworthy that we observed significant DNA cross-linking after as few as 6 seconds of MMC exposure and at concentrations well below what has been detected in the CE and aqueous humor. Our results suggest that current practices in MMC application during refractive surgeries may be increasing the potential for long-term and permanent effects on the health of the CE.

3.0 AGE-RELATED DYSTROPHIC CHANGES IN CORNEAL ENDOTHELIUM FROM DNA REPAIR DEFICIENT MICE

3.1 INTRODUCTION

The cornea is a remarkably transparent tissue that provides protection from environmental exposures and is critical for refracting incoming light. It is composed of three tissue layers (epithelium, stroma, and endothelium) each with distinct properties and functions. The corneal endothelium (CE) is the innermost and single cell layer that functions to maintain proper hydration of the corneal stroma and to allow nutrient and waste exchange with the aqueous humor. Functional CE cells are indispensable for maintaining corneal transparency. However, this single layer of cells is also very fragile and does not regenerate *in vivo* (Joyce 2003). Loss of CE cells as a consequence of disease or acute trauma therefore leads to irreversible corneal edema and blindness (Bourne and McLaren 2004). There is also a steady loss of CE cells in all individuals with aging, at a rate of 0.6% of central cell density per year (Bourne and McLaren 2004). Currently, corneal transplantation is the only therapeutic option for corneal edema (Bourne and McLaren 2004). In 2009, >42,000 individuals in the U.S.A. required a corneal transplant, with CE degeneration being a major cause of the need for transplant (Ghosheh, Cremona et al. 2008). The majority of corneal transplantation recipients are >60 years old. Hence, discovering the driving force behind spontaneous loss of CE cells with aging is critically important.

Aging-related changes of CE cells include progressive polymegathism (increased cell size to compensate for the loss of cell number), pleomorphism (variability in cell morphology), decreased ability to pump fluid from the corneal stroma, and increased permeability attenuating their function as a barrier (Bourne and McLaren 2004). In contrast to corneal epithelial cells and keratocytes (Hassell and Birk 2010), human CE cells have very limited proliferative potential *in*

vitro. CE cells from older donors (>50 years) have decreased proliferative capacity compared to cells from younger donors (<30 years) (Senoo and Joyce 2000). Furthermore, CE cells display numerous features of senescent cells including increased expression of the cyclin-dependent kinase inhibitors p21CIP1 and p16INK4a (Enomoto, Mimura et al. 2006), senescence-associated β -galactosidase staining (Mimura and Joyce 2006; Song, Wang et al. 2008), and decreased sensitivity to mitogenic stimulation *ex vivo* (Joyce 2005). Inhibition of p21 and p16 expression leads to increased CE proliferation *ex vivo*, demonstrating that these G1/S cell cycle inhibitors mediate replicative senescence (Joyce and Harris 2010).

It remains poorly understood why CE lacks regenerative ability. The age-related increase in senescence markers suggest that CE cells may have been exposed to endogenous stimuli that drive senescence. Senescence stimuli include critically short telomeres, DNA damage and activated oncogenes (Campisi and d'Adda di Fagagna 2007). Whereas telomeres do not appear to be a driving force behind CE senescence (Konomi & Joyce 2007), DNA damage does accumulate in CE cells as demonstrated by an increase in the presence of 8-hydroxy-2'-deoxyguanosine (8-OHdG), an endogenous oxidative DNA lesion, in corneal buttons from older donors compared to younger (Joyce, Zhu et al. 2008). Furthermore, γ H2AX foci, a marker of DNA double-strand breaks and cellular senescence, are increased in CE from older donors (Joyce, Harris et al. 2010). Endogenous genotoxins that could drive age-dependent accumulation of oxidative lesions include reactive oxygen species (Haigis and Yankner 2010), which are a by-product of oxidative phosphorylation. Because CE cells require high metabolic activity for continuous pump function, they may be exposed to greater oxidative stress than other cell types, and therefore prone to premature senescence (Joyce 2003; Joyce 2005; Mimura and Joyce 2006; Joyce, Zhu et al. 2008; Joyce, Harris et al. 2010). Exogenous sources of genotoxic stress to CE cells include the UV component of sunlight (Kolozsvari, Nogradi et al. 2002), exposure to DNA-damaging drugs during ocular procedures such as mitomycin C (MMC) (Roh, Cook et al. 2008), and free radicals generated during routine cataract surgery (Takahashi 2005).

To determine the effects of endogenous DNA damage on the CE, we characterized corneal tissues of DNA repair-deficient *Ercc1*^{-Δ} mice (Niedernhofer, Garinis et al. 2006). ERCC1-XPF is a highly conserved heterodimeric endonuclease essential in nucleotide excision repair of helix-distorting DNA lesions, interstrand crosslink repair and the repair of some double-strand breaks (Niedernhofer, Odijk et al. 2004; Ahmad, Robinson et al. 2008). Mice engineered

to express reduced levels of this nuclease display numerous symptoms and pathologies associated with advanced age and model a human progeroid syndrome (Weeda, Donker et al. 1997; Niedernhofer, Garinis et al. 2006). Using a genetic mutant defective in nuclear DNA repair allowed us to uniquely focus on the biological impact of endogenous DNA damage. This eliminates variables such as protein, membrane, lipid and mitochondrial damage, which confound experiments that employ using electrophilic genotoxins in normal hosts.

In this study we used a combination of imaging and histology to identify significant differences between CE of adult (4.5-6 mth-old) *Ercc1*^{-Δ} and normal littermate mice. Remarkably, many of the observed changes in *Ercc1*^{-Δ} mice were also observed in old (24-34 mth-old) normal mouse CE. These results provide direct experimental evidence that failure to repair endogenous DNA damage can drive aging and degeneration of the CE.

3.2 MATERIALS AND METHODS

Mice

Ercc1^{-Δ} were bred in an f1 background by crossing inbred mice heterozygous for each mutant allele in a C57Bl/6J and FVB/n genetic background. This prevents strain-specific pathology yet allows analysis of genetically identical mutant animals. Mice were given a unique identifier by ear punch. Genomic DNA was isolated from ear tissue using NucleoSpin 96 Tissue (Macherey-Nagel) and the genotype determined by PCR as previously described (Ahmad, Robinson et al. 2008). Wild-type (WT) littermates were used as young normal controls. Old WT mice were either in the same genetic background or purchased from NIA (f1 C57Bl/6; CJH, 34 mth-old males). Animal husbandry and experimental procedures were approved by the University of Pittsburgh IACUC.

Spectral Domain Optical Coherence Tomography (SD-OCT) Imaging

Mice were anesthetized with an intraperitoneal injection of ketamine (Ketaject, Phoenix Pharmaceuticals, St. Joseph, MI; 80 mg/kg) and xylazine (Xyla-ject, Phoenix Pharmaceuticals, St. Joseph, MI; 5 mg/kg) and imaged as previously described (Gabriele, Ishikawa et al. 2010). Pupils were dilated using Tropicamide (1%; Falcon Pharmaceuticals, Fort Worth, TX). A

custom contact lens was applied to the cornea to aid in focusing for retinal images. Mice were secured on a custom stage for imaging of the cornea and retina/optic nerve head. Volumetric images were acquired in both eyes (1.5x1.5x2.0 mm scans, 250x250 A-scans, 1024 pixels in depth, 4 repeated A-scans) at each location (Biotigen, Inc, Durham, NC).

Gross Imaging

Gross photos of mouse eyes were taken with a Leica MZFLIII high-resolution stereo fluorescence biomicroscope (Leica Microsystems Inc., Bannockburn, IL). Mice were anesthetized, as described above and immobilized with a three-point stereotactic mouse restrainer. Each whole cornea was focused, and images were obtained at a magnification of 25X.

Corneal Endothelial Confocal Imaging

Imaging of mouse central CE was accomplished by corneal confocal microscopy (Confoscan3; Nidek Technologies America, New Orleans, LA). Mice were sacrificed by CO₂ inhalation followed by cervical dislocation and immediately immobilized on a custom secure platform. A 40X objective optically coupled to the cornea with transparent gel (Viscotears; Novartis Ophthalmics, Duluth, GA) was focused onto the CE surface. The software (NAVIS; Lucent Technologies, Murray Hill, NJ) captured images from the CE through the corneal epithelium every 1.6 μm and stored them as an image stack for analysis of corneal thickness. Image stacks were inspected individually to determine the stromal-endothelium and stromal-epithelium transitions. Central thickness of the stroma was determined by counting the number of images from the epithelial peak scatter to endothelial peak scatter × 1.6 μm as previously described (Du, Carlson et al. 2009). Manual cell counting and area determination were performed with ImageJ (National Institutes of Health; <http://rsb.info.nih.gov/ij/>). Statistical analyses were carried out by ANOVA with Prism Graph Pad software (Prism; Graph Pad Software, San Diego).

Histology and Immunohistochemistry

Mouse eyes were enucleated using fine forceps. For paraffin sections, whole globes were injected with 2% paraformaldehyde (PFA) (Electron Microscopy Sciences, Hatfield, PA) and immersed in 2% PFA at 4°C until processing. Eyes were processed and embedded in paraffin wax. Eight μm thick serial sections were used for analysis. For corneal wholemount staining,

similar fixation was performed for 48 hours at 4°C in 2% PFA and then corneas were dissected from the globes. The corneas were rinsed in PBS, and stored at 4°C in 50% glycerol and 50% PBS (v/v) until further processing. For wholemount CD45 staining, corneas were washed in PBS and incubated in anti-mouse CD16/CD32 Fc γ III/II (BD Pharmingen, San Jose, CA) at 1:100 for 30 minutes to block nonspecific binding. Anti-mouse CD45-FITC (BD) was added at 1:100 and incubated overnight at 4°C. After multiple washes with PBS, phalloidin-546 (Invitrogen) was added at 1:50 together with 4',6-diamidino-2-phenylindole (DAPI) (0.5 μ g/ml) (Roche Molecular Biochemicals, Indianapolis, IN) and then incubated for 1 hour at room temperature. For ZO-1 staining, tissue was blocked in 10% heat-inactivated goat serum for 1 hour at RT followed by overnight incubation with anti-mouse ZO-1 (Invitrogen). Secondary antibody Alexa Fluor 488-conjugated goat anti-mouse (1:2,500) (Invitrogen-Molecular Probes, Eugene, OR) together with DAPI was added for 1 hour at RT. Omission of the primary antibody served as a negative control. The stained wholemounts were placed in aqueous mounting medium (Thermo Fisher Scientific, Pittsburgh, PA) on coverslip-bottom dishes and examined using an Olympus FluoView FV1000 confocal microscope (Olympus, Tokyo, Japan).

Scanning Electron Microscopy

Excised corneas were fixed overnight in 2.5% glutaraldehyde in PBS at 4°C. Corneas were washed three times in PBS, post-fixed for 1 hour in aqueous 1% osmium tetroxide, and then washed three times in PBS. Corneas were dehydrated through a graded ethanol series (30-100%), further dehydrated by three additional 15 minute washes with absolute ethanol. Next, the corneas were washed in heximethyldisilazane (HMDS) for 15 minutes and then removed to air dry. Corneas were then mounted onto aluminum stubs, grounded with silver paint, and sputter coated with 3.5 nm gold/paladium (Cressington Sputter Coater Auto 108, Cressington, Watford, UK). Images were taken using a JEOL JSM-6335F scanning electron microscope (Peabody, MA) at 3 kV.

Transmission Electron Microscopy and Descemet's Membrane Thickness

Corneas were fixed in cold 2.5% glutaraldehyde (Taab Chemical) in 0.1 M PBS (Fisher), pH 7.3. The corneas were rinsed in PBS, post-fixed in 1% osmium tetroxide (Electron Microscopy Sciences) with 0.1% potassium ferricyanide (Fisher), dehydrated through a graded series of

ethanol (30% - 90% - Reagent Alcohol, Fisher, and 100% - Ethanol 200 Proof, Pharmco) and embedded in Epon (Dodecenyl Succinic Anhydride, Nadic Methyl Anhydride, Scipoxy 812 Resin and Dimethylaminomethyl, Energy Beam Sciences). Using only central corneal regions, semi-thin (300 nm) sections were cut on a Reichart Ultracut, stained with 0.5% Toluidine Blue (Toluidine Blue O and Sodium Borate, Fisher) and examined under the light microscope. Ultrathin sections (65 nm) were stained with 2% uranyl acetate (Uranyl Acetate dihydrate, Electron Microscopy Sciences, and methanol, Fisher) and Reynold's lead citrate (Lead Nitrate, Sodium Citrate and Sodium Hydroxide, Fisher) and examined on Jeol 1011 transmission electron microscope. >10 measurements of DM thickness per image were made from multiple images at 5,000X magnification using ImageJ software. Averages and standard deviations were calculated from 4 WT mice (7 eyes total) and 5 hypomorphs (9 eyes total) and compared using Student's t-test with a $p < 0.05$ significance.

TUNEL Assay

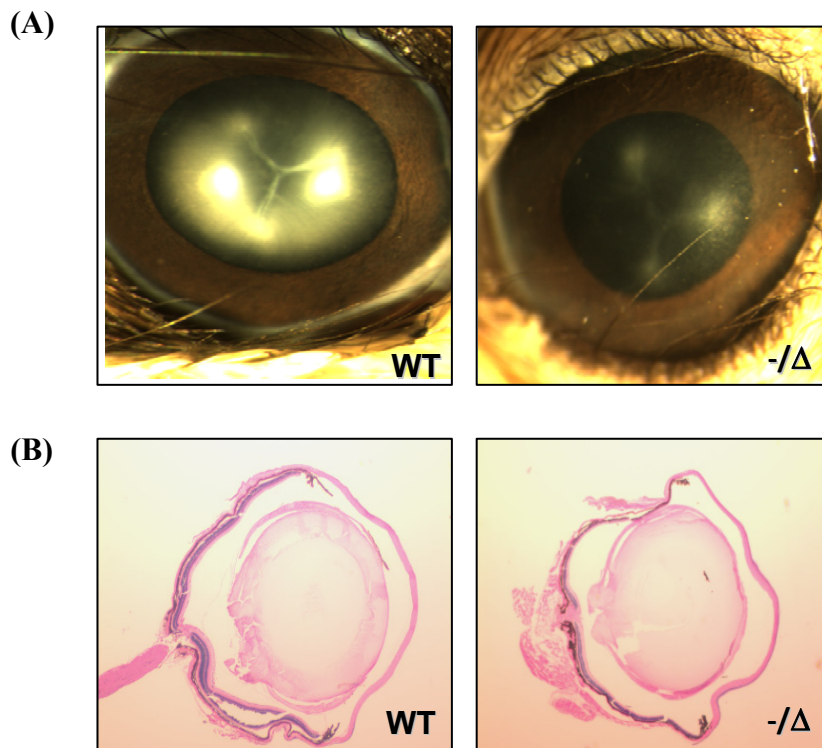
Paraffin sections were processed for TUNEL staining per the manufacturer's protocol (Roche, Indianapolis, IN). Briefly, sections were permeabilized in freshly prepared 0.1% Triton X-100 and 0.1% sodium citrate then rinsed in PBS. TUNEL reaction mixture (enzyme and buffer) was added to sections which were allowed to incubate for 60 minutes at 37°C in a humidified atmosphere in the dark. The negative control included no enzyme treatment and the positive control included DNase treatment prior to TUNEL staining. Sections were analyzed by fluorescence microscopy using 488 nm excitation.

3.3 RESULTS

3.3.1 *Ercc1*^{-Δ} mice have normal eye development

Ercc1^{-Δ} develop normally, but after reaching sexual maturation (at 8 wks of age) begin to display symptoms associated with aging, including dystonia, ataxia, loss of muscle mass,

kyphosis and ultimately incontinence (Gregg, Robinson et al. 2011). By this age, in contrast to age-matched controls, the *Ercc1*^{-Δ} mice have already developed tissue-specific degeneration and pathology similar to natural aging (Vo, Seo et al. 2010; Goss, Stolz et al. 2011; Gregg, Robinson et al. 2011). We did not detect any ocular developmental or structural defects in *Ercc1*^{-Δ} mice based on gross morphology (Fig. 3.1.A), histology (Fig. 3.1.B), or *in vivo* SD-OCT imaging of the anterior segment and retina/optic nerve head (Fig. 3.1.C). Images of gross morphology demonstrated normal orbits, fully developed iris with symmetric pupils and clear margins, normal conjunctival tissue, and non-vascularized corneas (Fig. 3.1.A). Anesthesia-induced cataracts occurred in both *Ercc1*^{-Δ} and age-matched WT mice as previously reported (Gabriele, Ishikawa et al. 2010), making it difficult to evaluate differences in lens transparency between animals (Fig. 3.1.A). Histological sections revealed the presence of apparently normal ciliary body, lens, retina, and optic nerve structures in *Ercc1*^{-Δ} mice (Fig. 3.1.B). These observations support the conclusion that the DNA repair-deficient mice undergo normal ocular development. Therefore any cellular differences observed between the eyes of WT and age-matched *Ercc1*^{-Δ} mice are likely the result of post-natal degenerative processes.



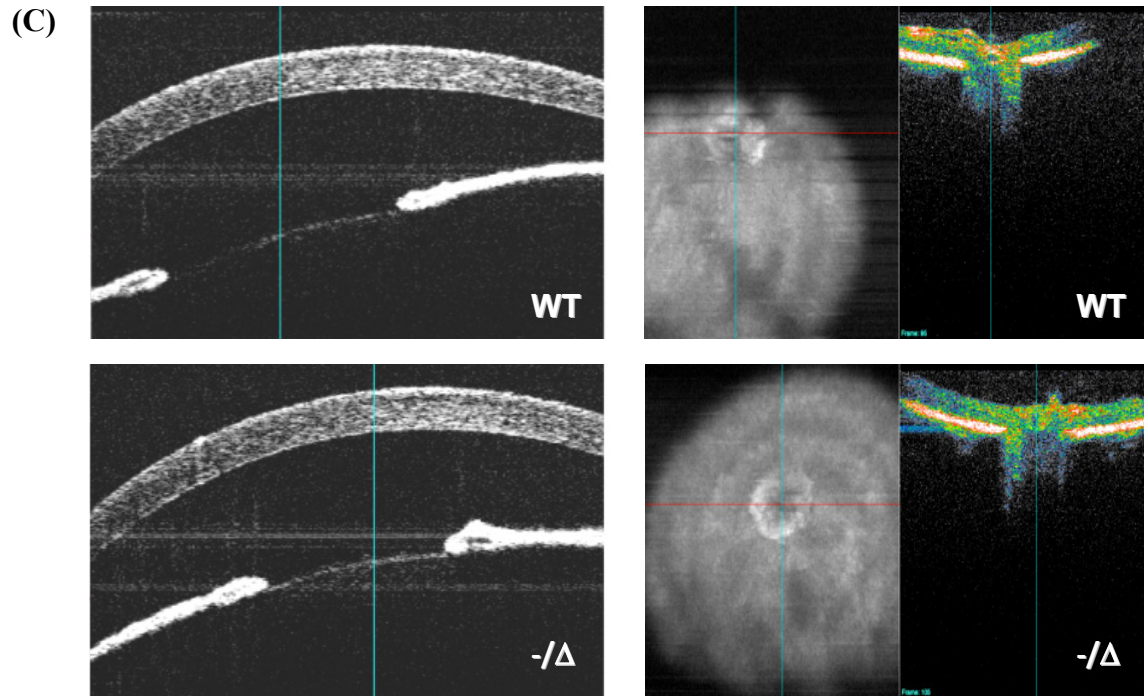


Figure 3.1: Ocular developmental and eye structure is normal in progeroid *Ercc1*^{-Δ} mice.
 (A) Representative images of eyes from age-matched WT and *Ercc1*^{-Δ} mice illustrating normal development of ocular structures in the mutant animals. (B) H&E sections of the entire globe from WT and *Ercc1*^{-Δ} mice. (C) In vivo SD-OCT of the anterior segment (top) and retina/optic nerve head (bottom) from WT and *Ercc1*^{-Δ} mice.

3.3.2 Dystrophic changes in CE from *Ercc1*^{-Δ} and naturally old WT mice.

To examine the morphology of the CE layer, we used confocal microscopy and corneal wholemount staining. Normal adult mice exhibited uniform CE cell shape and size (Fig. 3.2.A, left image). In contrast, *Ercc1*^{-Δ} mice displayed dystrophic changes including severe polymorphism and polymegathism (Fig. 3.2.A, middle image). These dystrophic changes were similar to the changes observed in the old WT mice (Fig. 3.2.A, right image). Polymorphism and polymegathism were also observed by corneal wholemount immunostaining (Fig. 3.2.B) using antibodies to ZO-1 to highlight cell-cell junctions and DAPI to stain nuclei. Large

polyploid, binuclear CE cells were also observed in *Ercc1*^{-Δ} mice and old WT animals, but not young WT adults (Fig. 3.2.C).

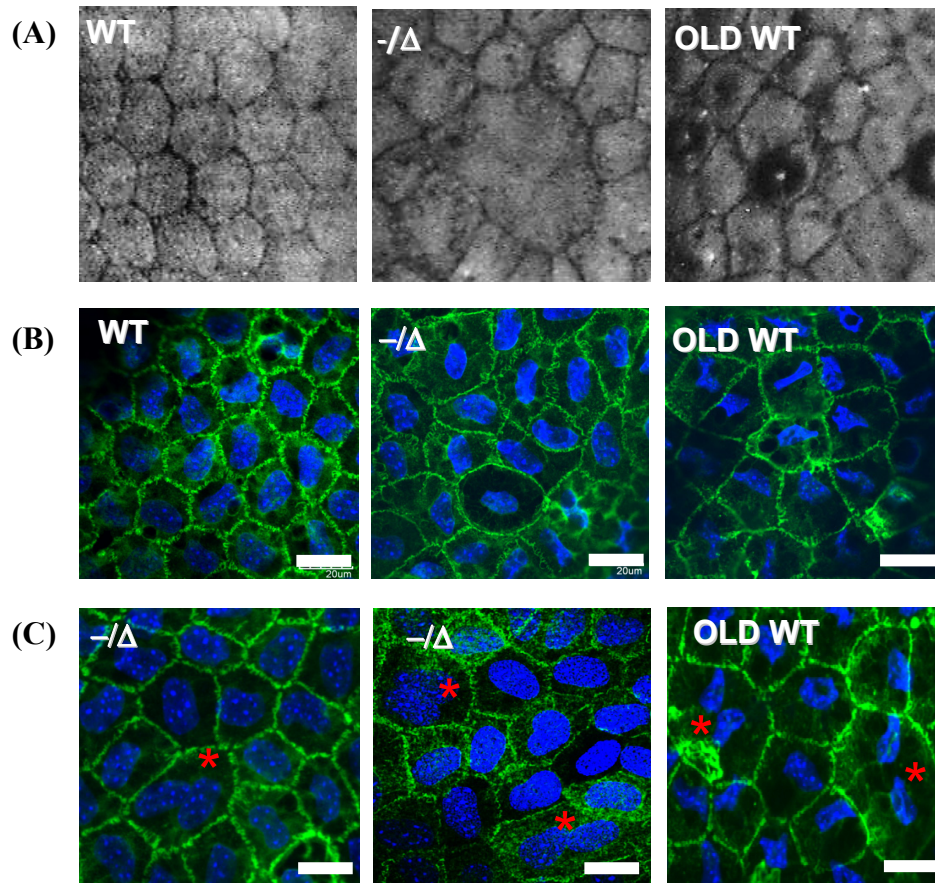


Figure 3.2: Premature onset of aging-related dystrophic changes in *Ercc1*^{-Δ} mouse CE. (A) Confocal microscopy images of the CE from a 6 mth-old WT mouse, 6 mth-old *Ercc1*^{-Δ} mouse and an old WT mouse (24 mth). (B) Wholemount immunostaining of the same specimens with ZO-1 (green) to highlight cell junctions and DAPI (blue) nuclei. Scale bars = 20 μm. (C) Representative images with large polyploid binuclear cells (red asterisk) in mutant and aged animals. Scale bars = 20 μm.

3.3.3 Decreased cell density with normal overall corneal thickness in *Ercc1*^{-Δ} and naturally old WT mice

Aging-related CE polymorphism and polymegathism indicate compensation for cell loss in the CE cell layer (Bourne and McLaren 2004). To determine if this was the case in the *Ercc1*^{-Δ} mice, we used images generated by corneal confocal microscopy to measure CE cell density and size in *Ercc1*^{-Δ}, WT littermates, and old WT mice. The CE cell density is significantly lower in *Ercc1*^{-Δ} mice compared to WT littermate controls (Fig. 3.3.A). Similarly, *Ercc1*^{-Δ} mice

had significantly increased mean cell size (Fig. 3.3.B). Changes similar to the *Ercc1*^{-Δ} mice were found in old WT mice, compared to young WT animals (Figs. 3.3.A,B). This is consistent with prior studies on aged WT C57BL/6 mice (Jun, Chakravarti et al. 2006). The dystrophic changes and decreased cell density, however, did not appear to affect overall central corneal thickness measured by SD-OCT (Fig. 3.3.C) or central stromal thickness measured by confocal microscopy (Fig. 3.3.D), as there were no significant differences between progeroid *Ercc1*^{-Δ} mice, their young-adult WT littermates or old WT mice.

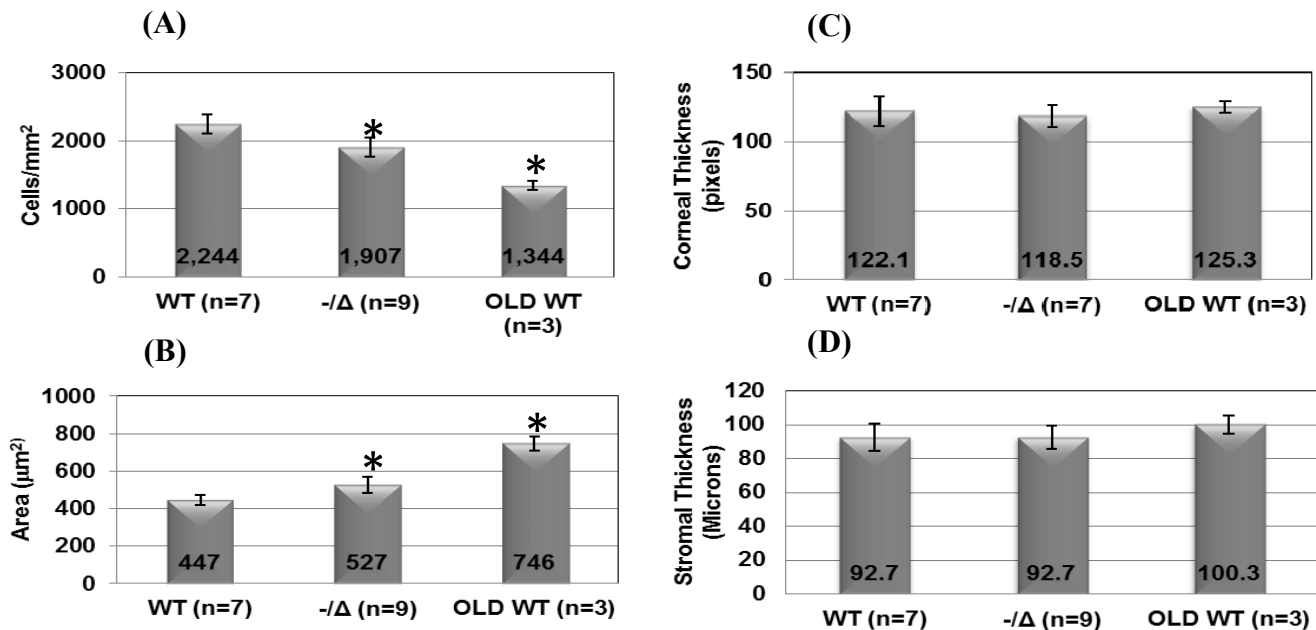
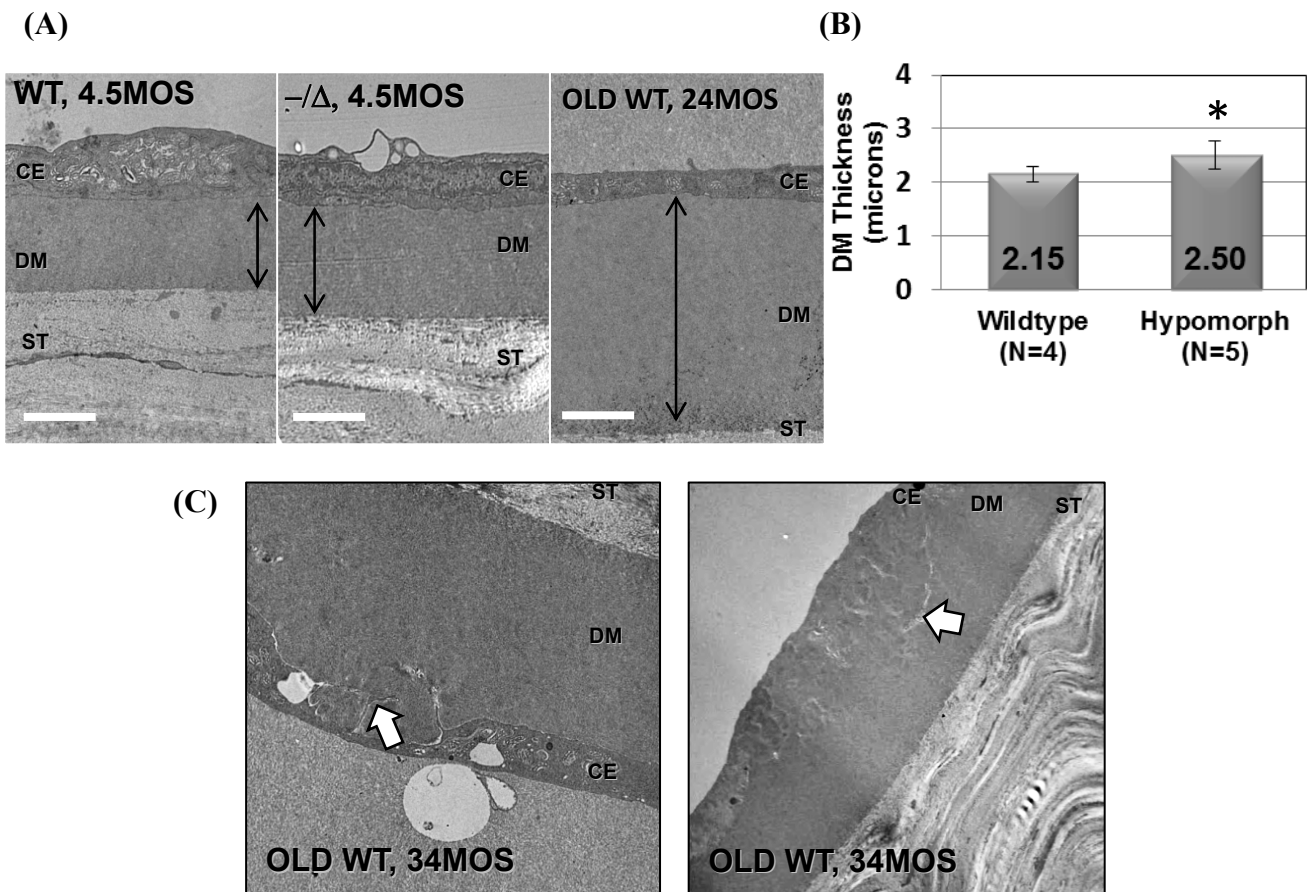


Figure 3.3: Loss of cell density in *Ercc1*^{-Δ} mouse CE. (A-B) Quantitative image analysis of confocal images used to calculate (A) cell density (cells/mm²) and (B) cell area (μm²) of 4.5-6 mth-old *Ercc1*^{-Δ} mice, normal littermate (WT), and old WT mice (34 mths of age). Error bars represent the standard deviation from analysis of 2 images (left and right eyes) from the indicated number of mice (n). An asterisk indicates significant difference relative to adult WT (p<0.05 for both ANOVA, Dunnett's). (C) Thickness of central corneas measured (in arbitrary pixels) from *in vivo* SD-OCT imaging. (D) Central corneal stromal thickness (μm) measured from confocal images.

3.3.4 Increased Descemet's membrane thickness and abnormal posterior banded collagen in *Ercc1*^{-Δ} mice.

Descemet's membrane (DM) is continuously secreted by CE cells throughout life and increased DM thickness is observed in aging humans (Johnson, Bourne et al. 1982) and mice (Jun, Chakravarti et al. 2006). Ultrastructurally, DM is comprised of an anterior banded zone

(ABZ) secreted during early development and a posterior non-banded zone (PNBZ) that accounts for age-dependent DM thickening. In certain disease states affecting the CE, banded collagen, believed to be Type VIII, can be observed in the PNBZ (Levy, Moss et al. 1996; Zhang, Bell et al. 2006). We prepared TEM sections from central cornea to measure central DM thickness and observe changes in DM. In *Ercc1*^{-Δ} mice, the DM thickness was significantly increased compared to WT littermates (Fig. 3.4.A,B). The DM was also thicker in old mice (Fig. 3.4.A, right image) as previously reported (Jun, Chakravarti et al. 2006). Interestingly, we also identified focal areas of DM defects in 34 mth-old WT mice (Fig. 3.4.C, white arrows). These DM defects were not observed in either the *Ercc1*^{-Δ} mice or WT littermates. A closer examination of DM from *Ercc1*^{-Δ} mice revealed areas of increased banded collagen (Fig. 3.4.E, white arrows) compared to WT littermates (Fig. 3.4.D, white arrows). Notably, this banded collagen was located posteriorly (closest to the cell layer) in the *Ercc1*^{-Δ} mice indicating more recent synthesis in contrast to the WT mice with more anteriorly located banded collagen, as has been previously reported (Jun, Chakravarti et al. 2006).



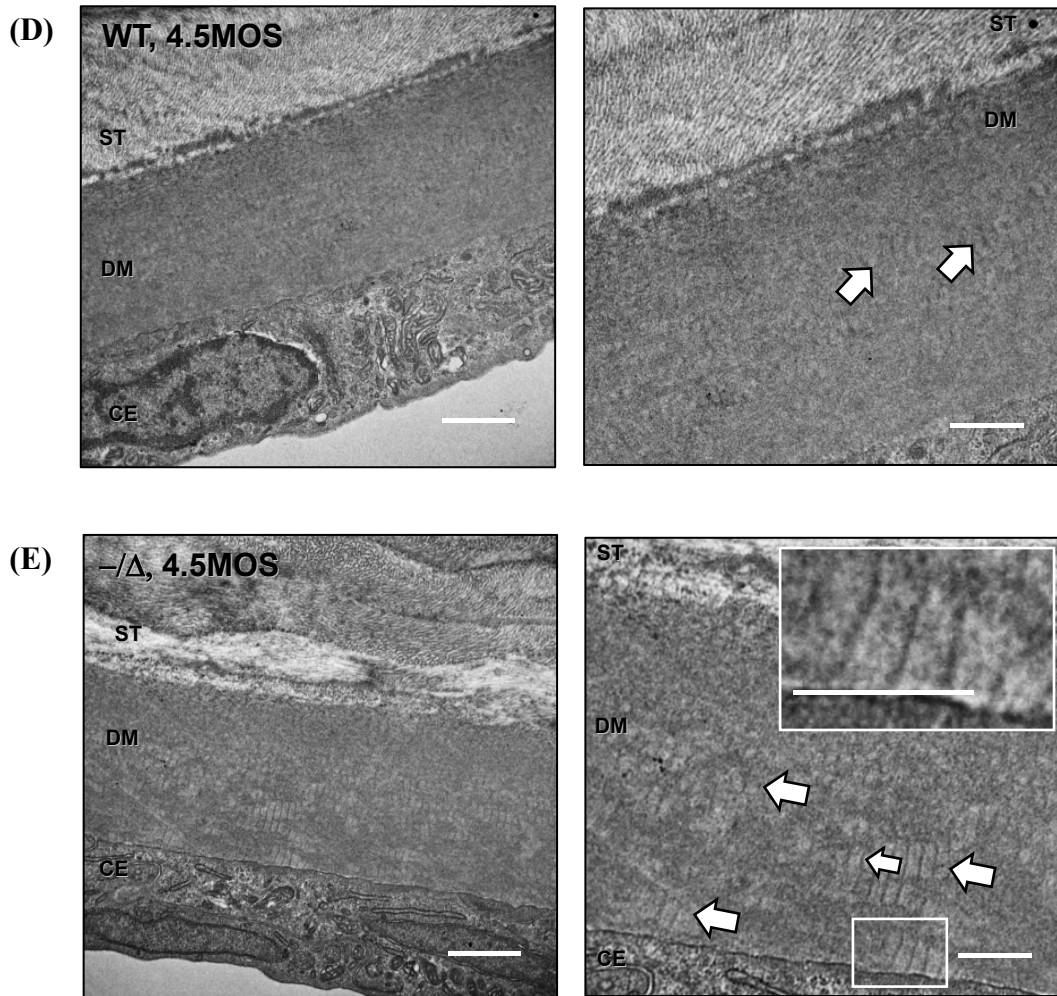


Figure 3.4: Premature thickening and abnormal deposition of Descemet's membrane in *Ercc1*^{-Δ} mice. (A) Representative TEM images displaying thickness of Descemet's membrane (DM) in WT (left), *Ercc1*^{-Δ} (center) at 4.5 mths of age, and old WT at 24 mths (right). The orientation from top to bottom is CE cell (CE), Descemet's membrane (DM, black arrow), posterior stroma (ST). Magnification = 10,000X. Scale bar = 2μm. (B) Graph shows average thickness±SD from central DM as measured from 4 WT mice (7 eyes total) and 5 *Ercc1*^{-Δ} mice (9 eyes total). Asterisk indicates statistically significant difference (Student's t-test, p<0.05). (C) DM defects in 34 mth old WT mice. Arrows indicate regions of abnormal DM. (D-E) Representative TEM images displaying collagen banding of Descemet's membrane (DM) in (D) WT and (E) *Ercc1*^{-Δ} mice at 4.5 mths of age. The orientation from top to bottom is stroma (ST), Descemet's membrane (DM), CE cell (CE). White arrows indicate areas of banded collagen. Scale bars indicate 1 μm in left images and 500 nm in right images. Inset in right image of *Ercc1*^{-Δ} mice (E) shows magnified area of interest (white box) and scale bar at 500 nm.

3.3.5 Presence of posterior projections arising from CE of *Ercc1*^{-Δ} mice.

Confocal image z-stacks were used to generate 3D corneal reconstructions. Figure 3.5.A demonstrates the presence of numerous heterogeneous lesions above the surface of the CE

monolayer in *Ercc1*^{-Δ} mice but not in their age-matched WT littermates. The lesions resemble corneal guttae, and were also observed in old WT CE. These posterior projections had variable size, shape, and reflectivity. The 3D reconstructions revealed that many of the projections in *Ercc1*^{-Δ} mice originated from the CE layer and projected into the anterior chamber (Fig. 3.5.B). However, we did not observe focal excrescences arising directly from Descemet's membrane in our Periodic acid-Schiff (PAS) stained paraffin (Supplemental Fig. S.1) or TEM sections (Fig. 3.3) of *Ercc1*^{-Δ} mice. Thus, the posterior projections in *Ercc1*^{-Δ} mice are most likely of cellular origin.

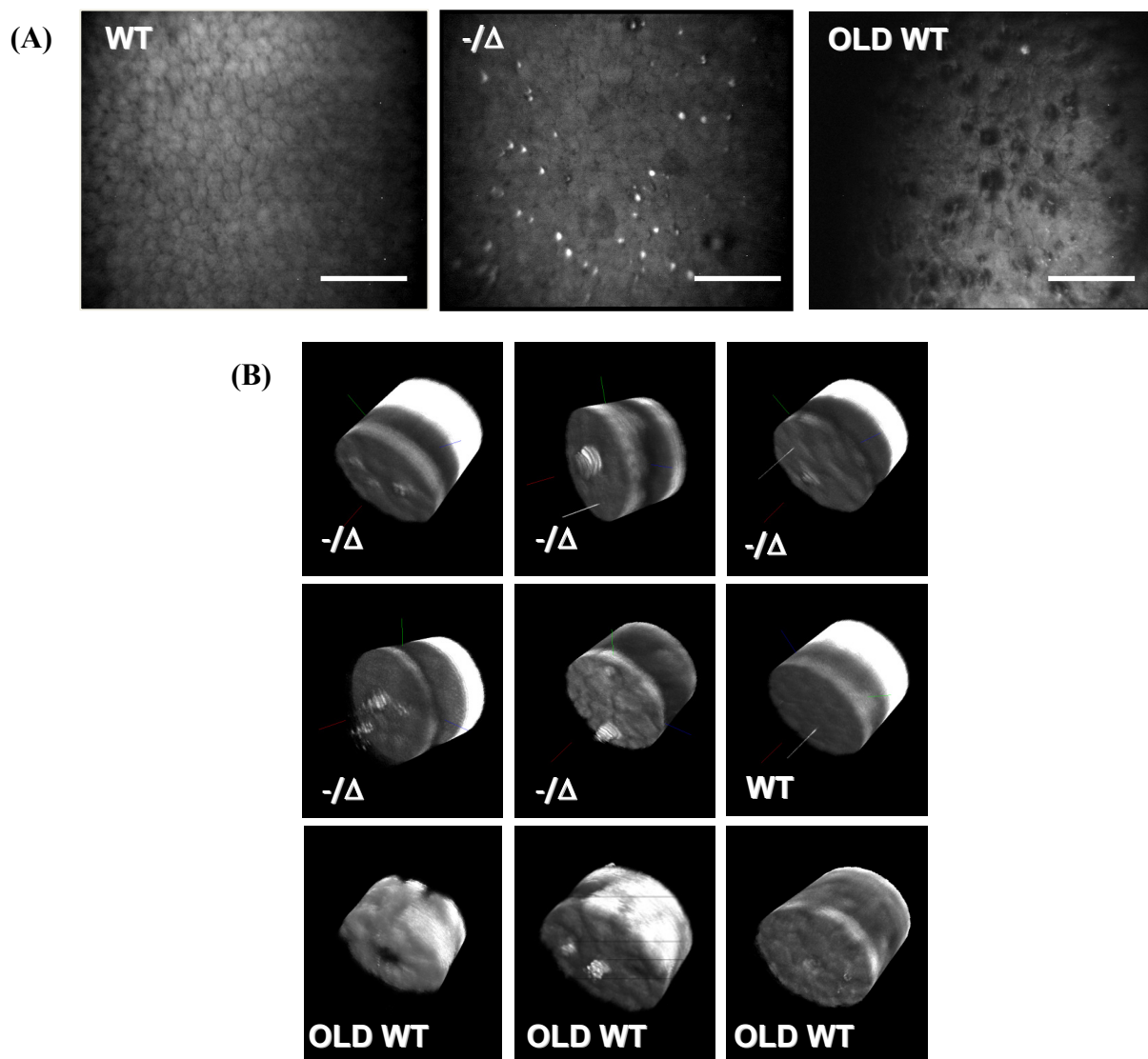


Figure 3.5: Premature onset of posterior projections originating from *Ercc1*^Δ CE. (A) Representative confocal images of CE from adult WT (left, 6 mths; far right, 34 mths), and *Ercc1*^Δ (middle, 4.5 mths) mice. Scale bar = 100 μm. (B) 3D reconstructions of corneas with the CE surface (facing left side of image) from the same mice.

3.3.6 Presence of CD45⁺ cells on *Ercc1*^{-Δ} mice CE.

The heterogeneous nature of the posterior projections (Fig. 3.5) in *Ercc1*^{-Δ} CE indicated the possibility that other cells interact with CE cells such as keratic precipitates (Guthoff, Zhivov et al. 2009). We observed occasional leukocytes in proximity to CE in histological sections of *Ercc1*^{-Δ} mouse corneas (Fig. 3.6.A), which were not found in their WT littermates. Wholemout immunostaining using CD45 as a general marker of leukocytes confirmed the presence of immune cells attached to the CE cell surface (Fig. 3.6.B). These CD45-positive cells were of various sizes and projected from the CE monolayer into the anterior chamber (Fig. 3.6.B, bottom image projection). Although not specific for cell type, SEM showed the presence of potential immune cells interacting with *Ercc1*^{-Δ} CE cells (Fig. 3.6.C).

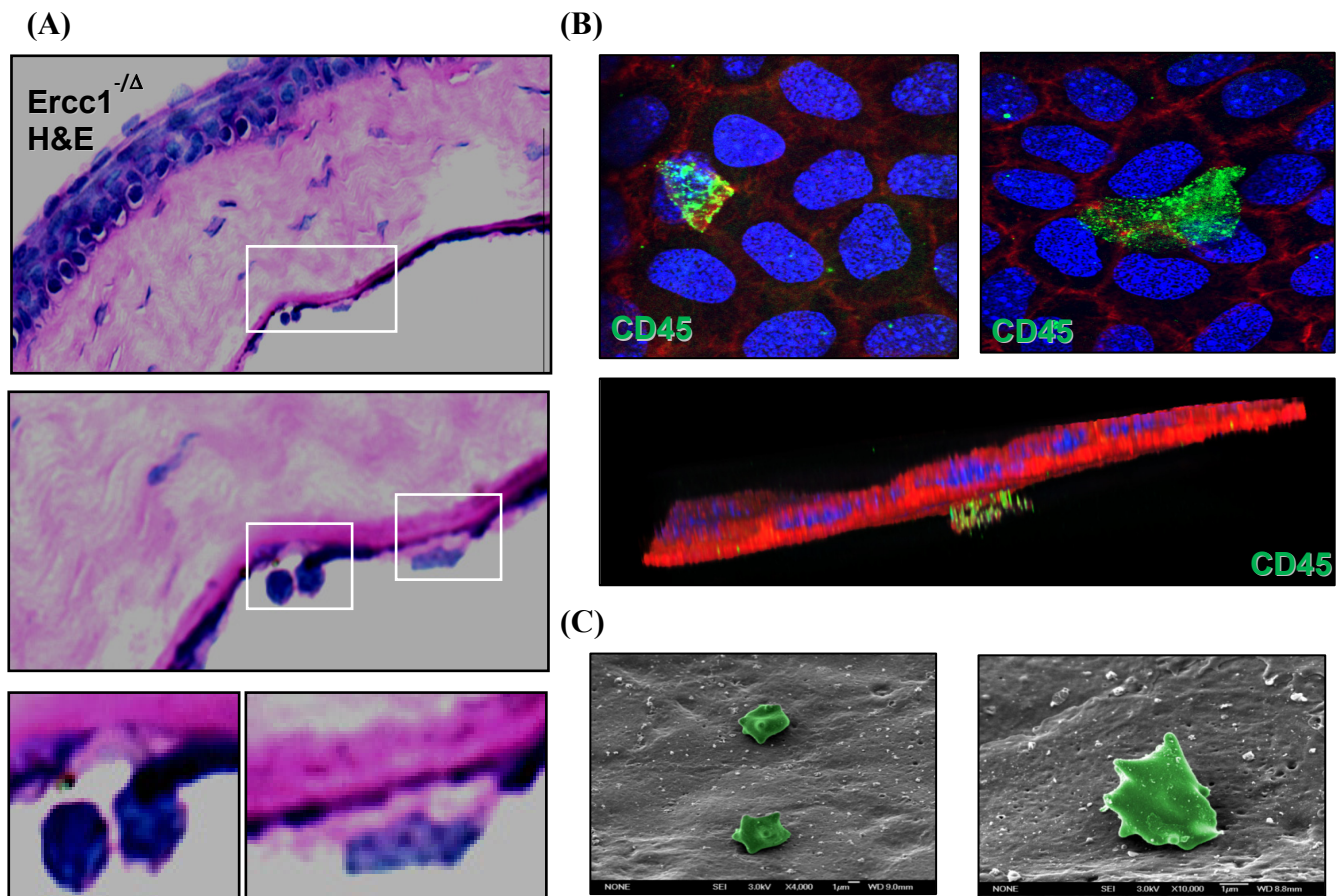


Figure 3.6: Inflammatory cells interact with *Ercc1*^{-Δ} mice CE. (A) H&E sections of *Ercc1*^{-Δ} mice CE revealing immune cells interacting with the CE. (B) Wholemout sections stained for CD45 (green) to detect leukocytes, phalloidin (red) and DAPI (blue). (C) Representative SEM image of the immune cells (pseudocolored green) interacting with CE from *Ercc1*^{-Δ} mice.

3.3.7 CE cells are lost by apoptosis in *Ercc1*^{-Δ} mice.

To probe the mechanism by which CE cells are lost in *Ercc1*^{-Δ} mice, we performed TUNEL staining of the CE layer. TUNEL staining of the CE layer confirmed the presence of apoptotic cells in *Ercc1*^{-Δ} mice but not WT littermates (Fig. 3.7.C). Immunostaining of wholemount sections for actin (Fig. 3.7.A) and histological sections (Fig. 3.7.B) revealed apoptotic cell extrusion, which is a process that removes dying cells from monolayers while maintaining barrier function (Rosenblatt, Raff et al. 2001). SEM captured the presence of a late-stage extruded apoptotic CE cell in the vicinity of a putative leukocyte (Fig. 3.7.D).

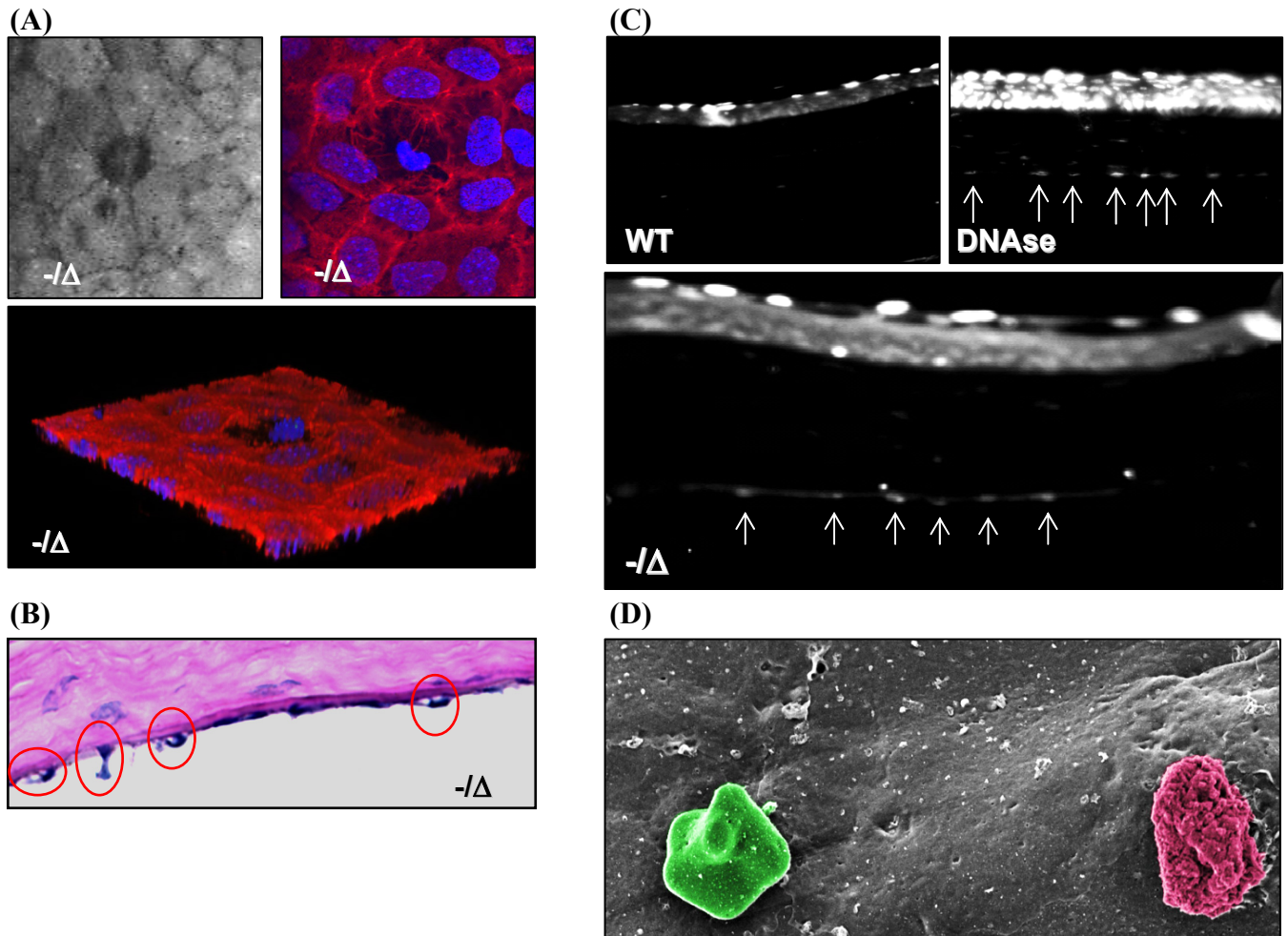


Figure 3.7: Apoptosis of CE in *Ercc1*^{-Δ} mice. (A) Representative confocal image (upper left) of the CE from an *Ercc1*^{-Δ} mouse showing a cell being extruded. Wholemount staining (upper right) with phalloidin (red) and DAPI (blue). Reconstruction from z-stack of images (lower panel). (B) H&E section demonstrating extruding CE cells. (C) TUNEL assay on paraffin sections. The right image is a positive control using DNase pre-treatment. WT demonstrates some superficial squamous epithelial cell apoptosis. The bottom image is cornea from *Ercc1*^{-Δ} mice. The arrows indicate TUNEL-positive cells. (D) SEM of extruding CE cell (pseudocolored red) and putative interacting immune cell (pseudocolored green).

3.4 DISCUSSION

In this study we demonstrated aging-related dystrophic changes in CE from DNA repair-deficient *Ercc1*^{-Δ} mice. Remarkably, 4.5-6 mth-old *Ercc1*^{-Δ} mice spontaneously developed degenerative changes typically seen in 2-3 yr-old WT mice. The prominent parallels between the *Ercc1*^{-Δ} and old WT mouse CE are increased polymorphism and polymegathism, polyploidy, decreased cell density, increased Descemet's thickness, and the presence of posterior projections that are most likely apoptotic CE cells and/or interacting leukocytes. This reflects a 4-6X acceleration of the appearance of aging-related changes in the CE due to DNA repair deficiency.

Many of the dystrophic changes seen in the *Ercc1*^{-Δ} and old WT mouse CE signify compensatory responses to cellular damage and loss and are also observed in human CE as a consequence of aging, trauma, disease or surgery (Bourne and McLaren 2004). For example, to accommodate for increasing cell loss, the remaining CE cells flatten, increase in size, and alter their morphology to cover the acellular area. The polyploid binuclear cells observed in young adult *Ercc1*^{-Δ} and old WT mice are also increased in aged and wounded human CE (Ikebe, Takamatsu et al. 1986). Increased polyploidy is positively correlated with exposure to cellular stress, senescence, and aging and is frequently observed in cells of liver, heart, and vascular tissues (Storchova and Pellman 2004). Increased DM thickness and changes in matrix composition are observed in disease states affecting the CE such as diabetes (Rehany, Ishii et al. 2000), Fuchs' corneal endothelial dystrophy (Levy, Moss et al. 1996; Zhang, Bell et al. 2006), and iridocorneal endothelial syndrome (Levy, McCartney et al. 1995).

An intriguing finding in our study was the presence of the "guttae-like" posterior projections in *Ercc1*^{-Δ} mice. Although these projections resembled guttae seen in Fuchs' corneal endothelial dystrophy, considered a premature aging disease of the CE (Bergmanson, Sheldon et al. 1999), we did not find any histological evidence that they were excrescences originating from Descemet's membrane. Wholemout staining further distinguished our projections from corneal guttae. Although we observed increased Descemet's thickness in *Ercc1*^{-Δ} mice, focal areas of extracellular matrix-based guttae, as were seen in 34 mth-old WT mice, were not detected in the progeroid mutant mice. The posterior projections in the *Ercc1*^{-Δ} mice appear instead to be apoptotic cells extruding from the CE monolayer or occasional CD45-positive leukocytes on the

surface of the CE. Interestingly, there were no histopathological signs of acute or chronic inflammation throughout the *Ercc1*^{-Δ} mouse corneal layers. Thus we hypothesize that senescence-associated secretory phenotype (SASP), which is driven by the accumulation of persistent DNA damage (Rodier, Coppe et al. 2009), is responsible for leukocyte accumulation. This process may facilitate the removal of damaged and apoptotic CE cells.

ERCC1-XPF deficient mice and humans display accelerated aging of numerous tissues including the skin, liver, kidney, brain, spinal cord, peripheral nerves, bone, and the hematopoietic system (McWhir, Selfridge et al. 1993; Weeda, Donker et al. 1997; Niedernhofer, Garinis et al. 2006; Lawrence, Sacco et al. 2008; Vo, Seo et al. 2010). Because ERCC1-XPF is an essential nuclease involved in numerous DNA repair pathways, a single DNA lesion driving tissue degeneration and premature aging has not been definitely identified. Deficiency in the nucleotide excision repair (NER) pathway alone does not lead to accelerated aging because NER-deficient *Xpa*^{-/-} mice display normal life span and do not display early onset of aging-related symptoms or pathologies (Dolle, Busuttill et al. 2006; Niedernhofer, Garinis et al. 2006; Grillari, Katinger et al. 2007). Thus, it has been hypothesized that DNA interstrand crosslinks, which are extremely cytotoxic and for which ERCC1-XPF is required for repair (Niedernhofer, Odijk et al. 2004), are the primary lesions that drive the premature aging observed in ERCC1-deficient mice and potentially contribute to normal aging (Weeda, Donker et al. 1997; Dolle, Busuttill et al. 2006; Niedernhofer, Garinis et al. 2006; Grillari, Katinger et al. 2007). Endogenous ICLs may arise as downstream byproducts of chronic oxidative stress and lipid peroxidation, which, for example, enhances the formation of malondialdehyde, a potent DNA crosslinking agent (Niedernhofer, Daniels et al. 2003; Grillari, Katinger et al. 2007). ICLs in CE may also be due to exogenous exposures to genotoxins such as the use of mitomycin C used during refractive procedures. Similar to the findings here, we established that therapeutic doses of mitomycin C rapidly induce DNA lesions (Roh, Cook et al. 2008).

Evidence from the current study supports a mechanism in which unrepaired nuclear DNA damage leads to CE cell death via apoptosis. This loss of cells in the CE monolayer, in turn drives the changes in CE cell morphology. Furthermore, the notion that DNA damage is driving force for these pathological changes is consistent with the elevated expression of senescence markers in CE cells from aged donors (Mimura and Joyce 2006; Joyce, Zhu et al. 2008; Song, Wang et al. 2008).

Fuchs' endothelial dystrophy is an idiopathic primary degenerative disease of the CE. Like aging-related degenerative changes, there is growing evidence for oxidative stress and oxidative DNA damage in both the nuclear and mitochondrial genomes of CE cells driving this degenerative disease (Jurkunas, Bitar et al. 2010). While the genetic components of Fuchs' dystrophy are currently under investigation, it will also be important to determine the stimuli and downstream cellular mechanisms (i.e. oxidative stress and apoptotic mechanisms) that propel CE degeneration in Fuchs' dystrophy.

In summary, our study provides strong genetic evidence that the CE is sensitive to unrepaired endogenous DNA damage. With this information future targeted approaches aimed at protecting, preventing, or reversing the effects of DNA damage may help to preserve or even enhance CE integrity. In addition, the study establishes that the *Ercc1*^{-Δ} mice are a rapid and accurate model system of aging-related degenerative changes of the CE for testing therapeutic strategies.

4.0 RAPID CHANGES IN CONNEXIN-43 IN RESPONSE TO GENOTOXIC STRESS STABILIZE CELL-CELL COMMUNICATION IN CORNEAL ENDOTHELIUM

Chapter 4 is adapted, with copyright permission from the Association for Research in Vision and Ophthalmology, from a published article. **Roh DS, Funderburgh JL. Rapid changes in connexin-43 in response to genotoxic stress stabilize cell-cell communication in corneal endothelium. *Invest Ophthalmol Vis Sci* 2011 Jul 15;52(8):5174-82.** Note that the figure numbers have changed, the “data not shown” are now supplemental figures found in the appendix, and section 4.3.6 and corresponding figure 4.9, and additional discussion were not included in the original manuscript.

4.1 INTRODUCTION

The corneal endothelium (CE) is a monolayer of neural crest–derived cells that is essential for corneal transparency. Located at the posterior surface of the cornea, the CE separates the cornea from the aqueous humor, relying on cell– cell junctions to control corneal hydration. The CE is a fragile cell layer that is vulnerable to the effects of intraocular surgery, systemic and ocular disease, and topical drugs (Bourne 2003; Bourne and McLaren 2004). In addition, endogenous oxidative stress appears to play a significant role in the degeneration of CE with age (Joyce, Zhu et al. 2009; Joyce, Harris et al. 2010) and in Fuchs’ dystrophy (Jurkunas, Rawe et al. 2008; Jurkunas, Bitar et al. 2010). Human CE does not regenerate in vivo, so existing cells must compensate for cell loss to maintain the pump and barrier functions required for corneal homeostasis. It is clear that surviving cells respond to CE cell loss by spreading to cover the posterior corneal surface. This spreading is associated with thinning of the cell layer (Joyce, Mekler et al. 1990) but the full range of physiological responses of the CE to cell loss has

not been characterized. CE function is dependent on the cell– cell junctions, which maintain the integrity of this monolayer. The goal of the present study was to examine how CE cells mediate these junctions in response to genotoxic stressors.

Gap junctions are intercellular channels composed primarily of the connexin family of proteins. These channels provide rapid intercellular transfer of small signaling molecules, such as nucleotides, inositol trisphosphate (IP₃), glutathione, and Ca²⁺ between connected cells (Alexander and Goldberg 2003). Such gap junction intercellular communications (GJIC) function in the maintenance of tissue homeostasis and influence cellular survival and death in response to oxidative stress (Lin, Yang et al. 2003; Ramachandran, Xie et al. 2007; Hutnik, Pocrnich et al. 2008) metabolic stress (Albright, Kuo et al. 2001; Lin, Yang et al. 2003), ischemia reperfusion injury (Nakase, Fushiki et al. 2003; Garcia-Dorado, Rodriguez-Sinovas et al. 2004), and genotoxic stress (Tekpli, Rivedal et al. ; Lin, Yang et al. 2003). Connexins may also mediate cell survival by GJIC-independent mechanisms in addition to functions associated with gap junctions (Decrock, Vinken et al. 2009).

With a half-life of 1.5 to 5 hours, connexin proteins respond rapidly to physiologic changes by altering gap junction coupling between cells. The Cx43 C-terminus contains 14 documented phosphorylation sites (Lampe and Lau 2004), and different phosphorylated species of Cx43 can be distinguished experimentally by SDS-PAGE. Aggregation of Cx43 into functional gap junction plaques, opening of the junctional pores, and Cx43 degradation have all been linked to site-specific phosphorylation of the Cx43 protein (Berthoud, Minogue et al. 2004). Given the pervasive role of connexins in maintenance of cell and tissue homeostasis, we hypothesized that exogenous genotoxic stress would alter homeostasis-regulating proteins such as Cx43 in the CE. Previously, we reported DNA damage in goat CE after brief doses of the DNA interstrand cross-linking agent mitomycin C (MMC) during procedures emulating photorefractive keratectomy (Roh, Cook et al. 2008). In this study, we identified specific changes that occur in Cx43 and in GJIC in CE as a result of genotoxic stress induced by exposures such as MMC. Determining how CE cells respond to various stressors may provide opportunities for CE protection and preservation.

4.2 MATERIALS AND METHODS

Cell culture and reagents

Primary bovine CE cells were isolated as previously described (Roh, Cook et al. 2008) and cultured in low glucose Dulbecco's modified Eagle's medium (DMEM; Invitrogen, Carlsbad, CA) supplemented with 10% fetal bovine serum and antibiotics/antimycotics in a humidified 5% CO₂, 37°C environment. Passage 1 to 4 cells, split 1:4, were used and grown 2 to 3 days past confluency for every experiment unless otherwise indicated. At least 24 hours before treatment with MMC, cycloheximide, forskolin, and epidermal growth factor (all from Sigma, Saint Louis, MO), the medium was changed to serum-free DMEM containing no antibiotics/antimycotics. MMC was added to cells by changing medium with prewarmed media containing 5 µM freshly diluted MMC. Primary bovine corneal fibroblasts were isolated and grown as previously described (Long, Roth et al. 2000).

Immunofluorescence

Cells were fixed in 3.2% paraformaldehyde (PFA) solution (Electron Microscopy Science, Hatfield, PA) in PBS for 20 minutes at room temperature. Permeabilization with 0.1% Triton X-100 (Thermo Fisher, Pittsburgh, PA) in PBS for 1 minute was followed by blocking with 10% heat-inactivated goat serum in PBS for 1 hour at room temperature. Cells were incubated with a polyclonal rabbit anti-Cx43 antibody to the C terminus (Invitrogen), monoclonal mouse anti-Cx43 to the C terminus (Millipore, Billerica, MA), or monoclonal mouse anti-zonula occludens-1 (ZO-1; Invitrogen) diluted 1:200 in 1% bovine serum albumin (BSA) in PBS solution overnight at 4°C. After multiple washes in PBS, cells were incubated for 1 hour at room temperature with species appropriate Alexa-conjugated secondary antibodies (Invitrogen) diluted to 0.8 µg/mL in 1% BSA in PBS containing 0.5 µg/mL 4',6-diamidino-2-phenylindole (DAPI; Invitrogen). Cells were observed on a laser scanning confocal microscope (Olympus Fluoview FV1000, Olympus, Center Valley, PA) and images captured and processed using Olympus Fluoview software. To quantify plaque size and intensity, ImageJ (developed by Wayne Rasband, National Institutes of Health, Bethesda, MD; available at <http://rsb.info.nih.gov/ij/index.html>) was used to manually trace Cx43 plaques in three separate

high magnification confocal images. Area and intensity values were calculated and compared with the Mann–Whitney *U* test.

Immunoblotting

Cells were lysed directly in 1X SDS sample buffer [1.6% sodium dodecyl sulfate, 0.06M Tris, 5.5% glycerol, and 0.002% bromophenol blue], scraped into tubes, heated at 95°C for 5 minutes, then sonicated until solubilized. For alkaline phosphatase treatment of cell lysates, cells were lysed in RIPA buffer (Thermo Fisher) [25 mM Tris-HCl pH 7.6, 150 mM NaCl, 1% NP-40, 1% sodium deoxycholate, 0.1% SDS] containing protease inhibitor cocktail (Sigma), sonicated, and incubated with 0.1 U/μL cell lysate of calf alkaline phosphatase (Sigma) for 1 hour at 37°C. Protein concentration was determined by Bio-Rad DC Protein Assay (Bio-Rad, Hercules, CA) and then 2-mercaptoethanol was added to a final concentration of 1% to the lysates and heated at 70°C for 20 minutes. An equal amount of protein was added to precast 4–20% gradient or 10% polyacrylamide gels (Bio-Rad) and electrophoresis was performed for 1 hour at 200 V. Protein was transferred to PVDF membrane (Millipore) and blocked for 1 hour at room temperature in 0.2 M Tris, 0.15 M NaCl, 0.01% thimeresol, 0.2% Tween-20, pH 7.4 (TTTBS) for ECL detection or with fluorescent blocker (Millipore) for Odyssey infrared imaging (LI-COR, Lincoln, NE). Membranes were incubated with the following primary antibodies as indicated: mouse anti-Cx43NT1, which recognizes the N-terminal region of Cx43 (Fred Hutchinson Cancer Center, Seattle, WA); rabbit anti-Cx43, which recognizes the C-terminal region of Cx43 (Invitrogen); mouse anti-ZO-1 (Invitrogen); and mouse anti- α -tubulin (Sigma), all diluted in 1% BSA in TTTBS or fluorescent blocker. Secondary antibodies included horseradish peroxidase (HRP)-conjugated goat anti-mouse and anti-rabbit antibodies (Santa Cruz Biotechnology, Santa Cruz, CA) for enhanced chemiluminescence (ECL) detection and IRDye800 and IRDye680 labeled secondary antibodies (LI-COR) for infrared imaging. Where indicated, blots were stripped for 15 minutes at room temperature (Restore Western Blot Stripping Buffer, Thermo Fisher Scientific, Rockford, IL). Chemiluminescent signal was visualized with ECL substrate (Millipore) followed by detection and capture of 16-bit images with a Bio-Rad FX imager (Bio-Rad), and fluorescent signal was detected with Odyssey infrared imaging system (LI-COR). Densitometry was performed using digital analysis software for ECL (Bio-Rad Quantity One) and fluorescent detection (LI-COR) followed by appropriate statistical analysis for comparisons

with GraphPad (GraphPad Software Inc., La Jolla, CA). All forms of Cx43 (phosphorylated and nonphosphorylated) were quantified in densitometry.

Immunoprecipitation

Cells were lysed directly in cold coimmunoprecipitation buffer [0.1% Nonidet P40, 25 mM Tris pH 7.4, 150 mM NaCl, 1 mM EDTA] containing HALT protease and phosphatase inhibitors (Thermo Fisher) and briefly sonicated until solubilized. Lysates were precleared with magnetic protein G beads (Millipore) for 1 hour at room temperature to remove any nonspecific binding of cell proteins to beads. The beads were discarded and then cleared lysates were incubated with 1 µg antibody per 500 µg of lysate using a rabbit polyclonal anti-Cx43 antibody (Invitrogen) overnight at 4°C. Beads were then washed multiple times with lysis buffer and heated at 95°C for 5 minutes in 1X SDS sample buffer with 2-mercaptoethanol. A magnetic rack was used to separate the beads from lysate before loading for SDS-PAGE separation. Mouse anti-ZO-1 (Invitrogen) and rabbit anti-Cx43 (Invitrogen) antibodies were used for immunoblotting.

Triton X-100 insolubility

Cells were lysed in cell lysis buffer containing 1% Triton X-100 and 1 mM EDTA with protease inhibitors (Sigma) and then chilled on ice for 30 minutes with mixing. Cell lysates were spun at 10,000 g for 30 minutes at 4°C. The soluble fraction was removed and the Triton X-100 insoluble pellet was further dissolved in 1X SDS buffer followed by sonication. Both the insoluble and soluble fractions were used for immunoblotting.

Live-cell imaging

CE cells grown on Biotech dishes (Biotech Inc., Butler, PA) to 70% to 80% confluency were transfected with 1 µg of Cx43-GFP plasmid (gift of Professor Matthias Falk, Lehigh University) using Lipofectamine 2000 (Invitrogen). This construct was previously described to have GFP at the most C-terminal end of Cx43 (Falk 2000), and 24 hours after transfection, cells expressing the Cx43-GFP fusion protein were imaged with the Nikon Eclipse TE200-E microscope (Nikon Instruments Inc., Melville, NY) on a heated stage with 5% CO₂. Images were captured using software (Metamorph, Molecular Devices, Sunnyvale, CA) every 2 minutes over a 4- to 6-hour period after treatment with MMC or medium alone. To determine internalization and degradation

frequency, Cx43–GFP assembled into cell surface plaques were identified and followed frame-by-frame exactly 24 hours after transfection. Plaques were counted if they were internalized and/or degraded by reduced fluorescent signal over a 3-hour timeframe. Comparison of the frequency of internalization/degradation events between medium and MMC-treated cells was performed using the Fisher exact test. A 2 × 2 contingency table was analyzed with GraphPad, with $P < 0.05$ being considered statistically significant.

Gap junction intercellular communication assays

Lucifer yellow (LY) dye (Sigma) scrape-load assays were performed by scraping confluent monolayers of CE cells with a sterile pipette tip in the presence of 1 mg/mL LY in warm PBS. After 2 minutes, cells were rinsed to remove LY dye solution and cells were immediately fixed in 3.2% PFA without permeabilization. Images were captured using a Nikon epifluorescent microscope. Dye transfer images were analyzed using ImageJ software by measuring the distance of dye transfer from the scrape wound at 10 different sites per image. Average distances were then analyzed with ANOVA and a post-hoc Tukey's test for multiple comparisons. $P < 0.05$ was considered statistically significant. For fluorescent recovery after photobleaching (FRAP), cells grown on 35-mm coverslip-bottom dishes were loaded with 1 μ M of Calcein-AM (Invitrogen) for 30 minutes at 37°C. Cells were allowed to recover for 1 to 2 hours then treated with 5 μ M MMC for 15 minutes. Individual cells were photobleached using a laser scanning confocal microscope (Olympus) and images of dye recovery were captured. ImageJ software was used to measure dye intensity in image stacks. Photobleached cells were normalized to control unbleached cells. Data were exported into GraphPad for exponential curve fitting and calculation of rate constants (k). Half-life of dye recovery ($t_{1/2}$) was calculated based on the formula: $t_{1/2} = \ln(2)/k$. The Student's t test was used for statistical comparison of $t_{1/2}$.

Live-cell assay for apoptosis (*not included in original publication*)

Cells were plated at equal density and grown to confluency in 24-well plates. Twelve hours prior to imaging medium was switched to serum- and antibiotic/antimycotic-free medium. Cells were loaded with 5 μ M caspase 3/7 detection reagent (CellEvent Caspase 3/7, Invitrogen) and then treated with 50 μ M MMC, 10 μ M AGA, or medium. This dye is non-fluorescent until a DEVD peptide sequence is cleaved by activated caspase 3/7. Then the dye binds DNA producing

a fluorogenic response indicative of apoptosis. Live-cell images were captured over a 18 hour period with the Nikon Eclipse TE200-E microscope on a heated stage with 5% CO₂. Images were captured using software (Metamorph, Molecular Devices) every hour using FITC excitation/emission filters. The number of caspase 3/7-positive cells, as indicated by nuclear fluorescence, was automatically counted in Metamorph and the mean of three individual wells was plotted over time.

4.3 RESULTS

4.3.1 Genotoxic stress to CE generates rapid changes in the Cx43 abundance and localization.

We previously reported the rapid induction of DNA lesions after brief exposure to low levels of MMC in CE cells (Roh, Cook et al. 2008). Within a similar timeframe, low dose MMC exposure induced an increase in total cellular Cx43 levels as detected by immunoblotting (Fig. 4.1.A). Increases occurred in each of the three characteristic protein bands representative of differentially phosphorylated Cx43 species present in most eukaryotic cells. The phenomenon was highly repeatable, with total cellular Cx43 increasing somewhat more than twofold 60 to 90 minutes after treatment. These results were confirmed using two Cx43 antibodies targeting different regions of Cx43, the C-terminal (Fig. 4.1.A, top) and the N-terminal (Fig. 4.1.A, bottom). The use of antibodies targeting different regions of the protein reduces the possibility that the observed quantitative changes result from epitope masking. Alkaline phosphatase (AP) treatment of whole cell lysates before electrophoresis dephosphorylates Cx43 collapsing the characteristic multiple bands into a single faster moving band (Fig. 4.1.B). The rapid and transient increase in Cx43 was maintained after AP treatment, indicating that total levels of Cx43, independent of phosphorylation state, occurred. A similar transient increase in cellular Cx43 was observed after exposure to other genotoxic agents, including ultraviolet-C radiation, etoposide, and hydrogen peroxide (Supplemental Fig. S.2)

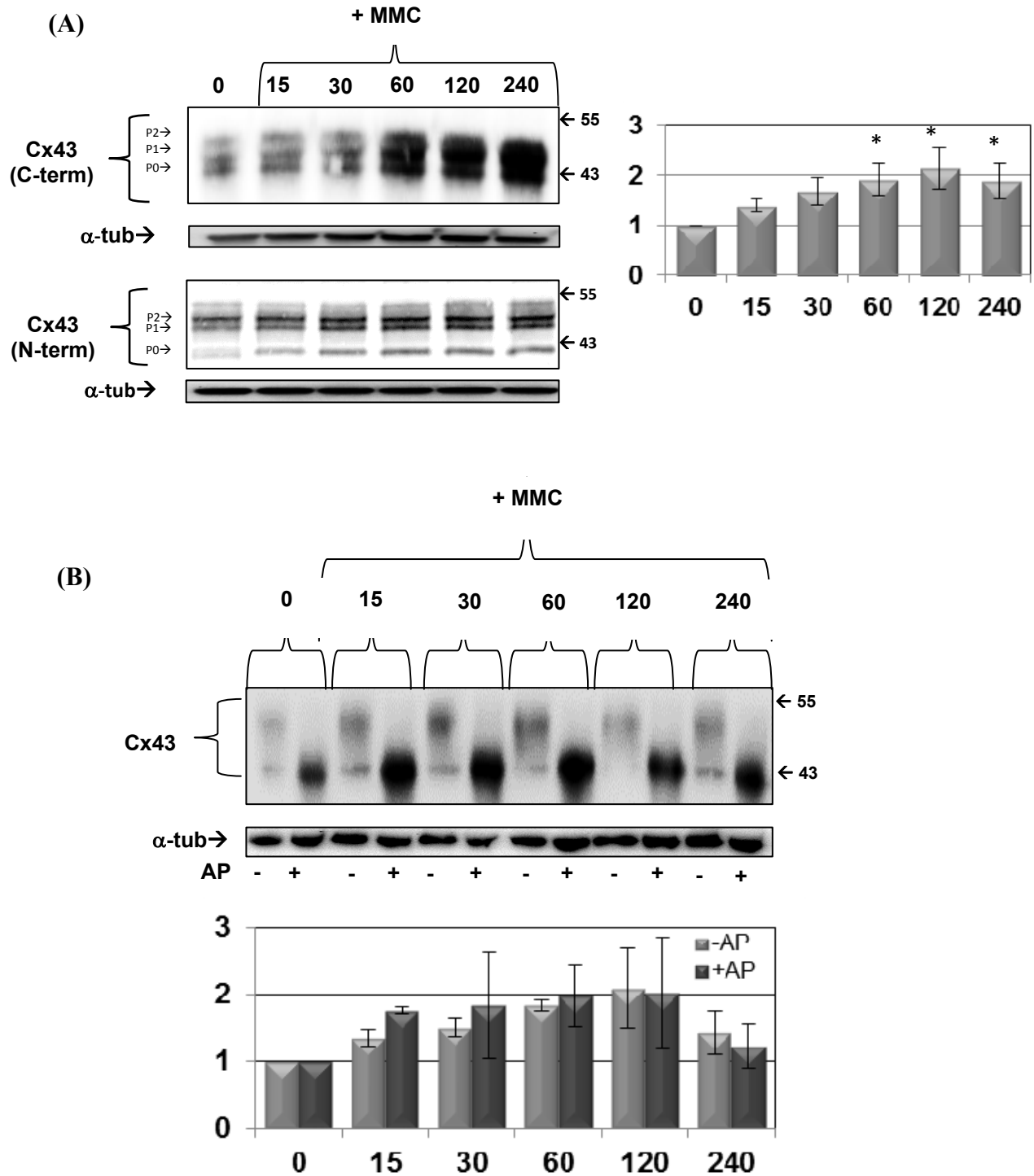
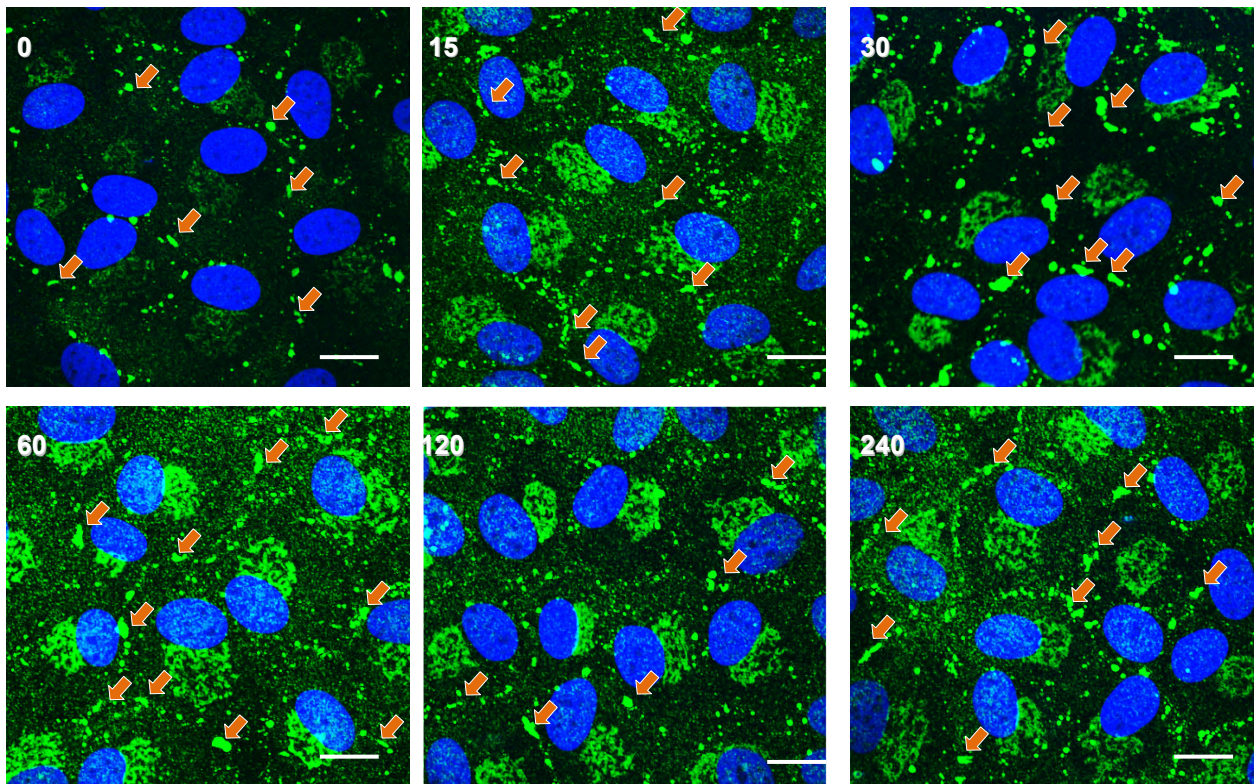


Figure 4.1: Rapid accumulation of Cx43 protein in response to genotoxic stress with mitomycin C. Cells were treated with prewarmed media containing 5 μ M MMC for indicated times in minutes. (A) Western blot for total Cx43 using C-terminal antibody (top) and N-terminal antibody (bottom) from independent experiments. Blots were stripped and reprobbed for α -tubulin as a loading control. Quantification to right is ratio of Cx43/ α -tubulin normalized to values at the “0” timepoint. Asterisks indicate statistically significant differences from time “0” (ANOVA, $p < 0.05$; Dunnett’s multiple comparison test, $p < 0.05$). Blots are representative of eight independent experiments and the mean fold change \pm SEM is shown in the graph. (B) Alkaline phosphatase (AP) treatments of cell lysates were followed by immunoblotting. Quantification in graph below is the ratio of Cx43/ α -tubulin normalized to “0” for either AP- or AP+. Differences between “-AP” and “+AP” at each time point were not statistically significant (2-way ANOVA, $p > 0.05$). Blot is representative of three independent experiments and the mean fold change \pm SEM is shown in the graph.

Immunostaining of CE cells (Fig. 4.2.A) revealed increased Cx43 at cell– cell interfaces, with an increased size of the punctate staining in this locale suggestive of increased accumulation of Cx43 in gap junction plaques. Staining also increased in perinuclear regions of the treated cells, suggesting recently synthesized Cx43 in transit to the cell surface to be increased as well. Cell fractionation of the treated cells found increased Cx43 largely in the Triton X-100 detergent-insoluble fraction (Fig. 4.2.C). Association with gap junction plaques confers detergent insolubility on connexin (Musil and Goodenough 1991); therefore, increases in insoluble Cx43 in response to MMC is consistent with immunostaining results, suggesting that MMC induces transport of the increased Cx43 into cell– cell junctional plaques. Similar changes were not observed in other cell– cell junction proteins, such as ZO-1, cadherin, and β -catenin, based on immunoblotting (Supplemental Fig. S.3)

(A)



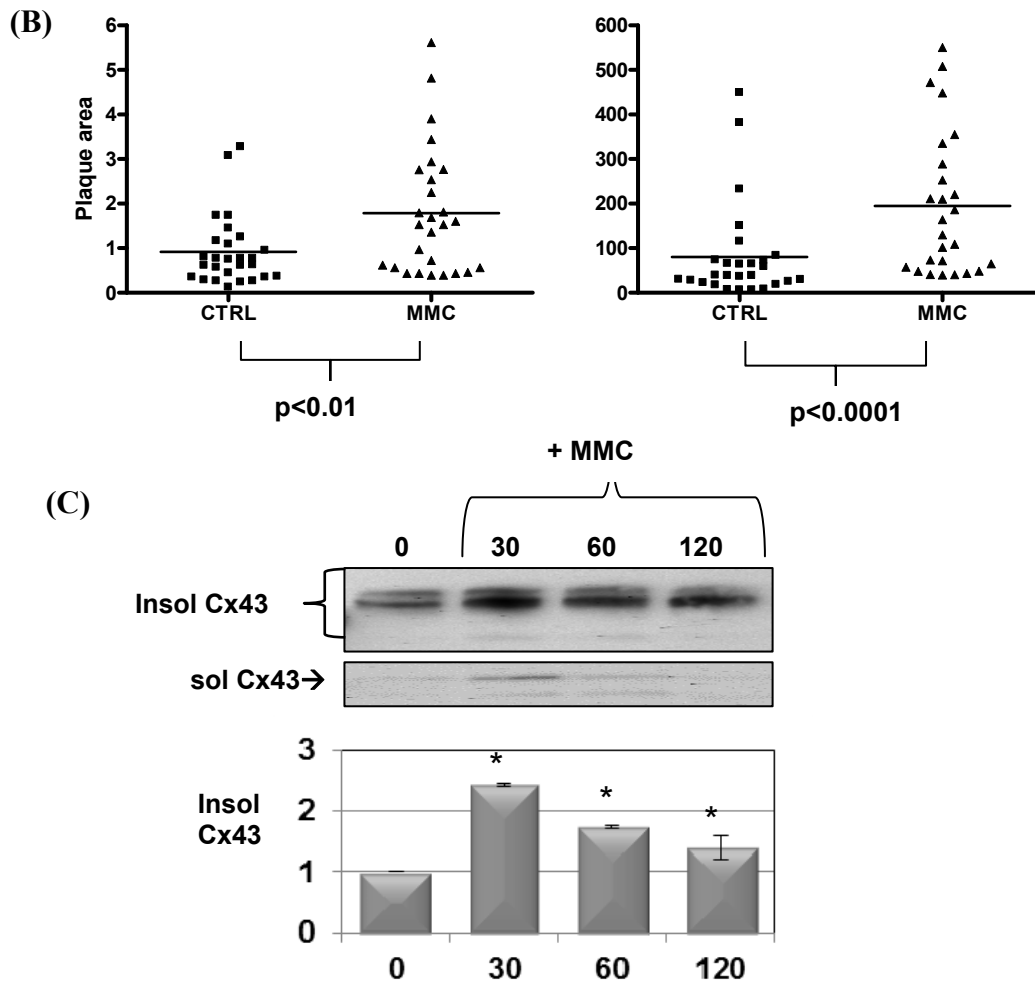


Figure 4.2: Changes in Cx43 gap junction plaque size and intensity after genotoxic stress. (A) Cells were treated with prewarmed media containing 5 μ M MMC for the indicated time in minutes then stained for Cx43 (green). DAPI (nuclei). Orange arrows indicate apparent gap junction plaques. (B) Gap junction plaques were imaged by confocal microscopy and analyzed for area μ m² and Cx43 fluorescence intensity (arbitrary units) after 60 minutes of 5 μ M MMC (n = 25 plaques) or medium alone (n = 25 plaques). Individual data points are shown along with the median. Area and intensity distributions were compared for statistically significant differences using the Mann–Whitney *U* test (area, $P < 0.01$; intensity, $P < 0.0001$). Similar results were obtained in three independent experiments. (C) Western blot for 1% Triton X-100 soluble and insoluble Cx43. Quantification below is insoluble Cx43 normalized to “0.” Asterisks indicate statistically significant differences from time “0” (ANOVA, $P < 0.05$; Dunnett’s multiple comparison test, $P < 0.05$). Results are representative of three independent experiments and the mean fold change \pm SEM is shown in the graph. Scale bar: (A) 20 μ m.

Quantitative image analysis of cells treated with MMC confirmed a significant increase in both the gap junction plaque area and Cx43 signal intensity compared to medium alone (Fig. 4.2.B) after 60 minutes of treatment with MMC. Previous studies have shown that interactions between Cx43 and the tight junction protein ZO-1 can regulate the size of Cx43 gap junctions. (Giepmans and Moolenaar 1998; Hunter, Jourdan et al. 2003; Hunter, Barker et al. 2005; Rhett, Jourdan et al. 2011) . To explore the potential involvement of ZO-1, we used

coimmunoprecipitation (Co-IP) and colocalization to examine changes in Cx43:ZO-1 association after MMC treatment. Co-IP revealed a relative decrease in the abundance of ZO-1 immunoprecipitating with Cx43 after 60 minutes of MMC treatment (Fig. 4.3.A). This alteration was also evident in images staining for ZO-1 and Cx43 (Fig. 4.3.B). Large Cx43 gap junction plaques displaying reduced ZO-1 co-localization occasionally were evident in untreated cells (Fig. 4.3.B), however these were present with significantly higher frequency in MMC-treated cells.

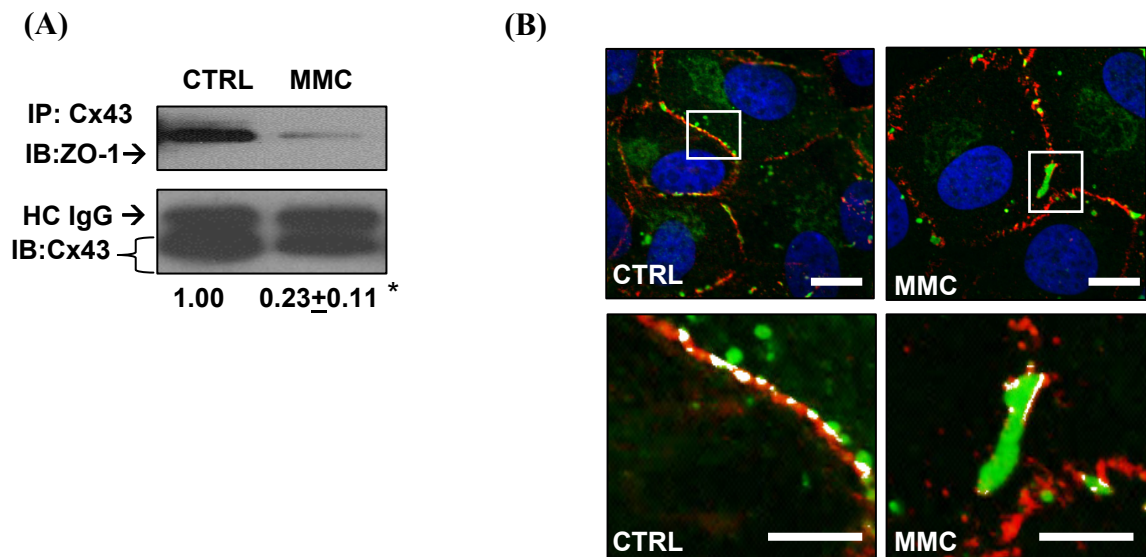


Figure 4.3: MMC induces alteration in Cx43 association with ZO-1. Cells were treated with prewarmed media containing 5 μ M MMC for 60 minutes or media alone (CTRL). **(A)** Coimmunoprecipitation with a rabbit polyclonal anti-Cx43 was performed followed by immunoblotting with mouse monoclonal anti-ZO-1. The blot was stripped and reprobed for Cx43. Quantification below is the ratio of ZO-1:Cx43, which is normalized to “CTRL.” Denatured heavy chain immunoglobulin G (IgG) is indicated as HC IgG. *Asterisks* indicate a statistically significant difference (Student’s *t*-test, $P < 0.001$). Results are representative of three independent experiments and mean fold change to “CTRL” \pm SEM is shown below. **(B)** Representative confocal images of a large gap junction plaque after MMC treatment. In the higher magnification inset (below), the areas of Cx43:ZO-1 colocalization are highlighted in white. Cx43 (green), ZO-1 (red), DAPI (blue). Scale bar, 10 μ m.

4.3.2 MMC treatment increases Cx43 stability.

Connexin protein half-life ranges from 1.5 to 5 hours in many cell types and organ systems (Musil, Cunningham et al. 1990; Beardslee, Laing et al. 1998). Treatment of cultured

CE with 10 $\mu\text{g}/\text{ml}$ cycloheximide (CHX) to inhibit protein synthesis was used to examine decay rates of Cx43. Treatment of cultured CE with 10 $\mu\text{g}/\text{mL}$ cycloheximide (CHX) to inhibit protein synthesis was used to examine decay rates of Cx43. In the untreated control, the half-life of decay was in the expected range of 1 to 2 hours (Fig. 4.4.A, left). Treatment with MMC, however, stabilized the Cx43, delaying degradation for up to 120 minutes (Fig. 4.4.A, right). After this period of stability, however, the decay rate returned to one similar to that of untreated cells.

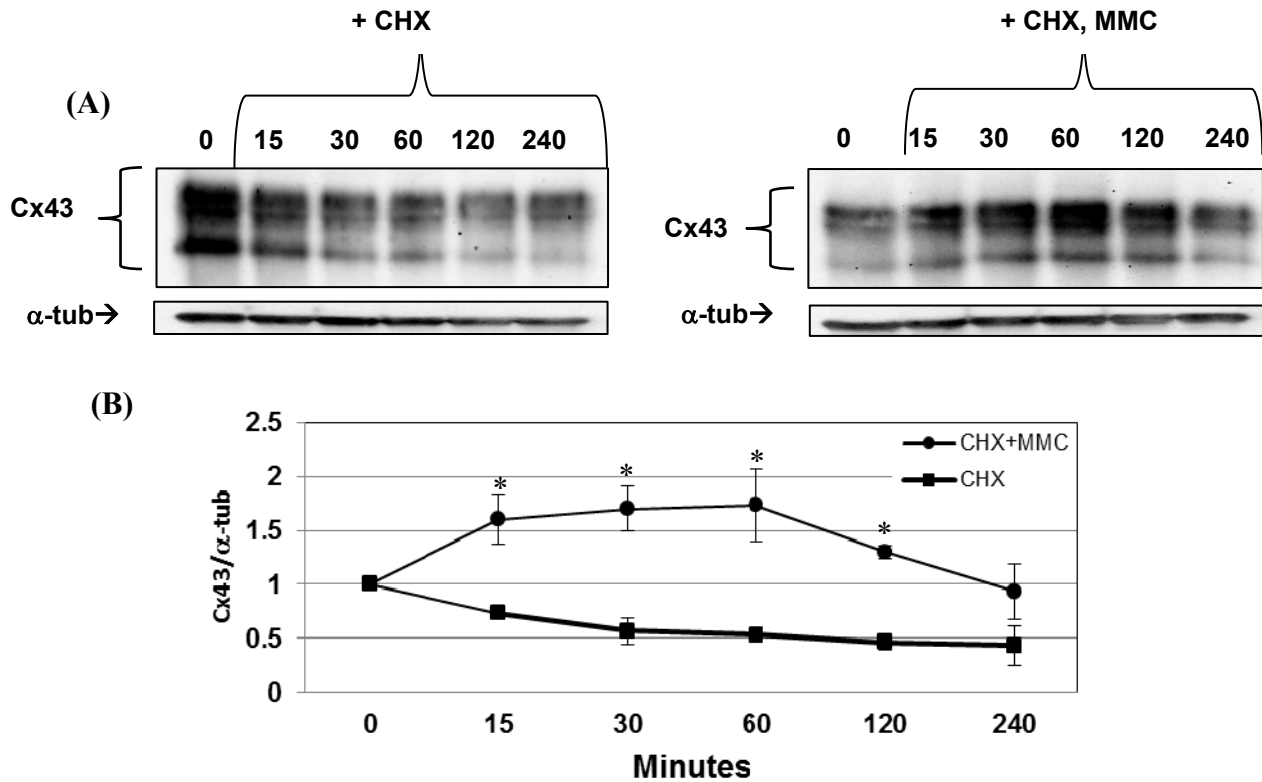
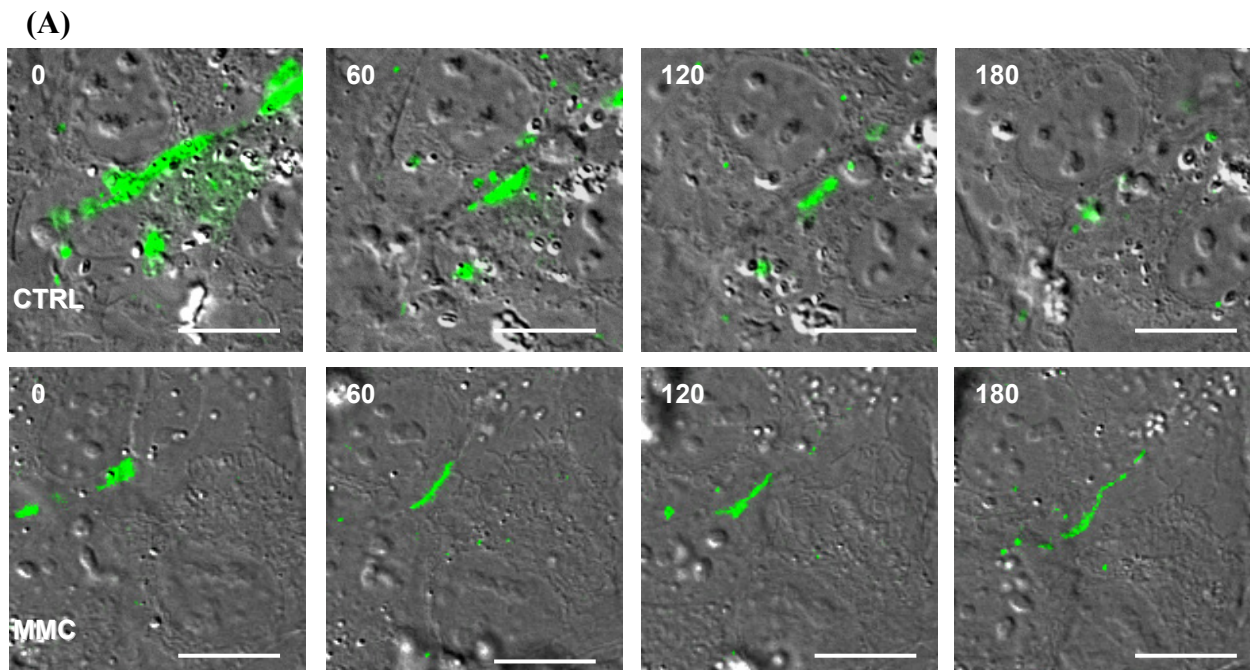


Figure 4.4: The stability of preexisting Cx43 is altered after MMC treatment. Cells were treated with prewarmed media containing 10 $\mu\text{g}/\text{mL}$ CHX with or without 5 μM MMC for indicated times in minutes. Blot shows total Cx43 using a C-terminal-specific antibody. Blots were stripped and reprobbed for α -tubulin as a loading control. Quantification below is ratio of Cx43/ α -tubulin normalized to the zero time (0) for “CHX” or “CHX + MMC.” *Asterisks* indicate statistically significant differences between “CHX” and “CHX + MMC” (2-way ANOVA, $P < 0.01$; Bonferroni multiple comparisons, $P < 0.05$). Results are representative of three independent experiments and mean fold change \pm SEM is shown in the graph.

4.3.3 Gap junction internalization is decreased after MMC treatment.

Degradation of Cx43 present in cell surface plaques occurs via processes involving the internalization of small and/or large endocytic double-membrane vesicles (Segretain and Falk 2004; Piehl, Lehmann et al. 2007; Falk, Baker et al. 2009). These processes can be followed directly by micrography using fluorescently tagged Cx43 (Falk 2000; Lauf, Giepmans et al. 2002; Falk, Baker et al. 2009). We examined this internalization and degradation of Cx43 after MMC treatment by live-cell imaging of CE that had been transiently transfected with a Cx43–GFP fusion protein (Hunter, Jourdan et al. 2003; Hunter, Barker et al. 2005). Figure 4.5 shows a series of images from live-cell video micrography after Cx43–GFP in MMC-treated cells or medium-only controls. Sixty-three individual plaques were identified and followed in the videos starting 24 hours after transfection at the time of MMC treatment. The presence or absence of each of these was scored 3 hours later to assess the relative stability of the plaque-associated Cx43 under the two conditions (Fig. 4.5.A). In medium-treated control transfected cells, 40 of 46 (89.6%) disappeared after 3 hours, whereas in the MMC-treated samples, only 8 of 17 (52.9%) of the plaques had been internalized and vanished (Fig. 4.5.B). This significant ($P < 0.01$) difference in plaque stability suggests that the reduced degradation of Cx43 identified in Fig 4.4 relates to alterations in the mechanism by which cells endocytose and degrade the gap junction plaques.



(B)

	INTERN/DEGRADE	NO CHANGE	% DEGRADED
CTRL	40	6	86.9
MMC	9	8	52.9
TOTAL	49	14	(p<0.01)

Figure 4.5: Genotoxic stress results in reduced internalization of Cx43 plaques. Seventy percent to 80% confluent cells were transfected with a Cx43–GFP plasmid. (A) Twenty-four hours after transfection, cells were treated with either medium (“CTRL,” upper figures) or medium with 5 μ M MMC (“MMC,” lower figures) and live-cell imaging was performed. Images were captured every 2 minutes over a 4- to 6-hour period after treatment. Images are stills of Cx43–GFP plaques over time in minutes. “CTRL” images illustrate an example of internalized and degraded plaques. MMC images illustrate a long-lived plaque. (B) To determine internalization and degradation frequency, Cx43–GFP assembled into cell surface plaques were identified and followed frame-by-frame exactly 24 hours after transfection. Plaques were counted if they were internalized and/or degraded by reduced fluorescent signal over a 3-hour timeframe. Statistical comparison of the frequency of internalization/degradation events between medium “CTRL” and MMC treated cells was performed using Fisher’s exact test, $P < 0.01$. Results are from two independent live-cell experiments tracking a combined 63 plaques (46 CTRLs, 17 MMCs). Scale bar: (A) 20 μ m.

4.3.4 Genotoxic stress increases forward trafficking of Cx43 into gap junctions.

To distinguish MMC effects in the formation of new membrane-associated Cx43 from its effects on Cx43 internalization/degradation, we examined transfer of Cx43 from the endoplasmic reticulum (ER) compartment to the cell surface after an 8-hour block with brefeldin A (BFA). BFA has been used in previous studies to investigate gap junction assembly because of its reversible inhibition of vesicle transport from the ER to the Golgi and subsequently to the cell surface (Laird, Castillo et al. 1995; Lauf, Giepmans et al. 2002). When BFA is removed, the transport of proteins is restored and the accumulation of proteins at the cell surface becomes briefly representative of the rate at which this forward trafficking process is occurring. Therefore, gap junction formation can be assessed after BFA removal. As shown in Fig 4.6, BFA treatment significantly reduced Cx43 at the cell surface (Fig. 4.6.A, BFA). After BFA washout and a 2-hour recovery, Cx43 appeared at the cell surface in gap junction plaques and in the perinuclear compartment in both control and MMC-treated cells (Fig 4.6.A, BFA + 2hr, BFA + MMC + 2hr). However, the presence of MMC led to a clear increase of Cx43 in plaques at the cell– cell interfaces (Fig 4.6.A, BFA + MMC + 2hr). These plaques were significantly larger than those formed without MMC (Fig. 4.6.B).

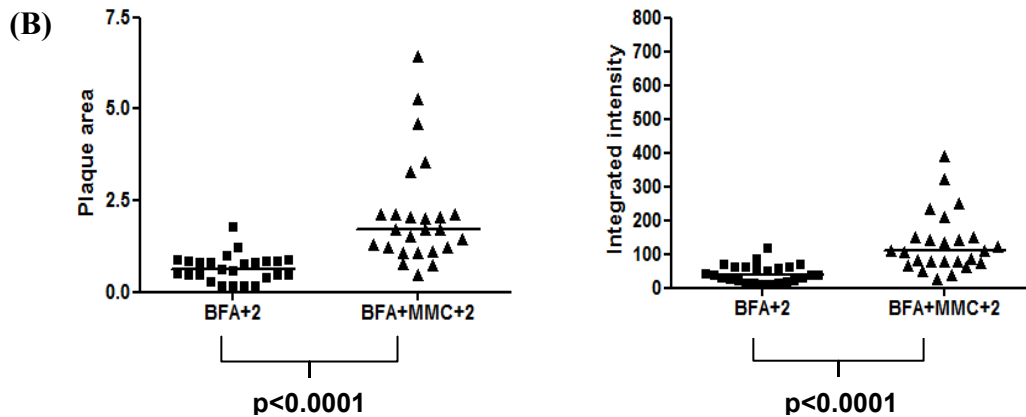
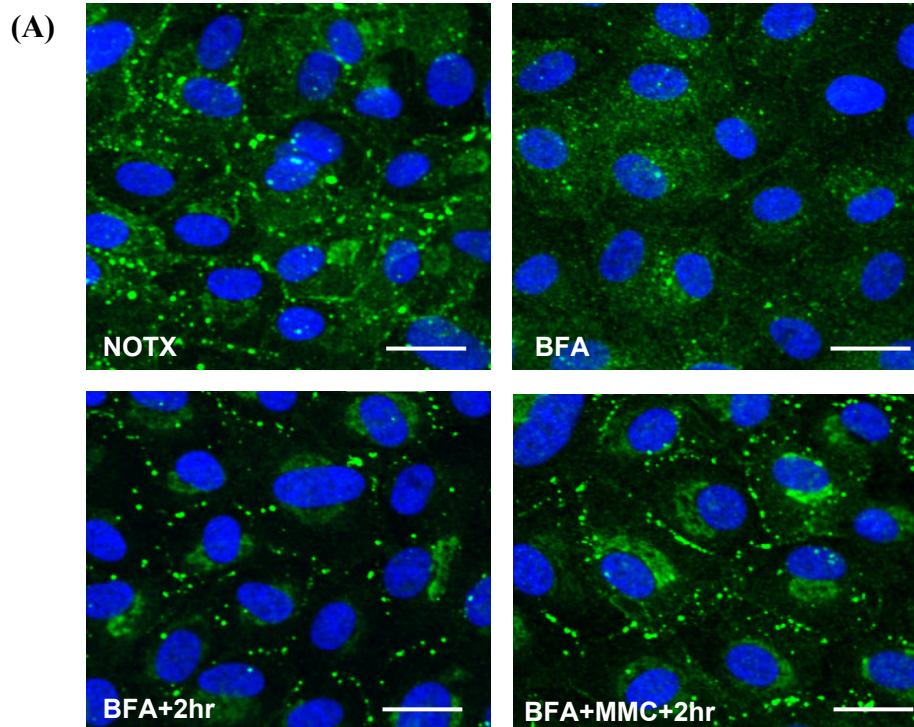
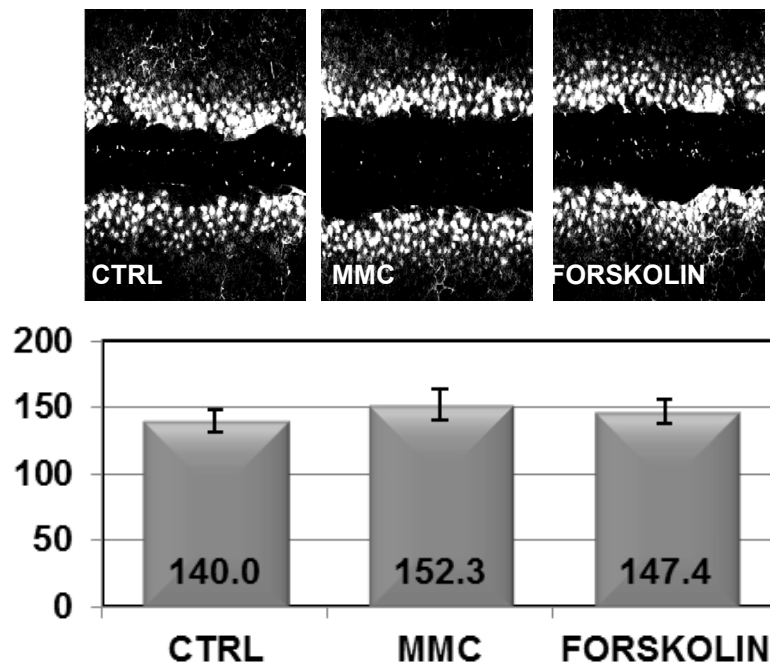


Figure 4.6: MMC induces increased assembly of gap junction plaques. Confluent monolayers were treated with prewarmed media containing 5 $\mu\text{g}/\text{mL}$ BFA for 8 hours followed by washout with warm medium and a 2-hour recovery. Five μM MMC was added as indicated during the 2-hour recovery period. (A) Representative confocal images of Cx43 (green) before treatment (NOTX), after 8 hour BFA (BFA), after recovery (BFA + 2hr), and after recovery in the presence of MMC (BFA + MMC + 2hr). DAPI (nuclei). (B) Gap junction plaques were imaged by confocal microscopy and analyzed for area (μm^2) and Cx43 fluorescence intensity (arbitrary units) similar to Figure 2B. BFA + 2hr ($n = 25$ plaques) or BFA + MMC + 2hr ($n = 25$ plaques). Individual data points are shown along with median. Area and intensity distributions were compared using the Mann–Whitney U test (area, $P < 0.0001$; intensity, $P < 0.0001$). Similar results were obtained in three independent experiments.

4.3.5 Gap junction communication is stabilized by MMC treatment.

LY dye, which transfers from cell to cell via gap junction channels, was used to assess the temporal rate of GJIC during a 2-minute incubation after scrape loading. As shown in Fig. 4.7.A, no significant differences were observed in the amount of dye transferred or the distance the dye moved comparing control and MMC-treated cells (Fig. 4.7.A). FRAP using Calcein AM, a similarly gap junction permeable dye, also revealed identical transfer kinetics between control and MMC-treated CE cells (Fig. 4.7.C). Forskolin is an agent known to maximize GJIC and markedly increases scrape-loaded dye transfer in many cell types (Dowling-Warriner and Trosko 2000; Paulson, Lampe et al. 2000; Romanello, Moro et al. 2001). In CE cells, however, forskolin produced no significant increase on the dye transfer rate (Fig. 4.7.A, far right panel). Both forskolin and MMC, however, increased dye transfer rates in primary bovine corneal fibroblasts (Fig. 4.7.B) suggesting that CE cells may be communicating via gap junctions at near maximal levels, making further increases in GJIC undetectable.

(A)



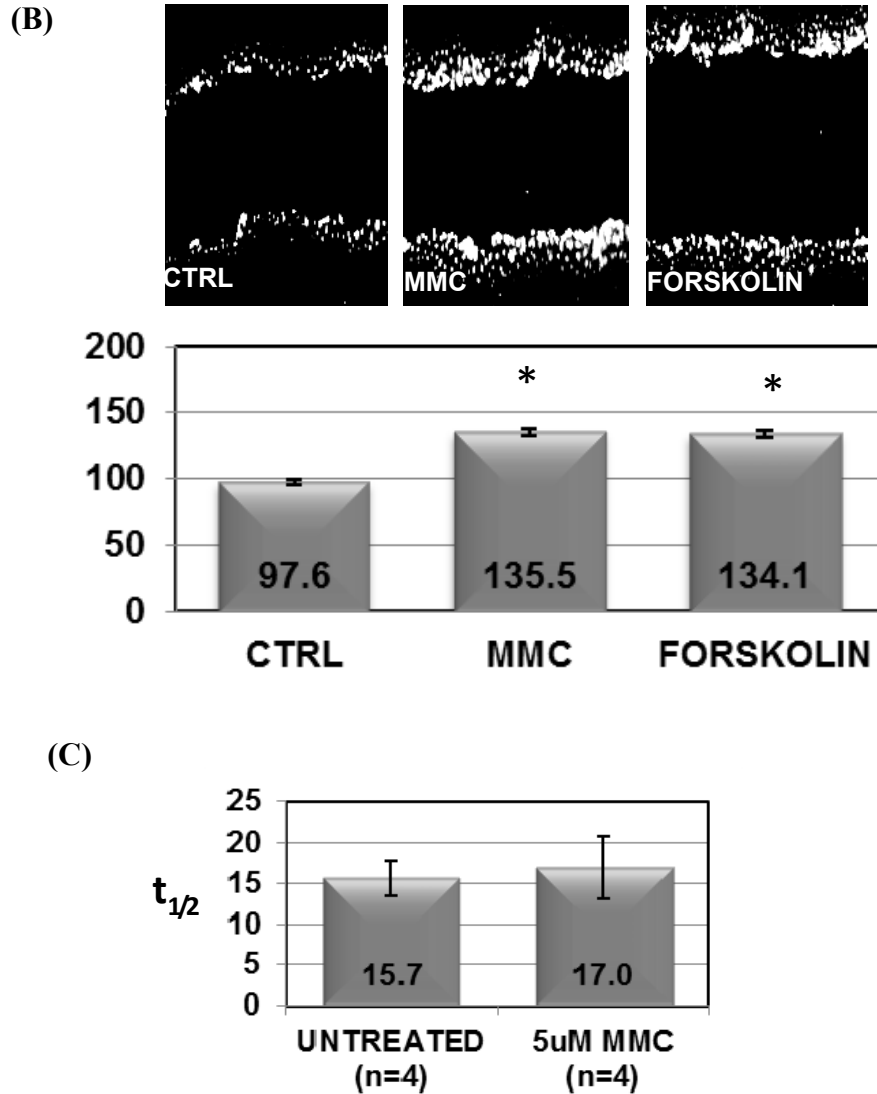


Figure 4.7: MMC and forskolin do not significantly increase GJIC. (A) Confluent monolayers were treated with prewarmed media containing 5 μ M MMC, 10 μ M forskolin, or medium alone (“CTRL”) for 30 minutes. Medium was replaced with 1 mg/mL Lucifer yellow (LY) dye in PBS and scrape-load dye transfer assay was performed as described in the Methods section. Ten individual sites were measured along different regions of the scrape wound for distance of LY dye transfer to determine cell– cell communication as shown in the graph below. Data points are mean distance \pm SD. There was no statistically significant difference between treatments (ANOVA, $P = 0.3$). (B) Confluent monolayers of bovine corneal fibroblasts were treated similar to (A). Asterisks indicate statistically significant differences (ANOVA, $P < 0.001$); Dunnett’s test: medium versus Forskolin ($P < 0.01$), medium versus MMC ($P < 0.01$). (C) FRAP was performed after loading confluent CE monolayers with 1 μ M calcein AM and observing dye recovery. Half-life of recovery in seconds ($t_{1/2}$) shown on the y-axis was compared between untreated ($n = 4$ cells) and MMC-treated ($n = 4$) cells. Mean \pm SD $t_{1/2}$ shown. No statistically significant difference was found between treatments (Student’s t test, $P = 0.8$).

To determine whether the increased Cx43 at the cell surface induced any alteration in gap junction function of CE cells, we inhibited GJIC using epidermal growth factor (EGF). EGF treatment has been shown to decrease GJIC in cultured cells through activation of the mitogen-activated kinase pathway (Abdelmohsen, Sauerbier et al. 2007). This response was clearly detected in CE cells using the LY dye transfer assay (Fig. 4.8). MMC-treated cultures partially rescued the EGF-induced GJIC inhibition, suggesting that increases in cell surface Cx43 induced by MMC are indeed functional in promoting intercellular communication.

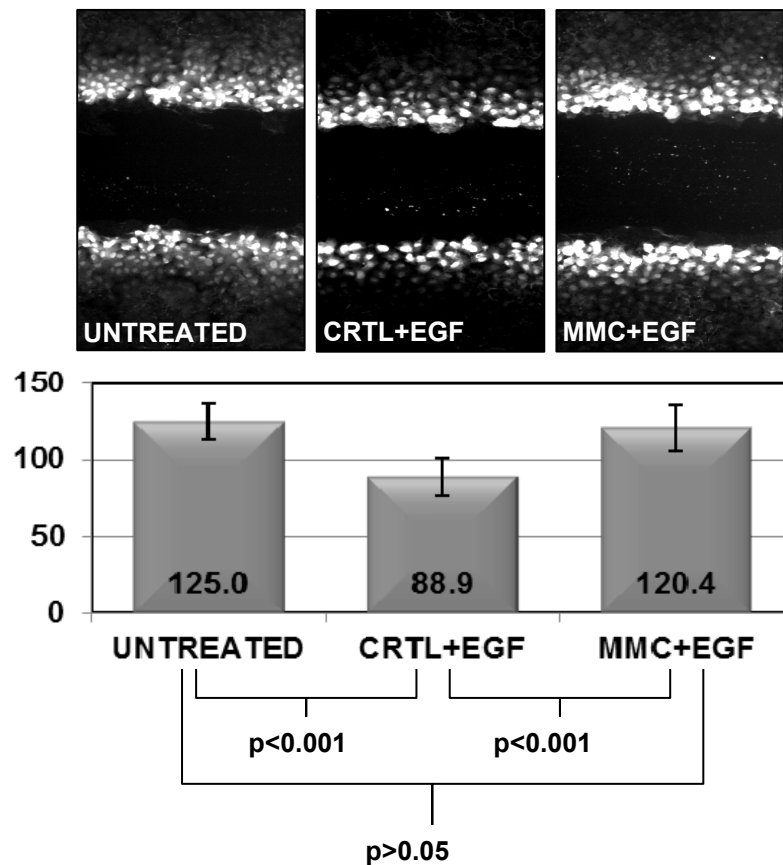


Figure 4.8: MMC treatment generates GJIC resistant to EGF-mediated downregulation. (A) Confluent monolayers were pretreated for 60 minutes with either prewarmed media containing 5 μ M MMC or medium (“CTRL”) alone. Medium was replaced with 100 ng/mL EGF for an additional 30 minutes and then GJIC was assessed with a scrape-load dye transfer assay as described in the Methods section. Ten individual sites were measured along different regions of the scrape wound for distance of LY dye transfer to determine cell– cell communication as shown in the graph. Data points are mean distance \pm SD of the dye transfer. ANOVA was used for statistical comparison among treatment groups ($P < 0.0001$). Tukey’s multiple comparison test reported untreated versus MED + EGF ($P < 0.001$), untreated versus MMC + EGF ($P > 0.05$), MED + EGF versus MMC + EGF ($P < 0.001$). Results are representative of two independent experiments.

4.3.6 GJIC protects against genotoxic stress-induced apoptosis

After we observed stabilization of GJIC during genotoxic stress, we assessed the role of GJIC in genotoxic stress-induced apoptosis. 18-alpha-glycerrhetinic acid (AGA) was used to inhibit GJIC during a high dose (50 μ M) of MMC. Cells were loaded with a fluorescent indicator of caspase 3/7 activation. The dye is non-fluorescent until apoptosis-induced activation of caspase 3/7 which cleaves the dye, translocating it to the nucleus and initiating its fluorescence. Live-cell imaging of confluent monolayers of equal cell numbers followed the progression of apoptosis. The combination of inhibition of GJIC with genotoxic stress (AGA+MMC) lead to an earlier onset of apoptosis compared to MMC alone (Fig. 4.9).

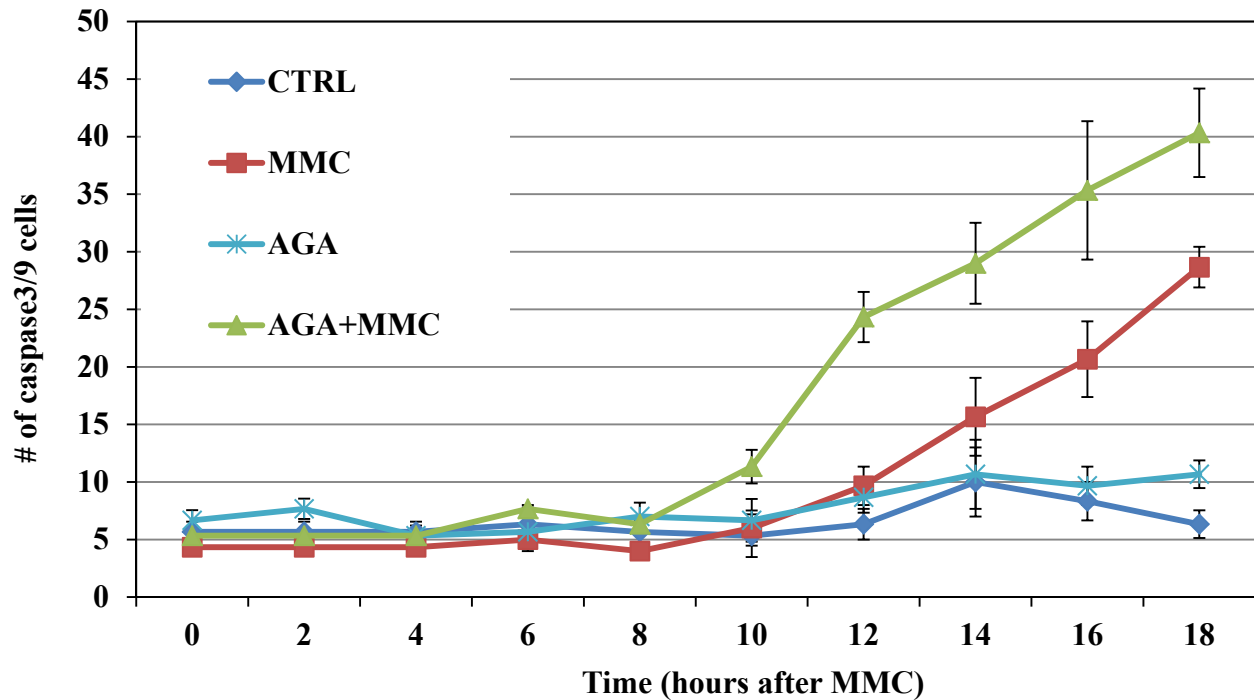


Figure 4.9: GJIC effect on acute genotoxic stress-induced apoptosis. CE cells were seeded at equal density then grown to confluency. Confluent CE cells were loaded with a fluorescent indicator of caspase 3/7 activity and imaged by live-cell imaging during acute genotoxic stress with 50 μ M MMC. 10 μ M 18- α GA (AGA) was used to inhibit GJIC. The number of caspase 3/7 positive cells, indicative of apoptosis, was calculated from live-cell images from each timepoint. The mean number of caspase 3/7-positive cells \pm SEM is shown in the graph from three independent cultures for each time point.

4.4 DISCUSSION

The CE is a nonregenerating tissue in which the total number of cells declines throughout life. As a result of damage or various acute stressors, this process can occur more rapidly. With cell loss, CE cells spread and flatten, covering a greater area. Apart from this process, little of the physiologic response to stressors in these cells is known, particularly regarding how cell– cell junctions are maintained. In the present study, we document several novel observations regarding how CE cells respond to an acute stress: Cx43 rapidly accumulates in detergent-insoluble plaques at cell– cell junctions; the plaques are stabilized, showing reduced endocytosis and degradation; transport of Cx43 from the ER to the cell surface is increased; and gap junction communication is stabilized against downregulation by EGF. These observations describe a previously unidentified response of CE cells to stress, rapidly increasing the abundance of functional gap junctions in the tissue.

The mechanism mediating this response is not straightforward. In initial experiments, we found no statistically significant increase in Cx43 mRNA (Supplemental Fig. S.4 therefore, the rapid change in Cx43 abundance in response to MMC seemed likely to involve decreased Cx43 degradation. A temporary halt to Cx43 degradation after MMC treatment was indeed observed (Fig 4.4) as was a significant reduction in endocytosis and dispersion of plaque-associated Cx43 (Fig 4.5), providing a mechanism that could be responsible for the observed increase in total cellular Cx43. Cx43 stabilization has been described in other cell types in response to stress. Long-lived gap junctions after arsenite and heat-shock exposure were observed in in CHO and S180 cell lines (VanSlyke and Musil 2005). In the case of CHO cells, cell surface Cx43 was stabilized by a mechanism dependent on functional proteasomal action (VanSlyke and Musil 2005). The CE response to MMC observed in this study could, therefore, be typical of a generalized cellular mechanism by which cells stabilize GJIC in response to stress.

Another potential effector of GJIC stabilization is ZO-1. ZO-1 is present in gap junctions, binding the C-terminal intracellular region of Cx43 (Giepman and Moolenaar 1998). We observed Cx43 but not ZO-1 to increase in response to MMC, and subsequently found a decreased association of ZO-1 with Cx43 by coimmunoprecipitation (Fig. 4.3). There is reason to believe that this reduced ZO-1:Cx43 ratio could contribute to the stress-induced Cx43 plaque stabilization. Association of Cx43 with ZO-1 has been linked to an increased endocytosis of

Cx43 (Barker, Price et al. 2002; Segretain, Fiorini et al. 2004; Bruce, Rothery et al. 2008); therefore, reduced association of Cx43 with ZO-1 in gap junction plaques (such as we observed) could delay or prevent Cx43 endocytosis and internalization. ZO-1 may also have an effect on the gap junction plaque size (Fig. 4.2). ZO-1 has been reported to regulate gap junction size by limiting access of ZO-1-associated Cx43 into preexisting gap junctions (Giepmans and Moolenaar 1998; Hunter, Jourdan et al. 2003; Hunter, Barker et al. 2005; Rhett, Jourdan et al. 2011). Reduced ZO-1 association with cell surface Cx43 is therefore consistent with the increased gap junction plaques we observed.

The *in vitro* CE layers used in this study did not appear to restrict the intercellular transmission of dyes via gap junctions (Fig. 4.7). However, in the presence of EGF—an agent that disrupts GJIC—it was clear that GJIC in MMC-treated cells was more resistant to this inhibition than control cells (Fig. 4.8). Therefore, the rapid alterations in Cx43 protein in response to genotoxic stress produce a cell–cell communication array that is more robust than that in nonstressed cells. This response gains relevance in light of the documentation that exposure to genotoxic stressors releases cytokines and growth factors (Prise and O'Sullivan 2009; Chang, Chou et al. 2010; Chen and Chang 2010; Novakova, Hubackova et al. 2010) that could compromise GJIC in the CE.

The tight junctions in CE cells serve to control movement of water and nutrients into the cornea (Srinivas 2010), but there is not yet a clearly demonstrated role for gap junctions in corneal physiology. Our results suggest that alterations in Cx43 may serve as survival factor for CE cells. In other biologic systems in which cells are subjected to physical stress or injury, gap junction coupling activation results in the mediation of injury or increased survival (Chew, Johnson et al. 2010; Qi, Chi et al. 2011). In the CE, upregulation of Cx43 mRNA and protein, via release of ciliary neurotrophic factor and its receptor, promote CE cell survival during oxidative stress and *ex vivo* corneal storage (Koh, Celeste et al. 2008; Koh, Cheng et al. 2009) (Koh 2002). Also, point mechanical stimulation of CE cell monolayers results in a Cx43-dependent increase in ATP release and calcium-wave propagation between cells (Gomes, Srinivas et al. 2006). Therefore, Cx43 and GJIC provide a response in CE to changes in cellular environment that is likely to represent a survival response.

The rapid rate at which CE responds to MMC suggests a mechanism not reliant on changes in gene expression but instead on posttranslation modifications of Cx43. Cx43 C-

terminal phosphorylation controls multiple aspects of this protein, including channel gating, subcellular localization, secondary structure, and stability (Solan and Lampe 2009). Increased phosphorylation of Cx43 C-terminal, for example is responsible for decreased ZO-1 binding (Chen, Pan et al. 2008). Site-specific Cx43 phosphorylation has also been linked to internalization and degradation of this protein (Solan and Lampe 2007). Casein kinase 1 is a likely candidate for an active participant in the response to MMC. Phosphorylation of Cx43 by casein kinase 1 has been proposed to stimulate incorporation of Cx43 into gap junction plaques (Cooper and Lampe 2002) and it appears to exert a general role in regulating the stability of its numerous substrates (Knippschild, Gocht et al. 2005). In addition, casein kinase 1 acutely responds to genotoxic stress resulting in increased kinase activity, changes in subcellular location, and increased mRNA and protein levels (Knippschild, Milne et al. 1997; Knippschild, Gocht et al. 2005; Alsheich-Bartok, Haupt et al. 2008; Inuzuka, Tseng et al. 2010).

In conclusion, we have documented rapid changes in Cx43 in response to genotoxic stress and identified the changes in binding partners and reduced degradation of Cx43. Mitomycin C is widely used in ocular surgery, and we recently showed that such treatment generates DNA cross-linking in CE (Roh, Cook et al. 2008). MMC, however, may not be the only genotoxic agent to which these cells are exposed. The high metabolic rate of the CE generates reactive oxygen species, which are capable of DNA damage (Cadet, Douki et al. 2003) and as a possible consequence, CE exhibits an accumulation of DNA modifications with increasing age (Joyce, Zhu et al. 2009; Joyce, Harris et al. 2010). The implications of the stabilization of Cx43 and GJIC on CE cell homeostasis/survival are yet to be fully elucidated but may serve to protect against detrimental effects of natural DNA damage and acute stress generated by agents such as MMC or ultraviolet light. Future areas of interest include determining the functional consequences of stabilized cell surface Cx43 and GJIC on CE cell viability. One potential function influencing cell survival may be to increase the intercellular transfer of cytoprotective molecules that increase survival and function of interconnected cells and/or disperse cytotoxic molecules and prevent their accumulation in any one cell.

(Additional discussion not included in original publication). The live-cell assay for apoptosis demonstrated a key finding by establishing GJIC as protective during genotoxic stress in CE cells. Fig. 4.9 shows that inhibition of GJIC accelerates genotoxic stress-induced apoptosis in CE cells. Therefore, the rapid accumulation of Cx43 in gap junctions and the

preservation of GJIC serves to enhance survival of the CE during acute genotoxic stress. The mechanisms that mediate survival through cell-cell communication may involve the dispersion of toxic molecules or spreading of survival factors. Although we did not test for changes in secondary messengers, intracellular Ca^{2+} and cAMP may be factors mediating survival. Ca^{2+} is thought to be the “killing messenger” that can propagate from cell to cell via gap junctions (Decrock, Vinken et al. 2009; Decrock, Vinken et al. 2011). Enhanced GJIC may prevent any one cell from accumulating high intracellular Ca^{2+} concentrations, which would normally lead to cell death. Alternatively, increased GJIC may allow for spreading of cAMP which has been shown to protect CE cells from staurosporine-induced apoptosis (Li, Allen et al. 2011). Interestingly, GJIC has been shown to decrease at the early onset of apoptosis which involved increased removal of gap junctions (Wilson, Close et al. 2000; Kalvelyte, Imbrasaite et al. 2003). Preventing the breakdown of gap junctions and/or the enhancement of GJIC may be an approach to improving the survival of CE cells during stress.

5.0 CASEIN KINASE 1 DELTA AS A REGULATOR OF CONNEXIN-43 AND GAP JUNCTION INTERCELLULAR COMMUNICATION DURING GENOTOXIC STRESS

5.1 INTRODUCTION

The gap junction protein connexin-43 (Cx43) is tightly regulated by phosphorylation of its intracellular C-terminus in conditions of both homeostasis and stress. Cx43 phosphorylation rapidly alters protein structure and conformation which has immediate impacts on localization, stability, binding partners, channel permeability, and the ability to form gap junctions (Solan and Lampe 2009). Numerous kinases have been implicated in Cx43 phosphorylation, each having a distinct effect on the life cycle of Cx43. The initial phosphorylation event can occur within minutes of synthesis and the maturation of the P0 to the P1 and P2 forms is believed to involve protein kinase A (PKA) and casein kinase 1, respectively (Solan and Lampe 2007). Stimulus-induced phosphorylation by other kinases such as src, Erk1/2, and protein kinase C (PKC), leads to distinct P0, P1, and P2 forms of Cx43 that drive channel closure and rapid disassembly of gap junctions (Lampe and Lau 2004). As Cx43 and GJIC are integrated with cell function, survival and death, understanding how the kinases and subsequent phosphorylation impacts gap junctions can help to enhance cellular responses during stress.

The delta isoform of casein kinase 1 (CK1 δ) was reported to be involved in the assembly of gap junctions and *in vitro* specifically phosphorylated serines 325, 328, 330 of Cx43 (Cooper and Lampe 2002). Mutation of these residues prevented the formation of gap junctions and an antibody generated against these sites localized to gap junction plaques exclusively (Lampe, Cooper et al. 2006). This Cx43 phosphorylation site has been linked with responses to cell and tissue injury. Ischemic-damaged heart tissue and hearts from a mouse model of oculodentodigital dysplasia (Cx43 mutation) with severe arrhythmias contained low levels of serine 325, 328,330 phosphorylation (Lampe, Cooper et al. 2006; Kalcheva, Qu et al. 2007).

Knock-in mice expressing a phosphomimetic version of these residues were resistant to ischemia-induced cardiac remodeling of gap junctions. In contrast, the phosphomutant knock-in mice were susceptible to stress-induced arrhythmias and gap junction remodeling (Remo, Qu et al. 2011). Therefore, it appears that phosphorylation of Cx43 by CK1 δ plays a unique and significant role in gap junction formation, stability and resistance to remodeling during stress and injury.

Our previous study (Roh and Funderburgh 2011) reported rapid changes in corneal endothelial (CE) Cx43 after acute genotoxic stress. This response included accumulation of Cx43 in gap junctions and stress-stabilized GJIC that was resistant to subsequent cytokine exposure (Roh and Funderburgh 2011). We later found that GJIC inhibition significantly accelerated genotoxic stress-induced apoptosis in CE cells and hypothesized that stabilization of Cx43 may be an important protective response. In this study we sought to determine a role for CK1 δ in genotoxic stress-stabilized gap junctions in CE, a fragile cell layer especially vulnerable to the effects of genotoxic stress (Joyce, Zhu et al. 2009; Joyce, Harris et al. 2010). Because CK1 δ is also involved in DNA damage signaling (Knippschild, Milne et al. 1997; Sakaguchi, Saito et al. 2000; Alsheich-Bartok, Haupt et al. 2008; Inuzuka, Tseng et al. 2010), we hypothesized that CK1 δ may link DNA damage responses to changes in Cx43. If Cx43 and GJIC stabilization have potential to preserve CE survival during stress then determining targeted methods to specifically modulate these processes will be beneficial in protecting CE from injury.

5.2 MATERIALS AND METHODS

Cell culture and reagents

Primary bovine CE cells and human corneal fibroblasts were isolated and cultured as previously described (Roh and Funderburgh 2011). HeLa cells (ATCC, Manassas, VA) were grown in DMEM containing 10% fetal bovine serum. Mitomycin C (MMC), brefeldin A (BFA), etoposide, cycloheximide (CHX), CKI-7, (all from Sigma, St. Louis, MO), PF670462 (Tocris Bioscience, Ellisville, MO), were freshly diluted in pre-warmed media and applied to cells. UVC treatments were performed using a UV light source (UVP, LLC., Upland, CA) with a UVC

filter. Cells were grown on 35-mm dishes and media was removed and saved in a separate container during UVC exposure then replaced immediately after. Intensity (Joules/m²) was pre-calculated using a UV meter (UVX Radiometer, UVP, LLC.).

Reverse Transcription Polymerase Chain Reaction (PCR)

Cells were collected by centrifugation after scraping into cold saline, RNA was isolated using RNeasy mini kit (Qiagen, Germantown, MD), and reverse transcribed to cDNA as previously described (Du, Funderburgh et al. 2005). Custom designed primers for bovine CK1δ (gene CSNK1D) were: 5' (GTTCCCTTGCCTTTTGACGAT) and 3' (GTGTCTCAACCGCTCCTCTC) which gave an expected 185 base pair product. PCR was carried out for 30 cycles of 15 minutes at 95°C and 60 minutes at 60°C after an initial incubation at 95°C for 10 minutes in an ABI7700 thermocycler (Applied Biosystems, Carlsbad, CA). PCR products were run on pre-cast DNA gels (BioRad, Hercules, CA) for 1 hour at 100V and bands were visualized with SYBR Gold (Invitrogen, Carlsbad, CA) under UV light.

Cx43 constructs

A cDNA construct (pGEX-2T, GE Life Sciences, Piscataway, NJ) encoding a GST fusion protein with the complete C-terminus of rat Cx43 (amino acids 236-382) was a kind gift of Dr. Steven Taffet, State University of New York Health Science Center, Syracuse, NY. The GST construct was transformed into BL21 *Escherichia coli* and expression was induced with 100 μM Isopropyl β-D-1-thiogalactopyranoside (IPTG). GST fusion protein was purified with pre-washed magnetic glutathione beads (Thermofisher, Pittsburgh, PA). A cDNA construct (pEGFP-N1, Clontech, Mountain View, CA) encoding full-length rat Cx43 fused with a C-terminal GFP was a kind gift of Dr. Matthias M. Falk, Lehigh University, Bethlehem, PA. This construct was further modified by PCR mutagenesis to mutate all serine residues 325, 328, 330 to alanines or aspartates. Primers were used to introduce mutations and included:

Serines → Alanines (GCA)

A-Front: GGGCAGGCCGGAGCAACAATTGCAAACGCACACGCCAGCCGTTTCGAT

A-Back: GCTGGGCGTGTGCGTTTGCAATTGTTGCTCCGGCCTGCCCATGCGATTT

B-Front: GCGCACTGCAGGCCACCATGGGTGACTGGAGTGCCTT

B-Back: CGCGCGGATCCGCAATCTCCAGGTCATCAGGCCGAGGCC

Serines → Aspartates (GAC)

A-Front: GGGCAGGCCGGAGACACAATTGACAACGACCACGCCCAGCCGTTTCGAT

A-Back: GCTGGGCGTGGTCGTTGTCAATTGTGTCTCCGGCCTGCCCCATGCGATTT

B-Front: GCGCACTGCAGGCCACCATGGGTGACTGGAGTGCCTT

B-Back: CGCGCGGATCCGCAATCTCCAGGTCATCAGGCCGAGGCC

PCR was performed to create two fragments (reaction 1: B-Front + A-Back; reaction 2: B-Back + A-Front), which were then combined with PCR (reaction 3: B-Front + B-Back), cut with *pstI* and *BamHI* and ligated into empty pEGFP-N1 vector pre-cut with *pstI* and *BamHI*. All mutations were verified by DNA sequencing. The resulting constructs were further modified to remove the GFP tag from the C-terminus by using the following primer which introduced stop codons:

A-Back_STOP: CTTCTCTCCGGCCGCGGATCCTTAAATCTCCAGGTCATCAGGCCGAGGCC

PCR was performed to copy the Cx43 encoding sequences and introduce the stop codons. The resulting products were cut with *PstI* and *NotI*. In addition, *PstI* and *NotI* were used to excise the sequence encoding GFP from the pEGFP-N1 vector followed by DNA ligation with the cut PCR products. Mutations were verified by DNA sequencing.

Immunostaining

Cells were grown on 35 mm dishes, fixed in 3.2% paraformaldehyde (PFA) (Electron Microscopy Science, Hatfield, PA), permeabilized with 0.1% Triton X-100 (ThermoFisher), and blocked as previously described (Roh and Funderburgh 2011). For staining of detergent insoluble proteins, cells were rinsed with saline and then covered with ice-cold 1% Triton X-100 in PBS for 30 minutes on ice, rinsed with PBS, and then fixed with PFA. Primary antibodies used for staining included rabbit polyclonal anti-Cx43 (Invitrogen), rabbit polyclonal anti-pCx43 serine 325, 328, 330, mouse monoclonal anti-Cx43 (Millipore, Billerica, MA), and goat polyclonal anti-CK1δ (OriGene, Rockville, MD).

Immunoblotting

Cells were lysed in 1X SDS sample buffer, heated at 95° C, and sonicated until solubilized as previously described (Roh and Funderburgh 2011). Primary antibodies used for immunoblotting were diluted in fluorescent blocker (Millipore) and included rabbit polyclonal anti-Cx43

(Invitrogen), rabbit polyclonal anti-pCx43 serine 325, 328, 330, mouse monoclonal anti-Cx43 (Millipore), and goat polyclonal anti-CK1 δ (OriGene). Secondary antibodies included IRDye800 and IRDye680 labeled secondary antibodies (LI-COR, Lincoln, NE) for infrared imaging. Fluorescent signal was detected with Odyssey infrared imaging system (LI-COR). Densitometry was performed using digital analysis software fluorescent detection (LI-COR).

Triton X-100 insolubility

Cells were lysed in cell lysis buffer containing 1% Triton X-100 and 1 mM EDTA with protease inhibitors (Sigma) and then chilled on ice for 30 minutes with mixing. Cell lysates were spun at 10,000 g for 30 minutes at 4°C. The soluble fraction was removed and the Triton X-100 insoluble pellet was further dissolved in 1X SDS buffer followed by sonication.

Co-immunoprecipitation

Cells were lysed directly in cold coimmunoprecipitation buffer [0.1% Nonidet P40, 25 mM Tris pH 7.4, 150 mM NaCl, 1 mM EDTA] containing HALT protease and phosphatase inhibitors (Thermo Fisher) and briefly sonicated until solubilized. Lysates were precleared with magnetic protein G beads (Millipore) for 1 hour at room temperature to remove any nonspecific binding of cell proteins to beads. The beads were discarded and then cleared lysates were incubated with 1 μ g antibody per 500 μ g of lysate using a rabbit polyclonal anti-Cx43 antibody (Invitrogen) or goat polyclonal anti-CK1 δ (OriGene) overnight at 4°C. Beads were then washed multiple times with lysis buffer and heated at 95°C for 5 minutes in 1X SDS sample buffer with 2-mercaptoethanol. A magnetic rack was used to separate the beads from lysate before loading for SDS-PAGE separation.

In vitro kinase assay

~5-10 μ g of GST-Cx43-CT fusion proteins bound to glutathione magnetic beads (ThermoFisher) were incubated with ~5,000 units of purified recombinant CK1 δ (New England Biolabs, Ipswich, MA) in 10 μ l reactions containing 5 μ M ATP, [γ -³²P]ATP (PerkinElmer Life Sciences Blu002, ~1 μ Ci), and 1 \times CK1 reaction buffer (50 mM Tris-HCl, 10 mM MgCl₂, 5 mM dithiothreitol, pH 7.5). Reactions were incubated at 30° C for 20 minutes followed by several washes in 1X CK1 reaction buffer using a magnetic rack to isolate the magnetic glutathione-

bound GST proteins. Phosphorylated protein was eluted in 1× SDS sample buffer, heated at 95°C for 5 minutes, and analyzed by SDS-PAGE on 10% pre-cast polyacrylamide gels (BioRad). Incorporation of [γ -³²P]ATP was detected by autoradiography of dried Coomassie-stained gels. For “cold” kinase assays, similar steps were taken with the exception of omission of [γ -³²P]ATP and detection of phosphorylated Cx43 serine 325, 328, 330 was done through immunoblotting with the pCx43 antibody (described below) and a mouse anti-GST antibody (GenWay, San Diego, CA). Inhibition of CK1 δ activity during kinase assays was achieved with the addition of 3 μ M PF670462 to the reaction mixture.

Generation and validation of a phosphospecific Cx43 antibody

Custom peptides were synthesized (ProSci Inc., Poway, CA) to generate an antibody that recognized Cx43 phosphorylated on serines 325, 328, 330 as previously reported (Lampe, Cooper et al. 2006). The phosphopeptide sequence (phosphorylated residues indicated by underlined residue and ‘(P)’) was: CQAGS(P)TIS(P)NS(P)HAQ and the cognate non-phosphopeptide sequence was: CQAGSTISNSHAQ which is conserved peptide sequence across multiple species including human, mouse, rat, and bovine. A commercial antibody production company (ProSci) was used to generate rabbit serum against the phosphopeptide. Phosphorylation-specific antibody was affinity purified by linking the phosphorylated peptide and the corresponding nonphosphorylated version to SulfoLink columns (ThermoFisher) and passing the serum first over a 2-ml column prepared with the nonphosphorylated peptide two times followed by a phosphopeptide-SulfoLink column according to the manufacturer's instructions. After washing, phosphorylation-specific antibody was eluted from the column with 0.1 M glycine-HCl, pH 2.8 and fractions were immediately neutralized with 1M Tris-HCl, pH 8.5. Antibody was concentrated using a spin column, dialyzed with PBS, and aliquoted and stored at -20° C until use. ELISA compared reactivity to the phosphopeptide and cognate nonphosphopeptide. 96-well plates were coated with 10 μ g/ml of each peptide dissolved in 50 mM carbonate binding buffer. Plates were blocked with 0.1% BSA in PBS with 0.02% thimerosal and serum was added in dilutions of 1:5,000, 1:25,000, 1:125,000 in triplicate. Goat anti-rabbit HRP (Santa Cruz Biotechnology, Santa Cruz, CA) was used with QuantaBlue substrate (Pierce) to detect antibody binding. Relative fluorescence at 325/420 nm was measured using a fluorometer. Calf intestinal alkaline phosphatase (AP) (Sigma) treatment of cell lysates

was performed as previously described (Roh and Funderburgh 2011) prior to SDS-PAGE to determine the phosphospecificity of the custom antibody. Similar AP treatment was used in immunostaining. HeLa cells were transfected with Cx43 constructs using Lipofectamine 2000 (Invitrogen) and analyzed by immunoblotting 24 hours after transfection.

RNAi of Cx43

Three siRNA oligonucleotides targeting bovine Cx43 (GJA1, NM_174068) were synthesized and included: 1) CCCACAUCAGGUGGAGUGUUUCCUU, 2) GGAGACAGAAACAAUUCUU, 3) CCGCAAUUACAACAAACAA (Invitrogen). Scrambled control siRNA oligonucleotide sequence was GGAACAGAAACUAUGACUU. Cells grown in serum-free medium were transfected with mixtures of all three siRNAs using Lipofectamine 2000 (Invitrogen) and assessed 48 hours later through immunoblotting with antibodies for pCx43 and total Cx43.

RNAi of CK1δ

Pre-designed GFP-labeled shRNA constructs (pGFP-V-RS, OriGene) targeting human CK1δ (CSNK1D, NP_001884.2) were used to manipulate CK1δ expression in human corneal fibroblasts. Sequences were the following: shRNA 72 (GGCAGCGGCTCCTTCGGAGACATCTATCT), shRNA 73 (TGCAGGAGAAGAGGTTGCCATCAAGCTTG). Scrambled shRNA (GCACTACCAGAGCTAACTCAGATAGTACT) served as a control. shRNA plasmids were transfected with Lipofectamine 2000 (Invitrogen) and assessed 48 hours later through immunostaining with antibodies for pCx43 and CK1δ (OriGene).

5.3 RESULTS

5.3.1 CK1 δ expression in CE

Expression of CK1 δ was examined by PCR and was detected in cultured bovine CE cells (Fig. 5.1.A). Immunostaining with a CK1 δ -specific antibody demonstrated localization throughout the cell, particularly in the peri-nuclear compartment, nucleus, and at the cell membrane (Fig. 5.1.B). Immunoblot analysis of Triton X-100 detergent soluble and insoluble fractions showed that a majority of CK1 δ is located in detergent-soluble portions of the CE cell (Fig. 5.1.C).

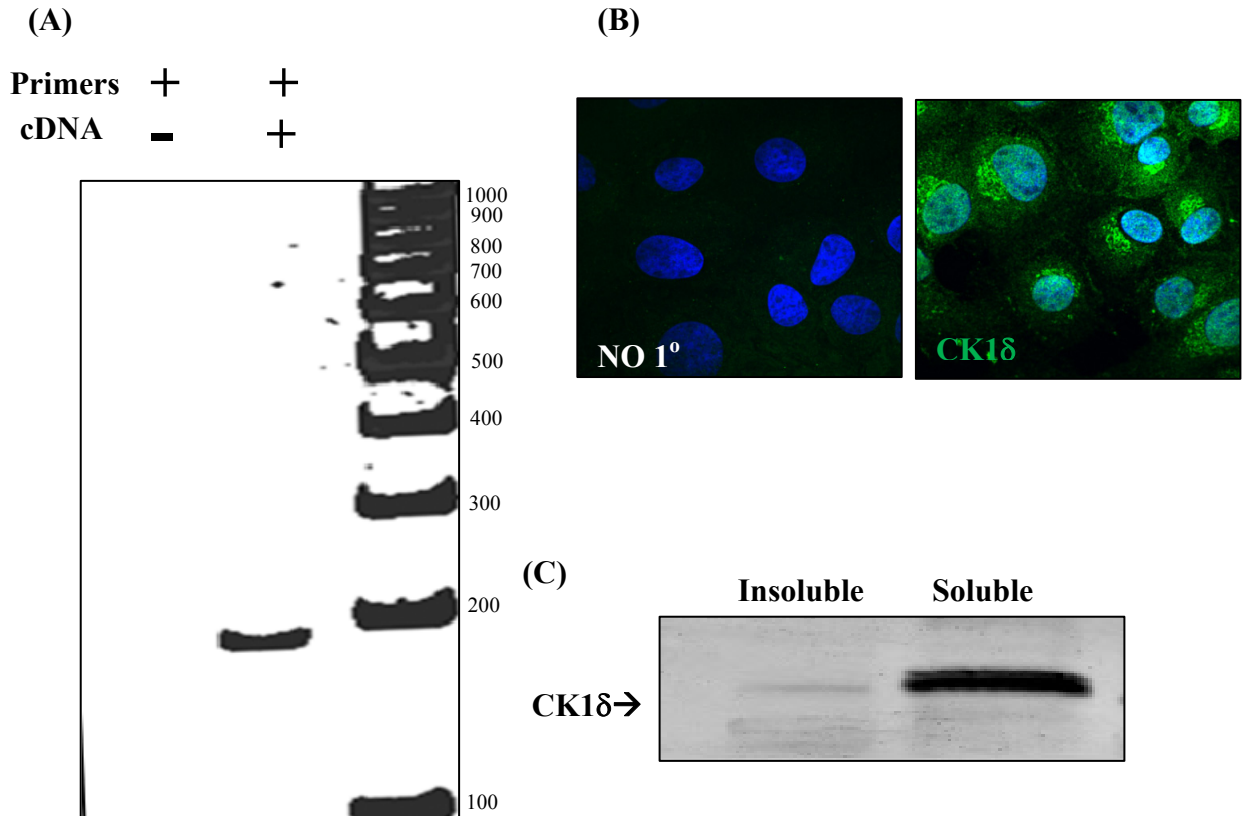


Figure 5.1: Expression of CK1 δ in bovine CE. (A) PCR data of bovine CSNK1D. Expected product size is 185 bp. Negative control excluded cDNA. (B) Immunostaining showing expression and localization of CK1 δ (green) and DAPI (nuclei). Negative control for staining included no primary antibody (NO 1 $^{\circ}$). (C) Immunoblot with CK1 δ antibody from 1% Triton X-100 insoluble and soluble fractions.

5.3.2 Increases in CK1 δ after genotoxic stress

CK1 δ is responsive to genotoxic stress through potential increases in mRNA, protein, and/or kinase activity as well as changes in substrate interactions (Knippschild, Milne et al. 1997; Sakaguchi, Saito et al. 2000; Alsheich-Bartok, Haupt et al. 2008). We observed increases in the total levels of CK1 δ protein based on immunoblotting from CE cells after MMC (Fig. 5.2.A) or UVC radiation (Fig. 5.2.B) exposure. Confirming this finding with immunostaining, the increase in CK1 δ was particularly evident in the peri-nuclear compartment and nucleus (Fig. 5.2.C). Notably, these increases were within the same timeframes we previously observed changes in Cx43 levels (Roh and Funderburgh 2011).

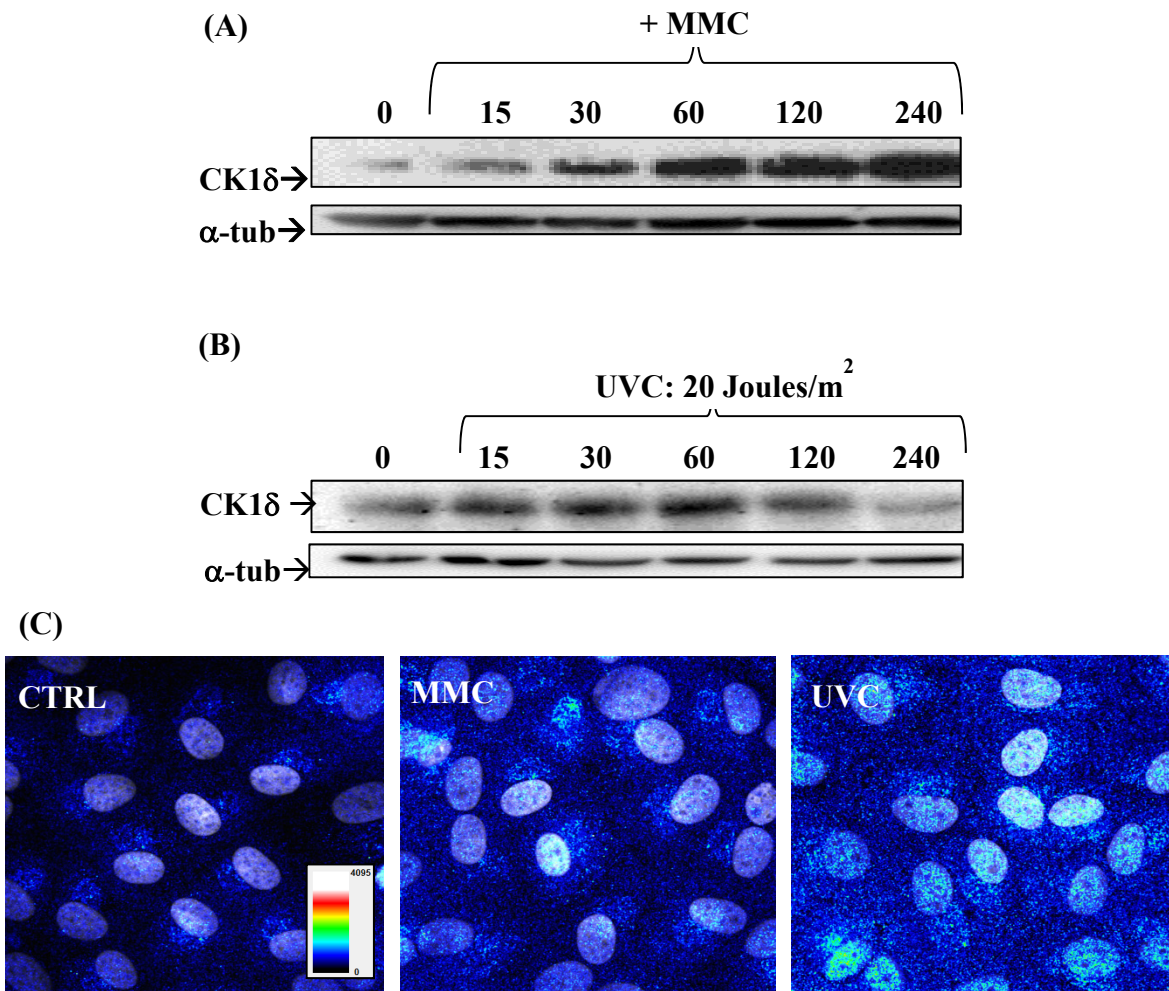
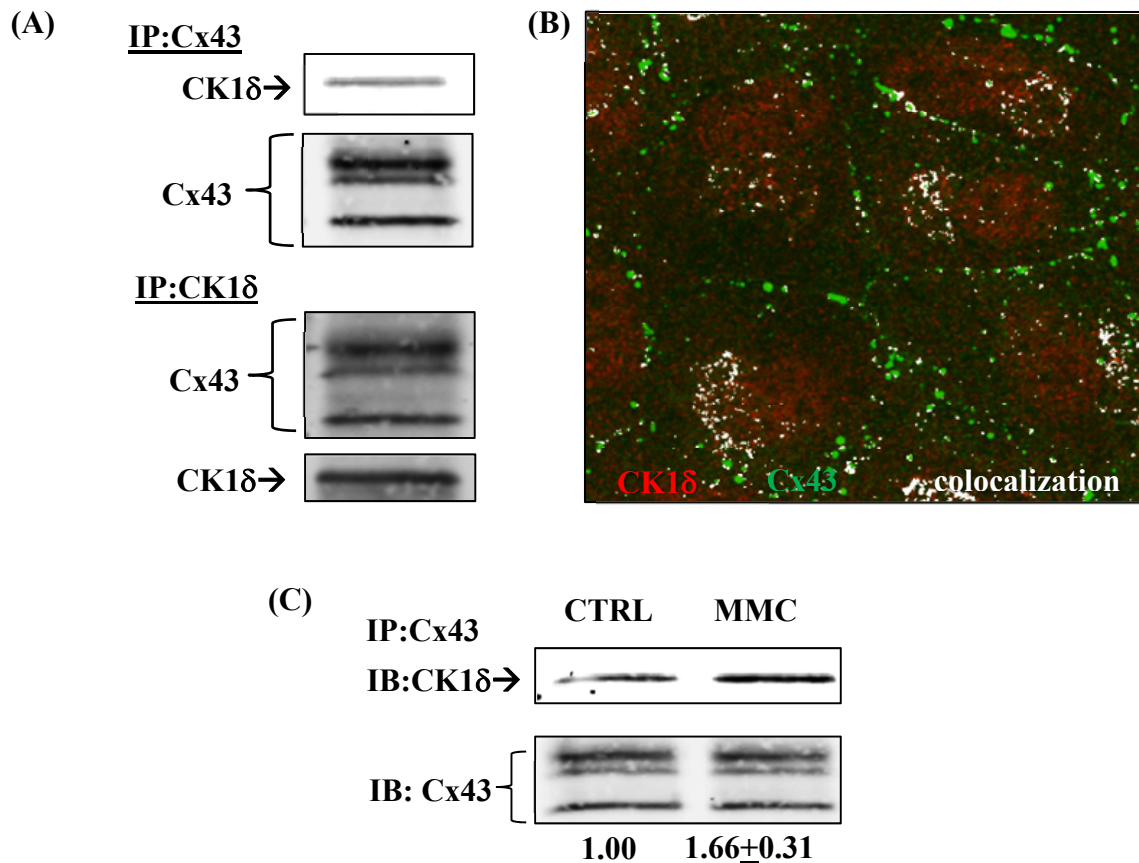


Figure 5.2: MMC and UVC treatment increases levels of CK1 δ . Confluent CE monolayers were treated with (A) 5 μ M MMC or (B) 20 J/m² UVC for the indicated time in minutes then assessed for CK1 δ levels through immunoblotting. (C) Immunostaining for CK1 δ after 60 minutes of treatment with medium (CTRL), 5 μ M MMC or 20 J/m² UVC. CK1 δ signal is pseudocolored and reflects intensity according to color scale shown (blue=lowest; white=highest). DAPI labels nuclei (gray scale).

5.3.3 Cx43: CK1δ localization in homeostatic and genotoxic stressed CE

In order to further characterize the interaction between CK1δ and Cx43 we used co-immunoprecipitation studies. IP with the Cx43 antibody demonstrated interaction with CK1δ and conversely IP with the CK1δ antibody demonstrated interaction with Cx43 (Fig. 5.3.A). CK1δ interacted with all forms (P0, P1, P2) of Cx43 despite being reported to only phosphorylate the P2 form (Cooper and Lampe 2002). To observe this interaction *in vivo* dual immunostaining with both antibodies was performed. This demonstrated Cx43:CK1δ co-localization in the peri-nuclear compartment as well as around the edges of some membrane-localized gap junction plaques (Fig. 5.3.B). To assess whether this interaction was dynamic after exposure to genotoxic stress we treated cells with 5μM MMC for 60 minutes after which, Co-IP showed an increase in the relative amount of CK1δ associated with Cx43 (Fig. 5.3.C). Immunostaining after exposure to various genotoxic stressors demonstrated that this increased interaction was in both the peri-nuclear and membrane compartments (Fig. 5.3.D).



(D)

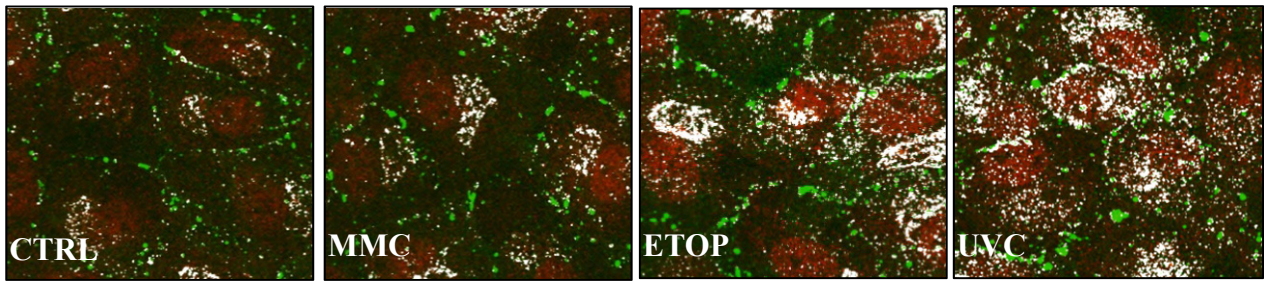


Figure 5.3: Dynamic interaction of Cx43 and CK1 δ in CE cells. (A) IP experiments demonstrating that Cx43 and CK1 δ interact in CE cell lysates. Upper blot uses Cx43 as IP-antibody and lower is reverse using CK1 δ as IP-antibody. (B) Immunostaining showing CK1 δ (red) and Cx43 (green) in CE cells. Areas of co-localization (white). (C) Co-IP after 60 minutes of 5 μ M MMC exposure or medium alone (CTRL). Quantification is CK1 δ /Cx43 then normalized to CTRL. Mean ratio \pm SEM from three experiments below. (D) Dual immunostaining similar to (B) after 60 minute exposure to 5 μ M MMC, 20 μ M etoposide, or 20 J/m² UVC.

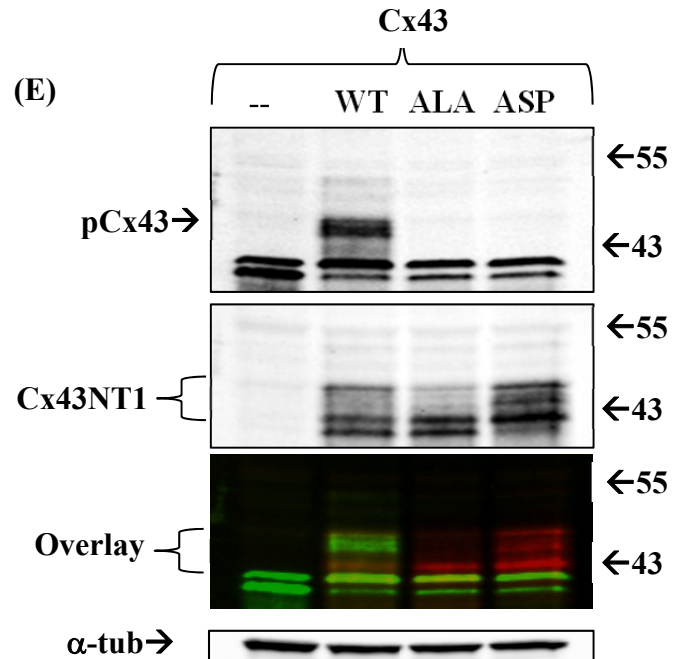
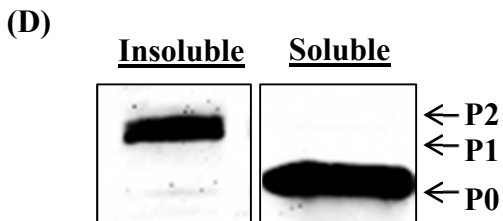
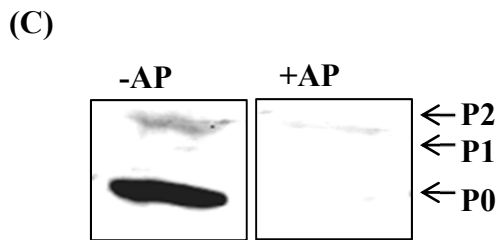
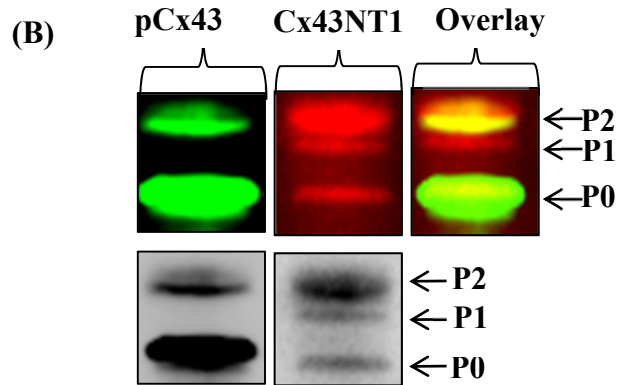
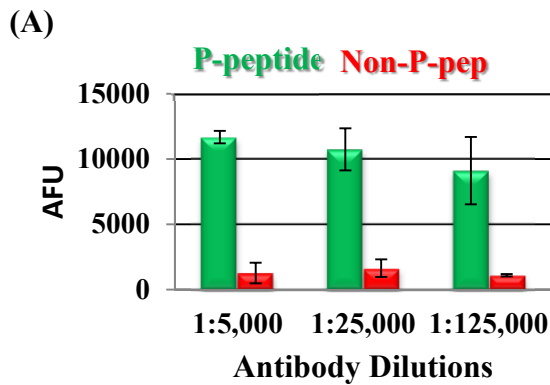
5.3.4 Antibody against Cx43 phosphorylated on serines 325, 328, 330

We created a peptide-based phosphospecific polyclonal rabbit antibody to Cx43 phosphorylated on serines 325, 328, 330 (named pCx43) to distinguish Cx43 specifically phosphorylated on this site. ELISA was used to test antibody specificity to a phosphopeptide and its cognate non-phospho counterpart. ELISA results demonstrated high reactivity with the phosphopeptide and negligible reactivity towards the nonphosphorylated peptide (Fig. 5.4.A). Immunoblotting simultaneously with two antibodies, the pCx43 antibody and total Cx43NT1 antibody, demonstrated that the pCx43 antibody recognized a portion of the P2 form of Cx43 (Fig. 5.4.B). Alkaline phosphatase (AP) treatment of cell lysates prevented antibody reactivity in immunoblotting (Fig. 5.4.C). In addition, expression of Cx43 constructs in Hela cells (which do not endogenously express Cx43) with these serines mutated to alanines or aspartates abolished pCx43 reactivity (Fig. 5.4.E) demonstrating the phosphospecific nature of antibody reactivity.

We observed a prominent P0-like band that was evident in immunoblotting, even in non-Cx43 expressing Hela cells. Detergent fractionation of cell lysates demonstrated that the pCx43 was mostly the P2 form in insoluble fractions (gap junction-associated Cx43) while the P0-like band was in the soluble fraction (Fig. 5.4.D). To determine the identity of this P0 band, we knocked down Cx43 with siRNA and did not observe similar decreases in the “P0” band (Fig. 5.4.F). In addition, immunoprecipitation from human corneal fibroblasts followed by peptide

mass fingerprinting was not able to detect connexin in this band. Therefore, pCx43 reacted with a soluble protein that migrated in a similar position as the P0 form of Cx43, but was not Cx43.

Immunostaining with the pCx43 antibody demonstrated localization at CE cell-cell interfaces co-localizing with a total Cx43 antibody (Fig. 5.4.I). This staining excluded the perinuclear compartment in CE cells that was evident with total Cx43, however, included filament-like cytoplasmic staining (Fig.5.4.I). Detergent extraction prior to staining eliminated the filamentous staining and demonstrated that the pCx43 antibody primarily recognized Cx43 in detergent-insoluble gap junction plaques (Fig. 5.4.J). Antibody reactivity during immunostaining could be prevented by AP treatment (Fig. 5.4.G) as well as pre-incubation with the phosphopeptide (Fig. 5.4.H).



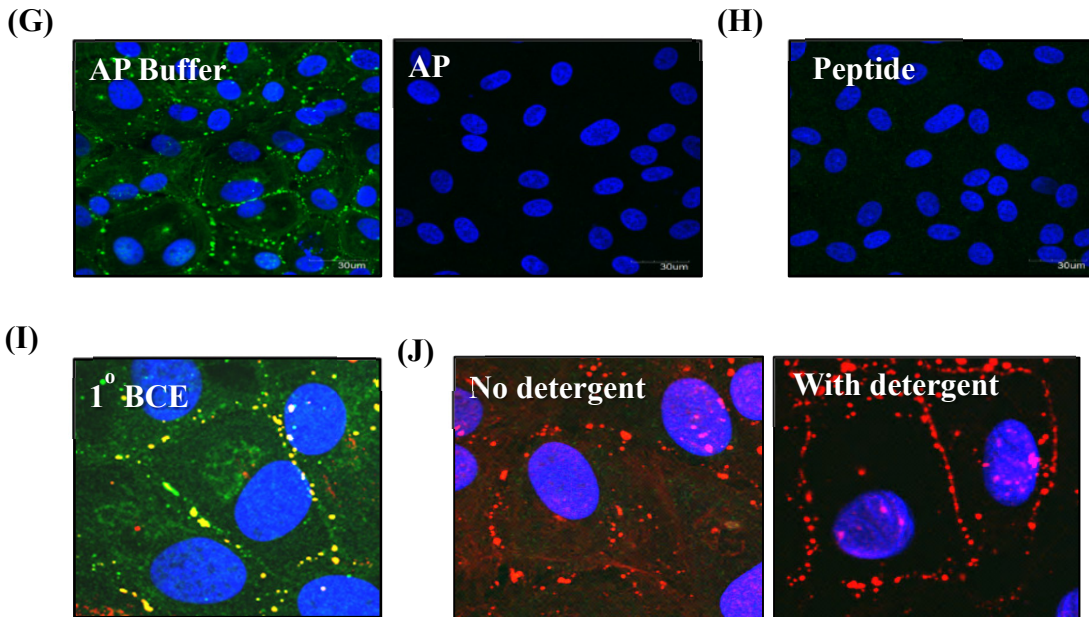
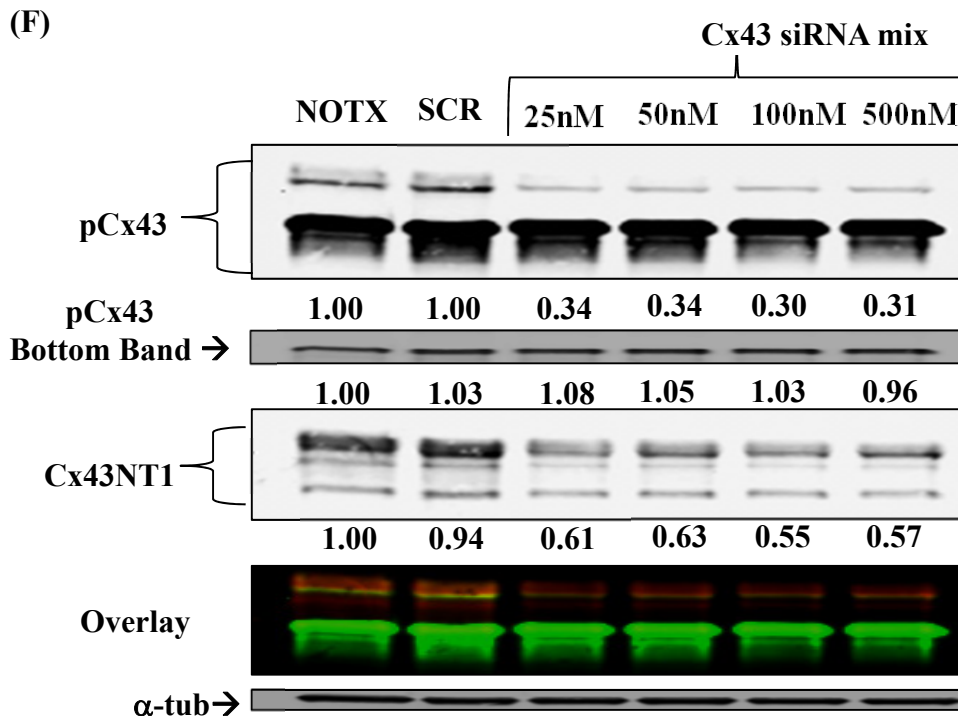


Figure 5.4: pCx43 antibody. (A) ELISA results testing pCx43 antibody reactivity against phosphopeptide and nonphosphopeptide. Results are mean \pm SD of triplicates of increasing antibody dilutions. (B) Dual immunoblotting with total Cx43NT1 (red) and pCx43 (green) antibodies. Areas of overlay appear yellow. P2, P1,P0 represent different forms of Cx43.(C) Alkaline phosphatase (AP) treatment of cell lysates and resulting pCx43 reactivity. (D) pCx43 reactivity after 1% Triton X-100 fractionation. (E) pCx43 reactivity in Hela cells transfected with Cx43 constructs. Wildtype (WT), Alanine (ALA), Aspartate (ASP) designate mutations in serines 325, 328, 330. (F) pCx43 reactivity after siRNA treatment against Cx43. pCx43 bottom band represents decreased exposure. Quantification below is ratio of pCx43 or Cx43NT1 to α -tubulin. (G) Immunostaining after AP treatment. pCx43 (green). (H) Immunostaining after incubation of antibody with phosphopeptide. (I) Dual immunostaining with total Cx43 (green) and pCx43 (red) in primary bovine CE. Overlay appears yellow. (J) Immunostaining after detergent extraction. pCx43 (red). DAPI stains nuclei blue in all images.

5.3.5 CK1 δ phosphorylates Cx43-CT on serines 325, 328, 330

In order to test the phosphorylation of Cx43 by CK1 δ , we used recombinant CK1 δ (rCK1 δ), lacking the autoregulatory C-terminus, in an *in vitro* kinase assay with recombinant Cx43 C-terminus fused to GST (GST-Cx43CT). rCK1 δ phosphorylated the C-terminus as indicated by autoradiography (Fig. 5.5.A, reaction 3) but did not phosphorylate GST alone (Fig. 5.5.1, reaction 2). This was inhibited by incubating the reaction with PF670462 (Fig. 5.5.A, reaction 4), which specifically inhibits both the δ/ϵ forms of CK1 (Cheong, Hung et al. 2011). Using GST-Cx43CT as a substrate, rCK1 δ created an epitope specific for the pCx43 antibody (Fig. 5.5.b, reaction 2) that was inhibited by incubation with PF670462 (Fig. 5.5.B, reaction 3).

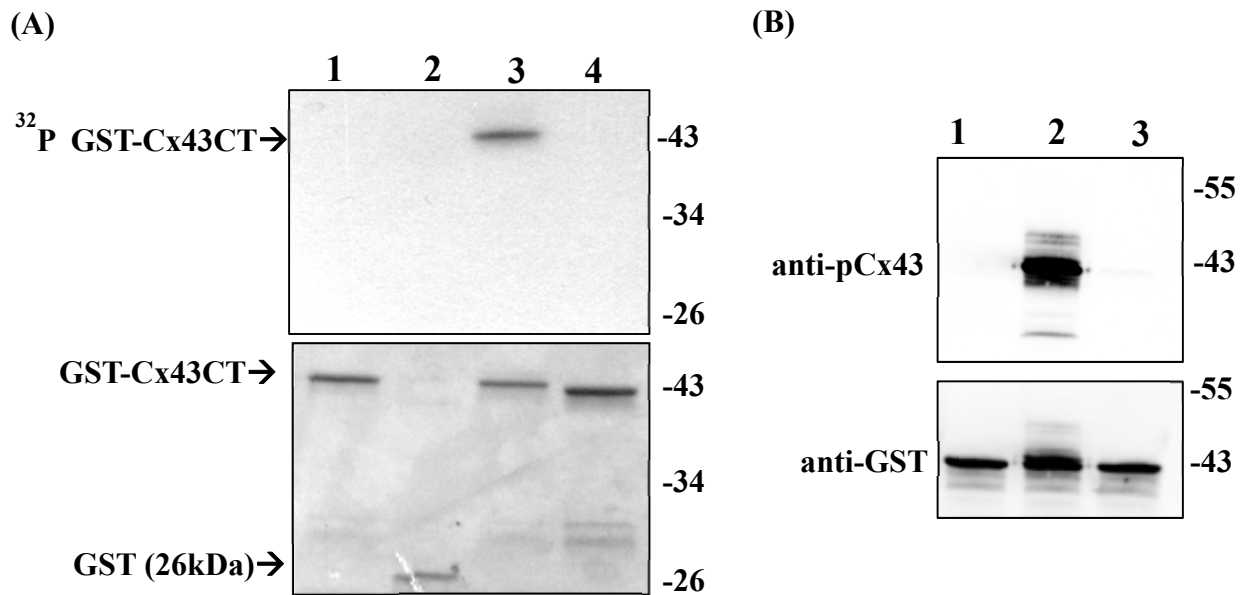
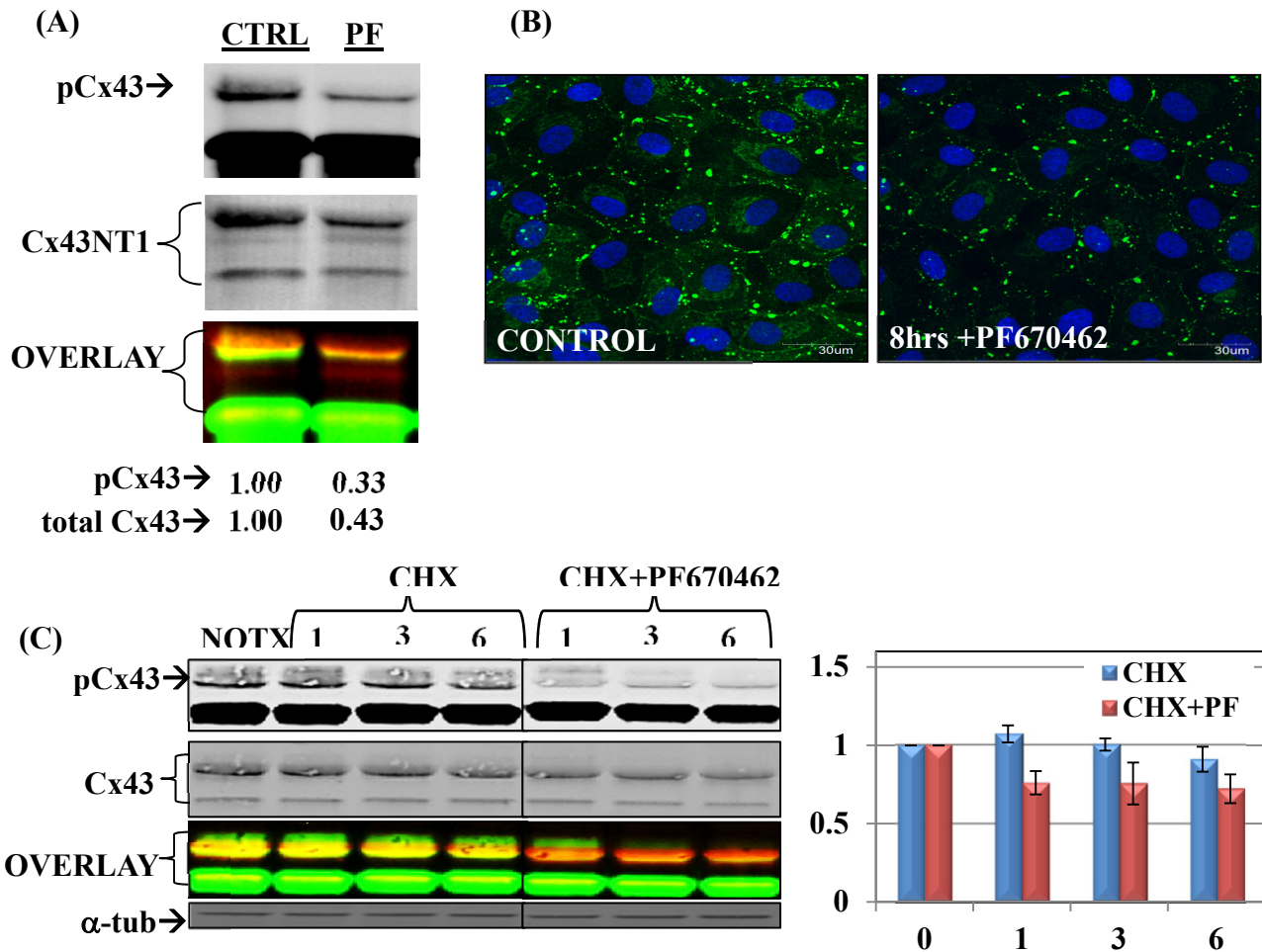
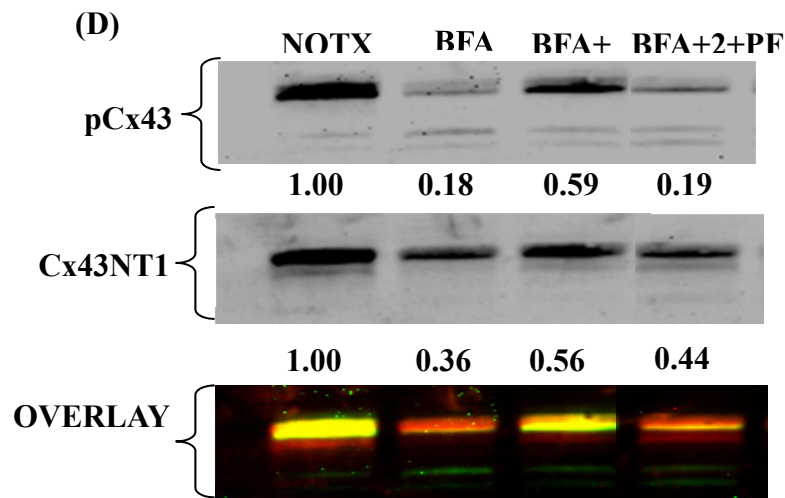


Figure 5.5: Recombinant CK1 δ phosphorylates Cx43 on specific residues *in vitro*. (A) Kinase assay testing ^{32}P incorporation into Cx43 C-terminal. 1) GST-Cx43CT alone (no rCK1 δ), 2) GST alone + rCK1 δ , 3) GST-Cx43CT + rCK1 δ , 4) GST-Cx43CT + rCK1 δ + PF670462. Upper is autoradiograph image of ^{32}P and lower is Coomassie stained gel. (B) "Cold" kinase assay testing phosphorylation of C-terminal serine 325, 328, 330. 1) GST-Cx43CT alone (no rCK1 δ), 2) GST-Cx43CT + rCK1 δ , 3) GST-Cx43CT + rCK1 δ + PF670462. Upper is immunoblot using pCx43 antibody and lower is immunoblot with GST antibody.

5.3.6 CK1 δ inhibitors reduce gap junction formation and Cx43 stability in CE

To determine the effect of CK1 δ inhibition on Cx43, PF670462 (specific for CK1 δ/ϵ) was used in CE cell cultures. Western analysis after 8 hour incubation with PF670462 demonstrated both reduced pCx43 and total levels of Cx43 (Fig. 5.6.A). Similar results were found with immunostaining as there was decreased Cx43 (Fig. 5.6.B). Therefore, it appeared that CK1 δ -mediated phosphorylation of Cx43 controlled Cx43 stability. To further test this we used cycloheximide chase experiments and found that including PF670462 decreased Cx43 abundance at a greater rate than with cycloheximide alone (Fig. 5.6.C). Next, to further distinguish CK1 δ 's role in gap junctions formation, cells were treated with brefeldin A followed by washout in the presence of PF670462. Cell surface Cx43 had reduced serine 325, 328, 330 phosphorylation with PF670462 and demonstrated string-like distribution of Cx43 unable to make larger aggregates like controls (Fig. 5.6.E). This was confirmed as PF670462 reduced Cx43 incorporation into the gap junction-associated detergent insoluble fraction (Fig. 5.6.D).





(E)

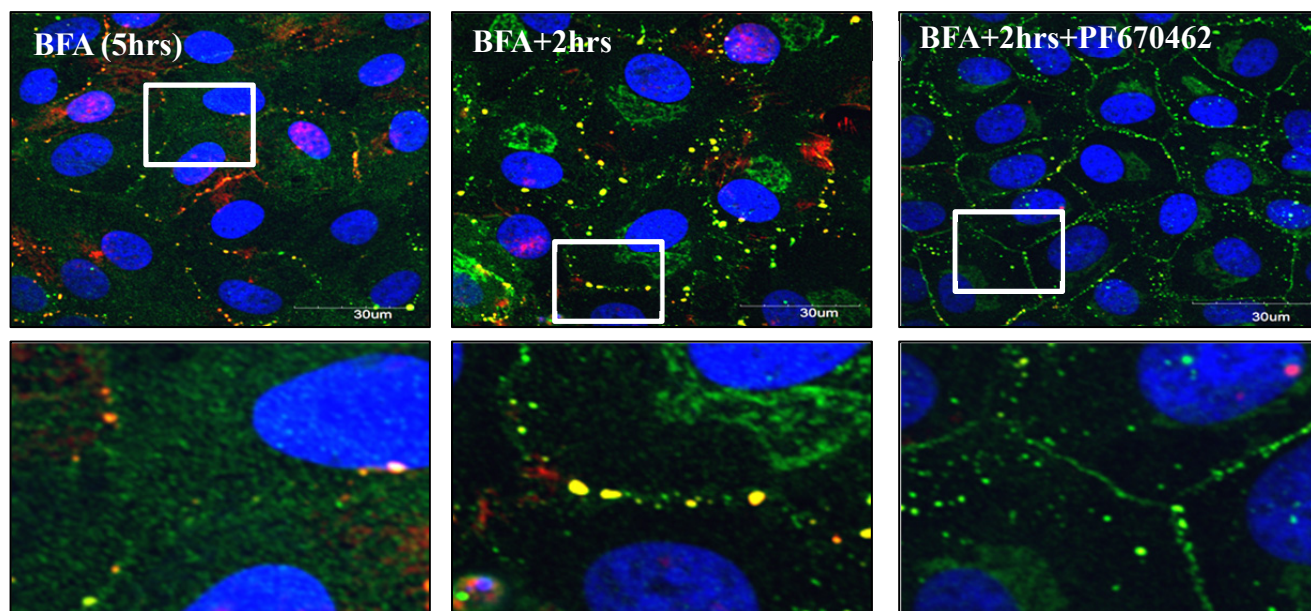


Figure 5.6: CK1 δ controls Cx43 stability and gap junction formation. (A) 8 hour treatment with PF670462 followed by dual immunoblotting with total Cx43NT1 (red) and pCx43 (green) antibodies. Areas of overlay appear yellow. (B) Similar treatment as in (A) followed by immunostaining with total Cx43 antibody (green). (C) CE cells treated with cycloheximide (CHX) with or without PF670462 for indicated times in hours. Dual immunoblotting with total Cx43NT1 (red) and pCx43 (green) antibodies. Areas of overlay appear yellow. Graph to right is mean \pm SEM of total Cx43/ α tub from two independent experiments. (D) Detergent insoluble fractions after brefeldin A (BFA) treatment with or without PF670462. BFA was used for 5 hours then washed out for 2 hours. Dual immunoblotting with total Cx43NT1 (red) and pCx43 (green) antibodies. Areas of overlay appear yellow. Quantification below is of pCx43 or total Cx43, normalized to control (NOTX). (E) Similar experiment to (D) followed by immunostaining with total Cx43 (green) and pCx43 (red) antibodies. Areas of overlay appear yellow and DAPI stains nuclei. White boxes are regions of interest magnified below.

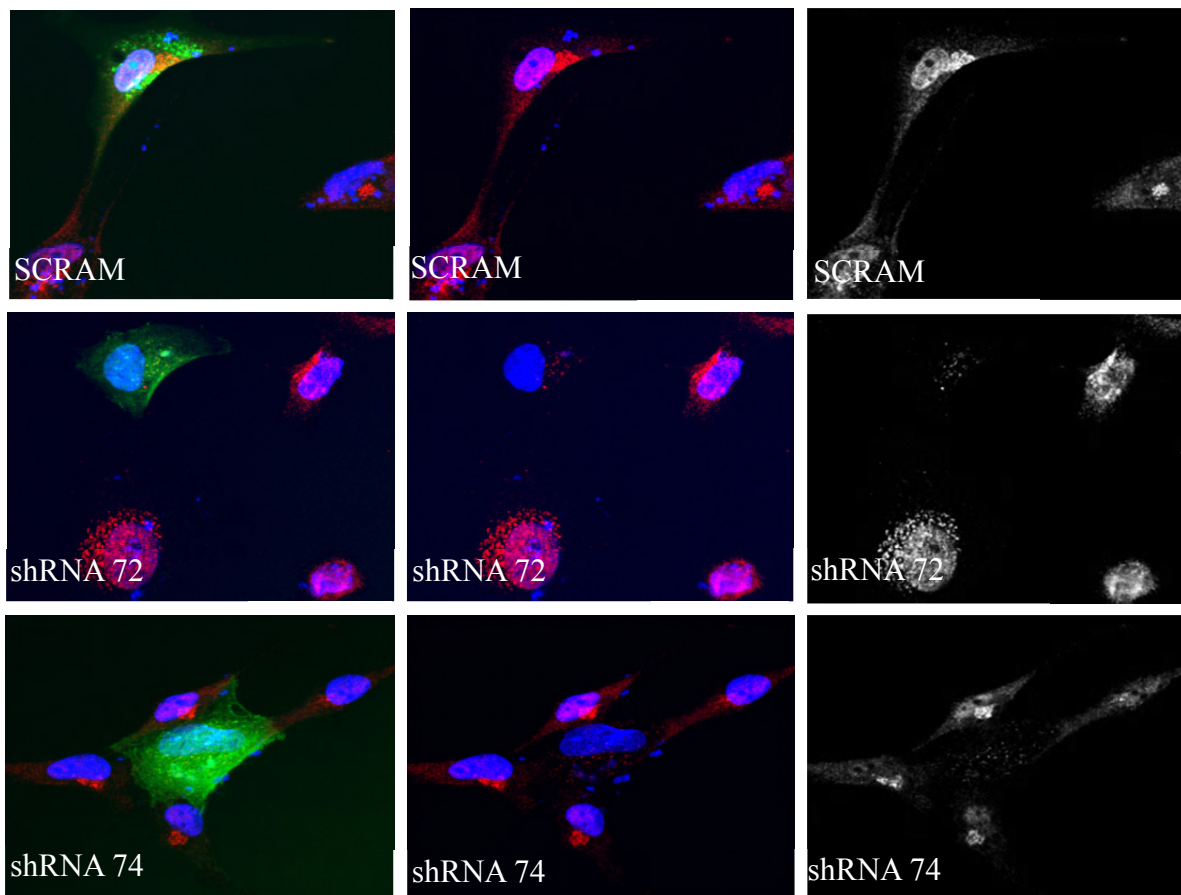
5.3.7 shRNAs against CK1 δ decreases pCx43 s325, 328, 330 in human corneal fibroblasts

Although PF670462 primarily inhibits CK1 δ , there is also potential for partial inhibition of CK1 ϵ . Therefore we used shRNAs specifically targeting CK1 δ to determine the effects on Cx43 phosphorylation. We were unable to knockdown CK1 δ in bovine cells with these shRNAs despite adequate transfection efficiency. Therefore, we used human corneal fibroblasts derived from corneoscleral rim donor tissue to observe the effects of CK1 δ knockdown. Using immunostaining we observed marked decreases in CK1 δ in the peri-nuclear and nuclear compartments with two separate shRNAs targeting CK1 δ (Fig. 5.7.A). Scrambled control shRNA did not affect CK1 δ . Because our shRNAs were GFP-labeled we then examined shRNA positive cells for pCx43 serine 325, 328, 330. The distribution of pCx43 was different from that of bovine CE cells being more peri-nuclear. However, shRNA-positive cells demonstrated a clear reduction in pCx43 levels (Fig. 5.7.B).

(A) GFP+DAPI+CK1 δ

DAPI+CK1 δ

CK1 δ alone



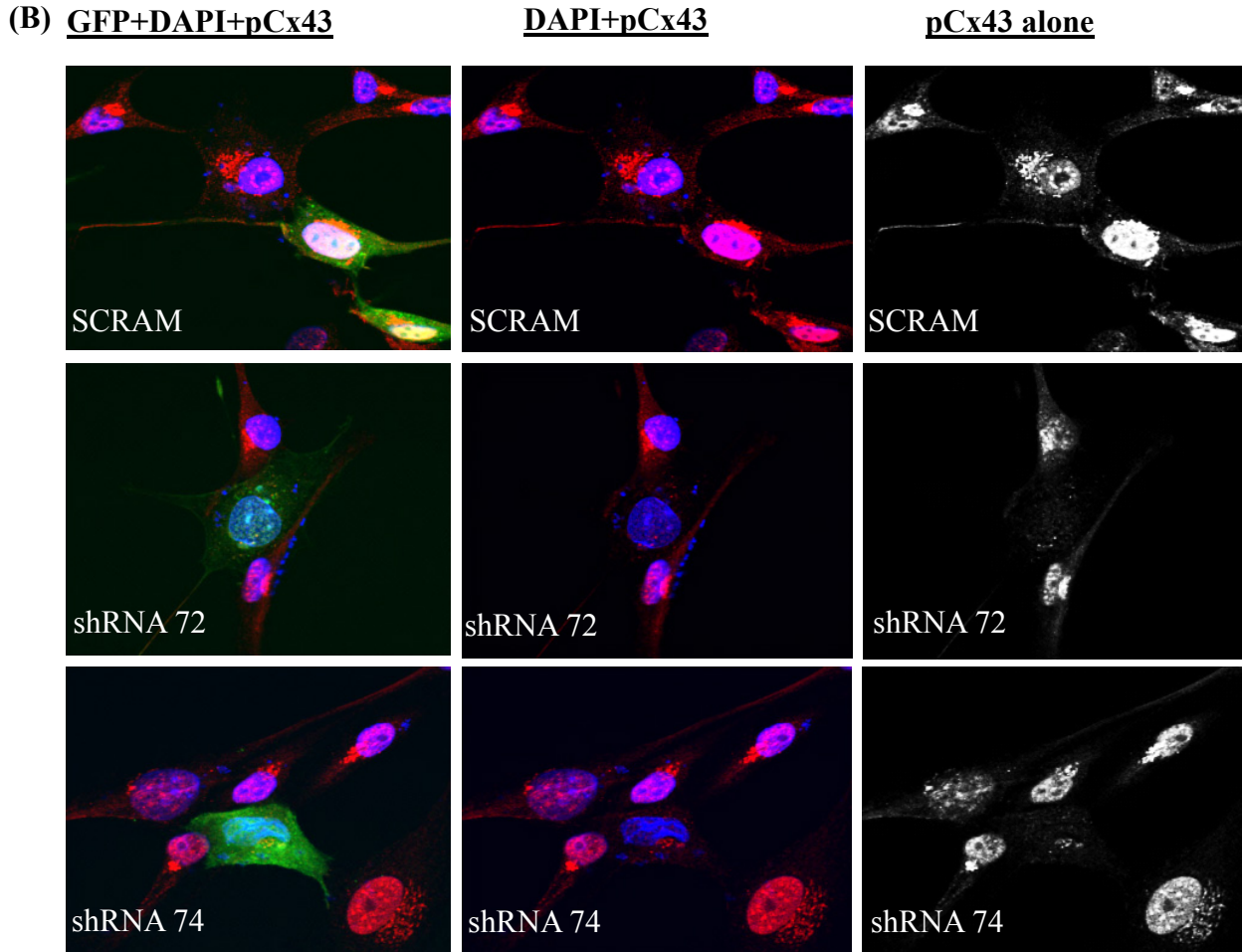


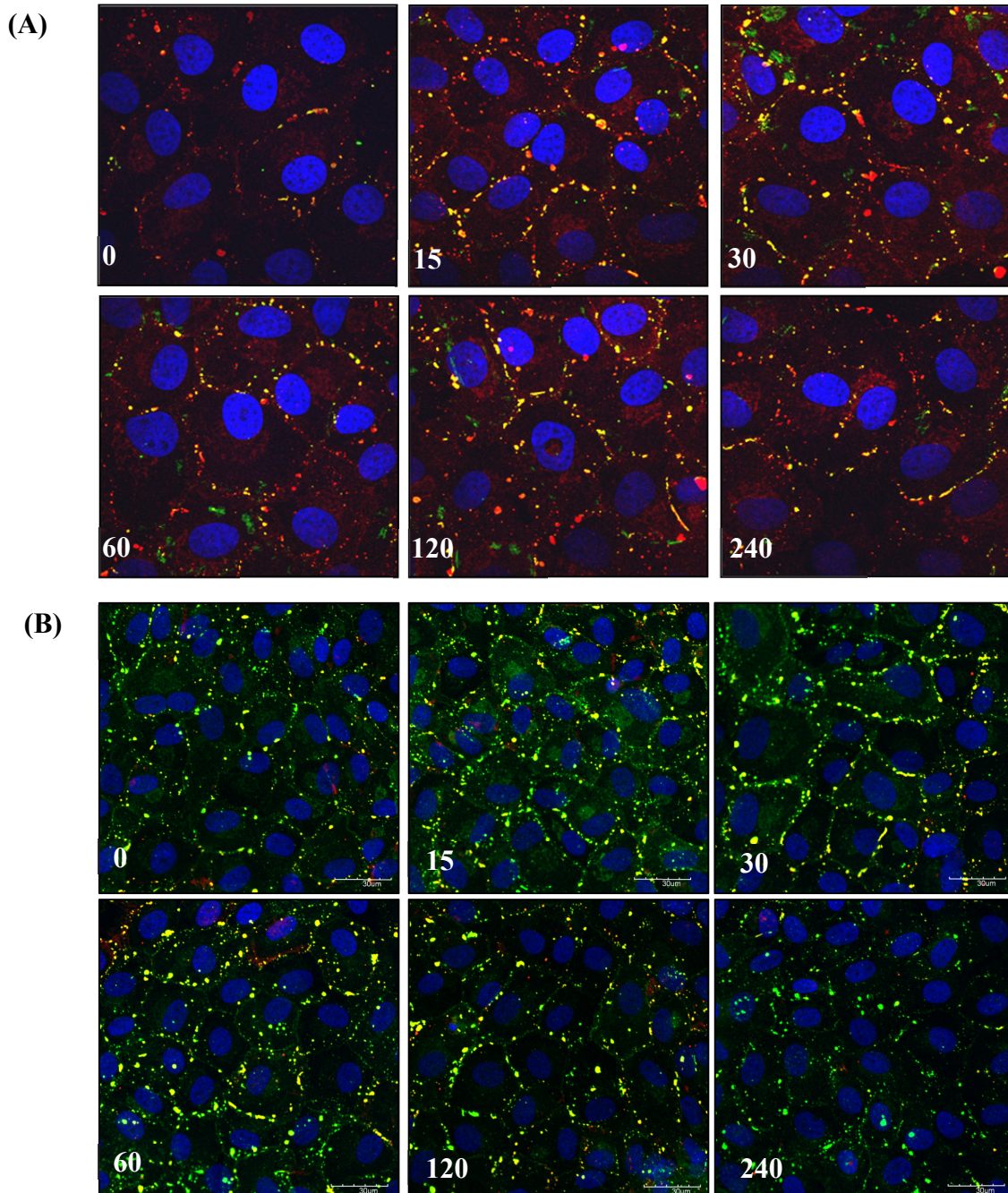
Figure 5.7: Effect of CK18 shRNA on pCx43. Human corneal fibroblasts were transfected with two shRNAs (shRNA 72 or shRNA 74) targeting CK18 or a scrambled shRNA (SCRAM). shRNA-transfected cells are GFP positive (green). (A) Immunostaining for CK18 (red) and DAPI. (B) Immunostaining for pCx43 and DAPI. Far right panels are grayscale to allow for easier viewing of CK18 or pCx43 alone.

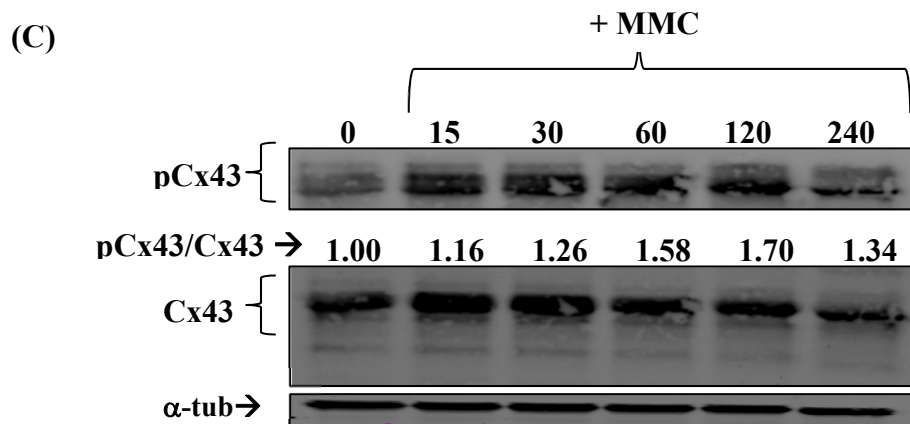
5.3.8 Genotoxic stress increases levels of pCx43 s325, 328, 330

Increases in total Cx43 were evident after genotoxic stress similar to our previous study (Roh and Funderburgh 2011). In order to distinguish the specific phosphorylated forms of Cx43 that were increased, we used our pCx43 antibody in immunoblotting and immunostaining after exposure to MMC and UVC. Dual staining with both total Cx43 and pCx43 antibodies demonstrated that large gap junction plaques were accumulating Cx43 phosphorylated on serines 325, 328, 330 after exposure to MMC and UVC (Fig. 5.8.A,B). We confirmed this result by

immunoblotting with both antibodies and found an increased proportion of total Cx43 phosphorylated on these residues after MMC. (Fig. 5.8.C).

Although we established a role for CK1 δ in regulation of Cx43 in homeostasis, we wanted to determine if this genotoxic stress-induced Cx43 accumulation was in part mediated by CK1 δ . Using CK1 inhibitors during genotoxic stress we found that the CK1 inhibitor CKI-7 prevented accumulation of Cx43 after MMC (Fig. 5.8.D).





(D)

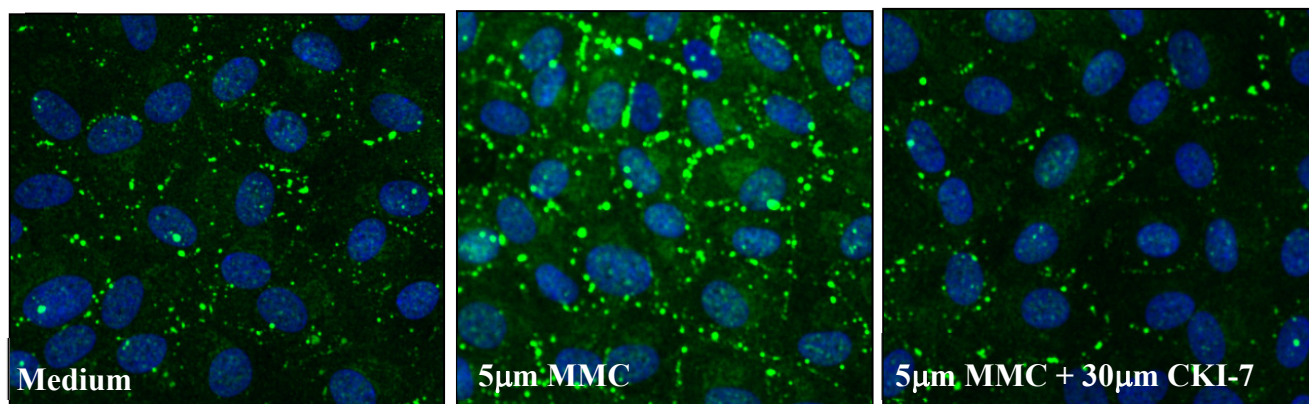


Figure 5.8: Genotoxic stress increases pCx43. (A) CE cells treated with 5 μM MMC for indicated time in minutes. Immunostaining of pCx43 (green) and total Cx43 (red). Overlay appears yellow. DAPI stains nuclei. (B) CE cells treated with 20 J/m^2 followed by recovery indicated by time in minutes. Immunostaining of pCx43 (red) and total Cx43 (green). Overlay appears yellow. DAPI stains nuclei. (C) Similar treatment as in (A) followed by immunoblotting with pCx43 and total Cx43 antibodies. Quantification is pCx43/Cx43/ α -tubulin and demonstrates increasing ratio. (D) 60 minute treatment with 5 μM MMC and 30 μM CKI-7. Immunostaining with total Cx43 (green) antibody. DAPI stains nuclei.

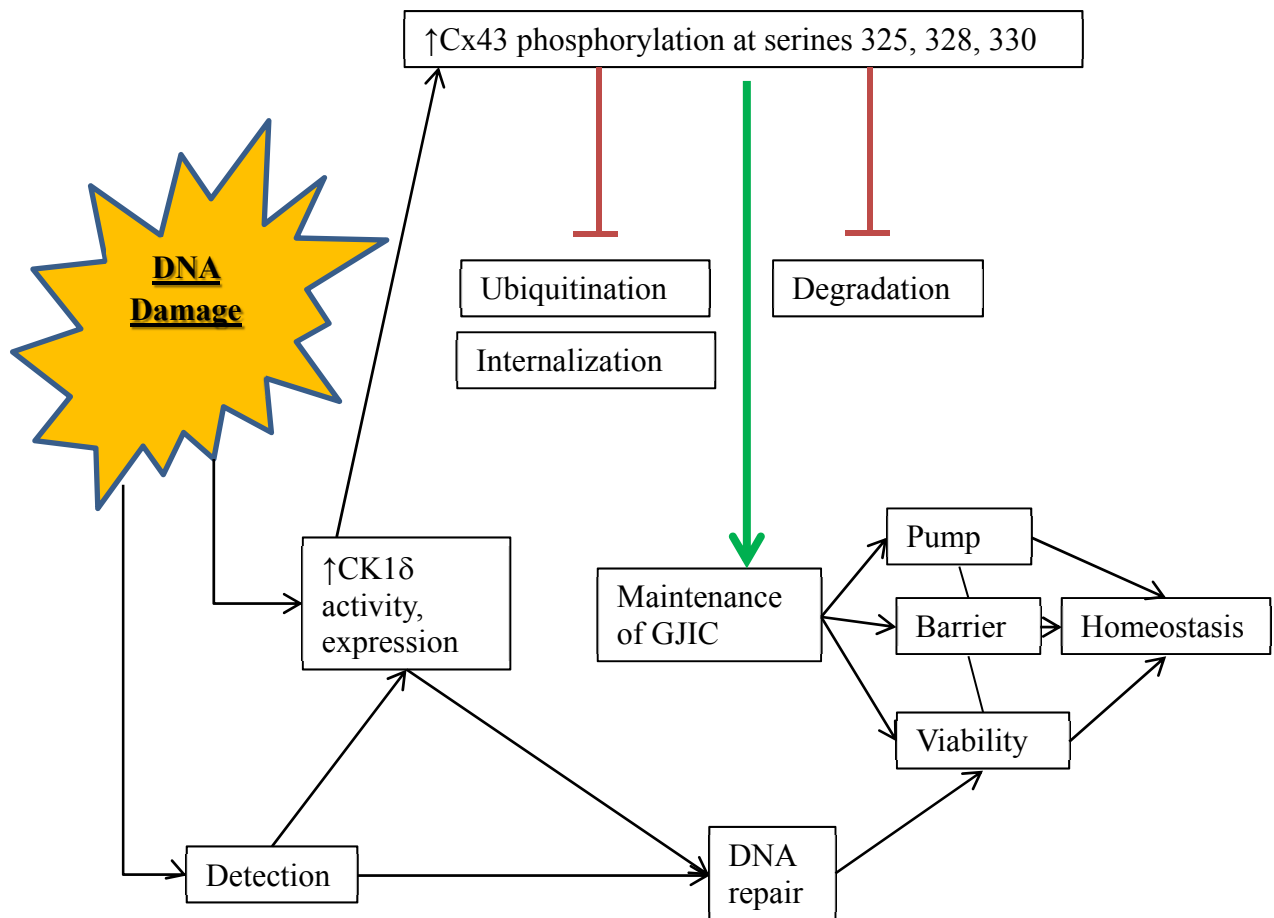


Figure 5.9: Potential model of events. In response to acute genotoxic stress, CE cells increase CK18 activity and expression. An unidentified molecular switch may be dephosphorylation of the C-terminal region of CK18 by protein phosphatases. As the kinase activity and levels of CK18 increase, so does its association and phosphorylation of Cx43. CK18 specifically phosphorylates serines 325, 328, 330 on the C-terminus which alters the trafficking, conformation, and binding partners. This phosphorylation allows for rapid accumulation into gap junction plaques and also prevents the binding of the cellular machinery involved in ubiquitination and internalization of cell surface Cx43. The rapid increase in gap junctions stabilizes intercellular communication from being disrupted allowing for the maintenance of CE functions. In addition, GJIC protects CE cells from DNA damage-induced apoptosis.

5.4 DISCUSSION

In this study we built upon our previous work characterizing genotoxic stress-induced changes in CE Cx43 and GJIC (Roh and Funderburgh 2011). In order to discern a potential signaling mechanism that was involved in these rapid changes in Cx43 we focused on CK18. We characterized the relationship between Cx43 and CK18 in CE cells and then further

distinguished CK1 δ 's role in regulating Cx43 in both homeostasis and after exposure to genotoxic stress. Our key findings include: (1) genotoxic stress simultaneously increases CK1 δ and (2) the presence of pCx43 in gap junction plaques; (3) CK1 δ is responsible for producing pCx43 in CE cells; (4) blocking CK1 δ reduces accumulation of Cx43 into large plaques associated with gap junctions; (5) reducing pCx43 via CK1 δ inhibition destabilizes Cx43 and gap junction plaques. These findings lead to the conclusion that the upregulation and stabilization of Cx43 and GJIC in response to genotoxic stress (Roh and Funderburgh 2011) is mediated by a transient increase in CK1 δ and an increased phosphorylation of specific residues in Cx43 by this kinase.

CK1 δ has ubiquitous expression patterns in numerous tissues and cells that account for its diverse roles in cell processes (Knippschild, Gocht et al. 2005; Lohler, Hirner et al. 2009). Cell-specific CK1 δ distribution is dependent on its catalytic activity as kinase activity has been shown to regulate CK1 δ sub-cellular localization (Milne, Looby et al. 2001). Genotoxic stress rapidly increased total levels of CK1 δ in CE cells (Fig. 5.2). Immunostaining showed increased CK1 δ was most pronounced in the peri-nuclear compartment and also in the nucleus (Fig. 5.2.C). The nuclear accumulation of CK1 δ in CE cells may be involved in the DNA damage response as CK1 δ has roles in p53 and MDM2 phosphorylation after genotoxic stress (Knippschild, Milne et al. 1997; Alsheich-Bartok, Haupt et al. 2008; Inuzuka, Tseng et al. 2010). The peri-nuclear accumulation may impact membrane trafficking of the many substrates of CK1 δ (Behrend, Stoter et al. 2000; Yu and Roth 2002; Yan, Spruce et al. 2007), including Cx43.

We evaluated the relationship between Cx43 and CK1 δ in CE cells using biochemical assays and immunostaining under non-stressed and stressed conditions. Co-IP documented the interaction between Cx43 and CK1 δ in cell lysates (Fig. 5.3.A). All forms of Cx43 were present in both IPs suggesting that CK1 δ is in complexes containing different forms of Cx43. Genotoxic stress to CE cells resulted in increased co-localization with Cx43 (Fig. 5.3.D) and Co-IP demonstrated that the relative amount of CK1 δ associated with Cx43 increased after MMC treatment (Fig. 5.3.C). This concentration of newly interacting Cx43 and CK1 δ may allow for increased downstream phosphorylation of Cx43 and influence subsequent gap junction formation.

To further characterize the functional consequences of CK1 δ -mediated phosphorylation of Cx43 (Fig. 5.5.A) *in vivo* we created, validated (Fig. 5.4) and used a phosphospecific antibody against Cx43 (pCx43). A key finding that links CK1 δ specifically to the pCx43 sites was that CK1 δ created the epitope for our pCx43 antibody by phosphorylating serines 325, 328, 330 (Fig. 5.5.B). pCx43 and gap junction formation was consistently blocked with inhibition of CK1 δ (Fig. 5.6). We observed long, string-like Cx43 staining with PF670462 incubation compared to the normal rounded and punctate gap junction plaques (Fig. 5.6.E) which may result from reduced ability for aggregation. These specific serine residues may control the ability for Cx43 to aggregate into gap junctions as other proteins phosphorylated by CK1 δ , such as tau, have increased aggregation after CK1 δ phosphorylation (Schwab, DeMaggio et al. 2000; Li, Yin et al. 2004; Hanger, Byers et al. 2007). In addition to gap junction formation, our results also suggest that CK1 δ phosphorylation controls overall Cx43 stability (Fig 5.6). Thus, as nascent Cx43 becomes progressively phosphorylated and is targeted to the periphery of gap junction plaques, those Cx43 molecules not phosphorylated on serines 325, 328, 330 by CK1 δ may become destined for degradation instead of becoming incorporated into gap junctions.

Genotoxic stress with MMC rapidly increases Cx43 in CE cells (Roh and Funderburgh 2011) which we found to include Cx43 phosphorylated on serine 325, 328, 330 (Fig. 5.8). We observed increases in CK1 δ after MMC and UVC treatment (Fig. 5.8) demonstrating a responsive nature of CE CK1 δ to genotoxic stress. Therefore, it appears that CK1 δ may have a distinct role in accumulation of Cx43 after DNA damage in CE cells. This may occur through two mechanisms. First, CK1 δ kinase activity may be elevated after genotoxic stress. CK1 δ has been shown to have higher kinase activity after DNA damage which stabilizes p53 levels (Knippschild, Milne et al. 1997; Sakaguchi, Saito et al. 2000; Inuzuka, Tseng et al. 2010). Future studies assessing CK1 δ activity towards Cx43 would specifically link DNA damage with increased active Cx43 phosphorylation. In a second potential mechanism CK1 δ expression may increase resulting in more interaction with Cx43, more phosphorylation, and enhanced gap junction assembly. This seems consistent with our data thus far as we had previously observed increased forward trafficking of Cx43 into gap junctions after MMC treatment (Roh and Funderburgh 2011).

The importance of phosphorylation of serine 325, 328, 330 and accumulation of Cx43 may be to enhance survival and maintain homeostasis as outlined in a hypothetical model (Fig. 5.9). The specific effects of increased serine 325, 328, 330 Cx43 phosphorylation may be to reduce interaction with internalization and degradative cellular machinery. As we found in our previous study (Roh and Funderburgh 2011), the relationship between Cx43 and ZO-1 was significantly reduced after genotoxic stress which may be a result of increased serine 325, 328, 330 phosphorylation. Changes in structure, charge, or binding partners may decrease the ability of ZO-1 to bind to the C-terminus which would result in enhancement of the connexon to gap junction transition (Rhett, Jourdan et al. 2011). Additionally, ubiquitination machinery which also controls Cx43 internalization and degradation (Kjenseth, Fykerud et al. 2010) may have reduced binding to Cx43 phosphorylated on serine 325, 328, 330. Determining the binding profile of Cx43 phosphorylated on serine 325, 328, 330 will help elucidate the machinery involved in this stabilization. In conclusion, because stabilization of Cx43 and GJIC appears to be protective in CE cells, identifying and manipulating the specific signaling pathways to enhance Cx43 stability and gap junction formation may be an approach to protect CE cells during acute genotoxic stress.

6.0 OVERALL CONCLUSIONS & SIGNIFICANCE

The corneal endothelium was recently characterized by the scientist and ophthalmologist William Bourne as “*the single layer of cells responsible for corneal clarity and maintain[ing] the window to the soul*” (Bourne 2010). This statement may have particular meaning to the over 42,000 individuals who receive corneal transplants in the United States, many of which are the result of corneal endothelial dysfunction. Professor Bourne goes on to state that “the reluctance [of the corneal endothelium] to divide is not understood” and that “future knowledge of the corneal endothelium will lead to improvements in the treatment of corneal disease” (Bourne 2010). It is becoming increasingly clear that there is a prominent role for DNA damage in the aging and fragility of the corneal endothelium and this knowledge will help us to understand new intricacies necessary to improve and develop treatments for corneal disease.

The documentation of a novel exposure to genotoxic stress (mitomycin C) during photorefractive keratectomy highlights the need for clinician and patient awareness during ocular procedures. Common clinical and surgical practice can induce DNA damage and must be taken into consideration given the vulnerability of the corneal endothelium. It is becoming more evident that the corneal endothelium is exposed to and impacted substantially by genotoxic stress from iatrogenic causes. Surprisingly, there are still current recommendations on how to use MMC in refractive surgery despite the evidence that it can affect corneal endothelial DNA.

The genetic mouse model of DNA repair deficiency further exemplifies the need to understand why the corneal endothelium succumbs to genotoxic stress in disease and aging. From this *in vivo* mouse study it is clear that the corneal endothelium is extremely sensitive and vulnerable to the effects of unrepaired endogenous DNA damage. Therefore, it is likely that DNA damage has a considerable role in the non-proliferative state of the corneal endothelium. Remarkably, the mice in our study did not receive exogenous or environmental DNA damaging exposures yet the corneal endothelium prematurely developed age-related degenerative changes.

This further implicates the high metabolic nature of the corneal endothelium and the byproducts of this metabolism, namely reactive oxygen species and their downstream targets, in degenerative changes. Chronic oxidative stress has been linked to the formation of endogenous DNA interstrand crosslinks believed to have role in aging. DNA damage in corneal endothelium must be taken into consideration while efforts to enhance the proliferation of these cells may bring about increased cell death or drastic alterations in cell behavior due to the accumulation of unrepaired DNA damage over decades of life. In addition, as corneal donor tissue from older donors is continuing to be used in corneal transplantations, the role of accumulating DNA damage should receive careful consideration in graft success and failure.

Finally, a greater understanding of how corneal endothelial cells respond to stress at the cellular level is essential in developing new methods to preserve them. In my studies I have only begun to implicate a role for gap junctions in protecting the corneal endothelium from injury and death in an acute setting. Although I found that gap junction intercellular communication was protective over an eighteen-hour period, additional time points will be necessary to evaluate this response during longer exposures to genotoxic stress. Further dissection of the molecular pathways driving this response and others can then be used as specific targets to preserve both the function and viability of these cells. The amelioration of corneal endothelial aging and degeneration, which can be expected to follow from understanding basic stress responses, should have significant impact on the vision and well-being of people far and wide.

APPENDIX A

SUPPLEMENTAL FIGURES

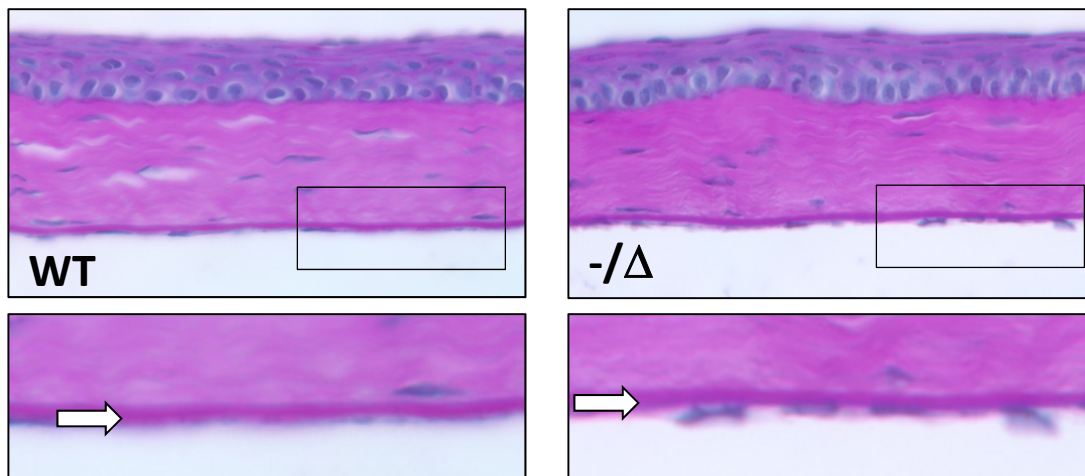


Figure S.1: PAS staining. Periodic Schiff staining (PAS) of mouse corneas from wildtype (WT) and *Ercc1*^{-Δ} mice at 27 weeks. Images below are magnification of upper images black boxes and highlight Descemet's membrane (white arrows).

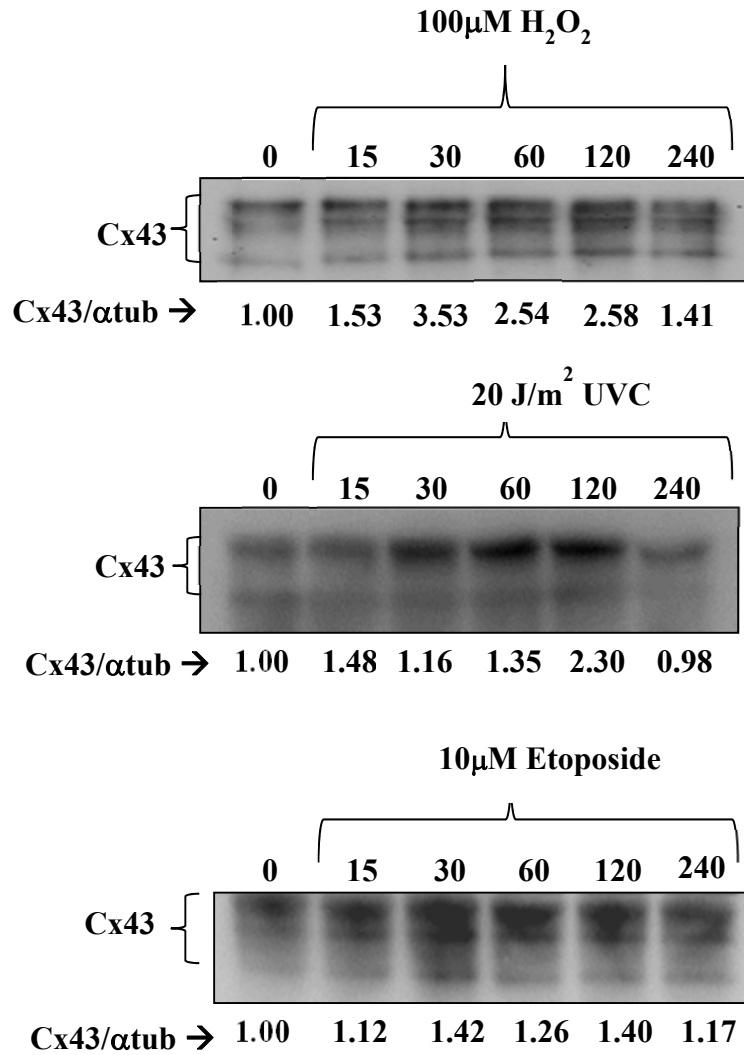


Figure S.2 Cx43 accumulation after genotoxic stress. Confluent CE cells treated with 100 μM H₂O₂, 20 J/m² UVC, and 10 μM etoposide for the indicated times in minutes. Immunoblotting with a total Cx43 antibody and α-tubulin antibody (not shown). Quantification is ratio of Cx43/α-tubulin

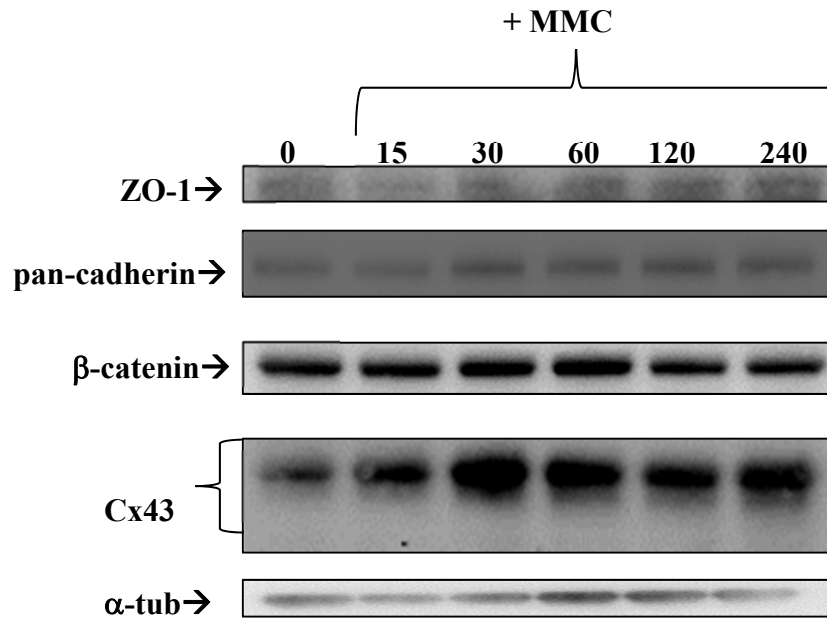


Figure S.3: Cell-cell junctions after MMC. Confluent CE cells treated with 5 μ M MMC for the indicated times in minutes. Immunoblotting with antibodies against ZO-1, cadherins, β -catenin, Cx43, and α -tubulin.

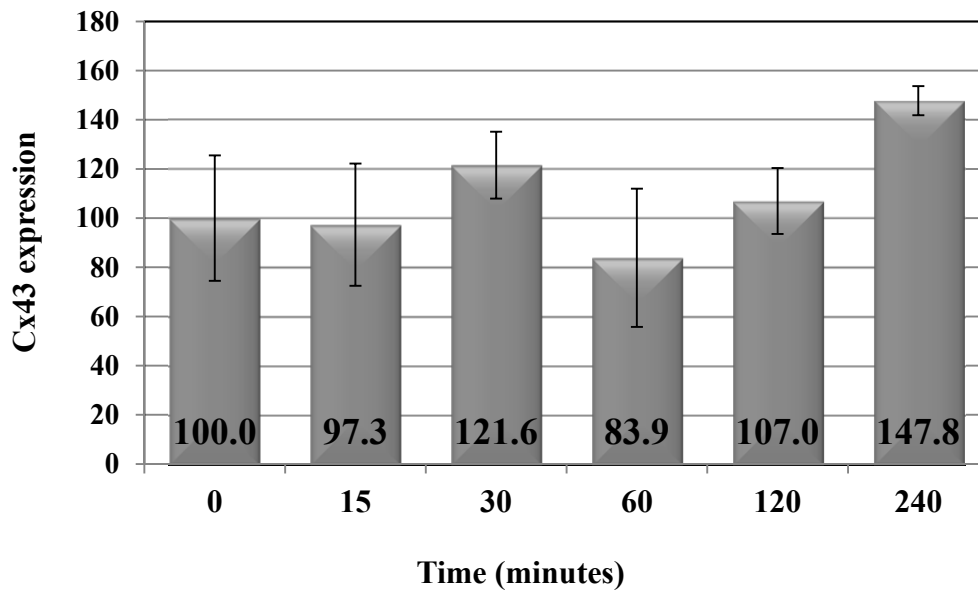


Figure S.4: Cx43 expression after MMC. Confluent CE cells treated with 5 μ M MMC for the indicated times in minutes. Quantitative RT-PCR was used to quantify Cx43 expression. Data is normalized to time "0".

BIBLIOGRAPHY

- Abbas, T., M. Olivier, et al. (2002). "Differential activation of p53 by the various adducts of mitomycin C." J Biol Chem **277**(43): 40513-40519.
- Abdelmohsen, K., E. Sauerbier, et al. (2007). "Epidermal growth factor- and stress-induced loss of gap junctional communication is mediated by ERK-1/ERK-2 but not ERK-5 in rat liver epithelial cells." Biochem Biophys Res Commun **364**(2): 313-317.
- Abraham, L. M., D. Selva, et al. (2006). "Mitomycin: clinical applications in ophthalmic practice." Drugs **66**(3): 321-340.
- Ahmad, A., A. R. Robinson, et al. (2008). "ERCC1-XPF endonuclease facilitates DNA double-strand break repair." Mol Cell Biol **28**(16): 5082-5092.
- Albright, C. D., J. Kuo, et al. (2001). "cAMP enhances Cx43 gap junction formation and function and reverses choline deficiency apoptosis." Exp Mol Pathol **71**(1): 34-39.
- Alexander, D. B. and G. S. Goldberg (2003). "Transfer of biologically important molecules between cells through gap junction channels." Curr Med Chem **10**(19): 2045-2058.
- Alsheich-Bartok, O., S. Haupt, et al. (2008). "PML enhances the regulation of p53 by CK1 in response to DNA damage." Oncogene **27**(26): 3653-3661.
- Avisar, R., I. Avisar, et al. (2008). "Effect of mitomycin C in pterygium surgery on corneal endothelium." Cornea **27**(5): 559-561.
- Azzam, E. I., S. M. de Toledo, et al. (2003). "Expression of CONNEXIN43 is highly sensitive to ionizing radiation and other environmental stresses." Cancer Res **63**(21): 7128-7135.
- Banaz-Yasar, F., R. Tischka, et al. (2005). "Cell line specific modulation of connexin43 expression after exposure to ionizing radiation." Cell Commun Adhes **12**(5-6): 249-259.
- Barker, R. J., R. L. Price, et al. (2002). "Increased association of ZO-1 with connexin43 during remodeling of cardiac gap junctions." Circ Res **90**(3): 317-324.
- Beardslee, M. A., J. G. Laing, et al. (1998). "Rapid turnover of connexin43 in the adult rat heart." Circ Res **83**(6): 629-635.
- Bedei, A., A. Marabotti, et al. (2006). "Photorefractive keratectomy in high myopic defects with or without intraoperative mitomycin C: 1-year results." Eur J Ophthalmol **16**(2): 229-234.
- Behrend, L., M. Stoter, et al. (2000). "Interaction of casein kinase 1 delta (CK1delta) with post-Golgi structures, microtubules and the spindle apparatus." Eur J Cell Biol **79**(4): 240-251.
- Ben-Yehoyada, M., L. C. Wang, et al. (2009). "Checkpoint signaling from a single DNA interstrand crosslink." Mol Cell **35**(5): 704-715.

- Bensimon, A., R. Aebersold, et al. (2011). "Beyond ATM: The protein kinase landscape of the DNA damage response." FEBS Lett **585**(11): 1625-1639.
- Bergmanson, J. P., T. M. Sheldon, et al. (1999). "Fuchs' endothelial dystrophy: a fresh look at an aging disease." Ophthalmic Physiol Opt **19**(3): 210-222.
- Berthoud, V. M., P. J. Minogue, et al. (2004). "Pathways for degradation of connexins and gap junctions." Cardiovasc Res **62**(2): 256-267.
- Bissen-Miyajima, H. (2008). "Ophthalmic viscosurgical devices." Curr Opin Ophthalmol **19**(1): 50-54.
- Boamah, E. K., D. E. White, et al. (2007). "Mitomycin-DNA adducts induce p53-dependent and p53-independent cell death pathways." ACS Chem Biol **2**(6): 399-407.
- Bonanno, J. A. (2003). "Identity and regulation of ion transport mechanisms in the corneal endothelium." Prog Retin Eye Res **22**(1): 69-94.
- Bonanno, J. A. (2011). "Molecular mechanisms underlying the corneal endothelial pump." Exp Eye Res.
- Bourne, W. M. (2003). "Biology of the corneal endothelium in health and disease." Eye (Lond) **17**(8): 912-918.
- Bourne, W. M. (2010). "Corneal endothelium--past, present, and future." Eye Contact Lens **36**(5): 310-314.
- Bourne, W. M. and J. W. McLaren (2004). "Clinical responses of the corneal endothelium." Exp Eye Res **78**(3): 561-572.
- Bourne, W. M., L. R. Nelson, et al. (1997). "Central corneal endothelial cell changes over a ten-year period." Invest Ophthalmol Vis Sci **38**(3): 779-782.
- Bruce, A. F., S. Rothery, et al. (2008). "Gap junction remodelling in human heart failure is associated with increased interaction of connexin43 with ZO-1." Cardiovasc Res **77**(4): 757-765.
- Burtner, C. R. and B. K. Kennedy (2010). "Progeria syndromes and ageing: what is the connection?" Nat Rev Mol Cell Biol **11**(8): 567-578.
- Cadet, J., T. Douki, et al. (2003). "Oxidative damage to DNA: formation, measurement and biochemical features." Mutat Res **531**(1-2): 5-23.
- Calera, M. R., H. L. Topley, et al. (2006). "Connexin43 is required for production of the aqueous humor in the murine eye." J Cell Sci **119**(Pt 21): 4510-4519.
- Campisi, J. and F. d'Adda di Fagagna (2007). "Cellular senescence: when bad things happen to good cells." Nat Rev Mol Cell Biol **8**(9): 729-740.
- Carones, F., L. Vigo, et al. (2002). "Evaluation of the prophylactic use of mitomycin-C to inhibit haze formation after photorefractive keratectomy." J Cataract Refract Surg **28**(12): 2088-2095.
- Catarino, S. M., J. S. Ramalho, et al. (2011). "Ubiquitin-mediated internalization of Connexin43 is independent on the canonical endocytic tyrosine-sorting signal." Biochem J.
- Chabner, B. A., P. C. Amrein, et al. (2006). Antineoplastic Agents. Goodman and Gilman's The Pharmacological Basis of Therapeutics, 11th Edition. B. LL, L. JS and P. KL. New York, NY McGraw Hill.
- Chang, S. W. (2004). "Early corneal edema following topical application of mitomycin-C." J Cataract Refract Surg **30**(8): 1742-1750.

- Chang, S. W. (2005). "Corneal keratocyte apoptosis following topical intraoperative mitomycin C in rabbits." J Refract Surg **21**(5): 446-453.
- Chang, S. W., S. F. Chou, et al. (2010). "Dexamethasone reduces mitomycin C-related inflammatory cytokine expression without inducing further cell death in corneal fibroblasts." Wound Repair Regen **18**(1): 59-69.
- Chen, J., L. Pan, et al. (2008). "Domain-swapped dimerization of ZO-1 PDZ2 generates specific and regulatory connexin43-binding sites." EMBO J **27**(15): 2113-2123.
- Chen, T. C. and S. W. Chang (2010). "Effect of mitomycin C on IL-1R expression, IL-1-related hepatocyte growth factor secretion and corneal epithelial cell migration." Invest Ophthalmol Vis Sci **51**(3): 1389-1396.
- Cheong, J. K., N. T. Hung, et al. (2011). "IC261 induces cell cycle arrest and apoptosis of human cancer cells via CK1delta/varepsilon and Wnt/beta-catenin independent inhibition of mitotic spindle formation." Oncogene.
- Chew, S. S., C. S. Johnson, et al. (2010). "Role of connexin43 in central nervous system injury." Exp Neurol **225**(2): 250-261.
- Chowdhury, D., M. C. Keogh, et al. (2005). "gamma-H2AX dephosphorylation by protein phosphatase 2A facilitates DNA double-strand break repair." Mol Cell **20**(5): 801-809.
- Chung, D. J., C. H. Castro, et al. (2006). "Low peak bone mass and attenuated anabolic response to parathyroid hormone in mice with an osteoblast-specific deletion of connexin43." J Cell Sci **119**(Pt 20): 4187-4198.
- Cooper, C. D. and P. D. Lampe (2002). "Casein kinase 1 regulates connexin-43 gap junction assembly." J Biol Chem **277**(47): 44962-44968.
- Corwin, W. L., J. M. Baust, et al. (2011). "The unfolded protein response in human corneal endothelial cells following hypothermic storage: Implications of a novel stress pathway." Cryobiology.
- Cotrina, M. L., J. H. Lin, et al. (2008). "Adhesive properties of connexin hemichannels." Glia **56**(16): 1791-1798.
- Crawford, K. M., S. A. Ernst, et al. (1995). "NaK-ATPase pump sites in cultured bovine corneal endothelium of varying cell density at confluence." Invest Ophthalmol Vis Sci **36**(7): 1317-1326.
- de Benito-Llopis, L., M. A. Teus, et al. (2007). "Effect of mitomycin-C on the corneal endothelium during excimer laser surface ablation." J Cataract Refract Surg **33**(6): 1009-1013.
- De Silva, I. U., P. J. McHugh, et al. (2000). "Defining the roles of nucleotide excision repair and recombination in the repair of DNA interstrand cross-links in mammalian cells." Mol Cell Biol **20**(21): 7980-7990.
- Decrock, E., M. Vinken, et al. (2011). "Calcium and connexin-based intercellular communication, a deadly catch?" Cell Calcium.
- Decrock, E., M. Vinken, et al. (2009). "Connexin-related signaling in cell death: to live or let die?" Cell Death Differ **16**(4): 524-536.
- DelMonte, D. W. and T. Kim (2011). "Anatomy and physiology of the cornea." J Cataract Refract Surg **37**(3): 588-598.
- Diakonis, V. F., A. Pallikaris, et al. (2007). "Alterations in endothelial cell density after photorefractive keratectomy with adjuvant mitomycin." Am J Ophthalmol **144**(1): 99-103.
- Dolle, M. E., R. A. Busuttil, et al. (2006). "Increased genomic instability is not a prerequisite for shortened lifespan in DNA repair deficient mice." Mutat Res **596**(1-2): 22-35.

- Dollfus, H., F. Porto, et al. (2003). "Ocular manifestations in the inherited DNA repair disorders." Surv Ophthalmol **48**(1): 107-122.
- Dowling-Warriner, C. V. and J. E. Trosko (2000). "Induction of gap junctional intercellular communication, connexin43 expression, and subsequent differentiation in human fetal neuronal cells by stimulation of the cyclic AMP pathway." Neuroscience **95**(3): 859-868.
- Downey M, D. D. (2006). "gammaH2AX as a checkpoint maintenance signal." Cell Cycle **5**(13): 1376-1381.
- Dronkert, M. L. and R. Kanaar (2001). "Repair of DNA interstrand cross-links." Mutat Res **486**(4): 217-247.
- Du, Y., E. C. Carlson, et al. (2009). "Stem cell therapy restores transparency to defective murine corneas." Stem Cells **27**(7): 1635-1642.
- Du, Y., M. L. Funderburgh, et al. (2005). "Multipotent stem cells in human corneal stroma." Stem Cells **23**(9): 1266-1275.
- Dupre-Crochet, S., A. Figueroa, et al. (2007). "Casein kinase 1 is a novel negative regulator of E-cadherin-based cell-cell contacts." Mol Cell Biol **27**(10): 3804-3816.
- Edelhauser, H. F. (2006). "The balance between corneal transparency and edema: the Proctor Lecture." Invest Ophthalmol Vis Sci **47**(5): 1754-1767.
- Elias, L. A., D. D. Wang, et al. (2007). "Gap junction adhesion is necessary for radial migration in the neocortex." Nature **448**(7156): 901-907.
- Engler, C., C. Kelliher, et al. (2010). "Unfolded protein response in fuchs endothelial corneal dystrophy: a unifying pathogenic pathway?" Am J Ophthalmol **149**(2): 194-202 e192.
- Enomoto, K., T. Mimura, et al. (2006). "Age differences in cyclin-dependent kinase inhibitor expression and rb hyperphosphorylation in human corneal endothelial cells." Invest Ophthalmol Vis Sci **47**(10): 4330-4340.
- Falk, M. M. (2000). "Connexin-specific distribution within gap junctions revealed in living cells." J Cell Sci **113** (Pt 22): 4109-4120.
- Falk, M. M., S. M. Baker, et al. (2009). "Gap junction turnover is achieved by the internalization of small endocytic double-membrane vesicles." Mol Biol Cell **20**(14): 3342-3352.
- Flenniken, A. M., L. R. Osborne, et al. (2005). "A Gja1 missense mutation in a mouse model of oculodentodigital dysplasia." Development **132**(19): 4375-4386.
- Fraunfelder, F. W. (2006). "Corneal toxicity from topical ocular and systemic medications." Cornea **25**(10): 1133-1138.
- Fry, R. C., T. J. Begley, et al. (2005). "Genome-wide responses to DNA-damaging agents." Annu Rev Microbiol **59**: 357-377.
- Fuchsluger, T. A., U. Jurkunas, et al. (2011). "Anti-apoptotic gene therapy prolongs survival of corneal endothelial cells during storage." Gene Ther.
- Fukuchi, T., Y. Hayakawa, et al. (2002). "Corneal endothelial damage after trabeculectomy with mitomycin C in two patients with glaucoma with cornea guttata." Cornea **21**(3): 300-304.
- Gabriele, M. L., H. Ishikawa, et al. (2010). "Reproducibility of Spectral-Domain Optical Coherence Tomography Total Retinal Thickness Measurements in Mice." Invest Ophthalmol Vis Sci.

- Gagnon, M. M., H. M. Boisjoly, et al. (1997). "Corneal endothelial cell density in glaucoma." Cornea **16**(3): 314-318.
- Gaietta, G., T. J. Deerinck, et al. (2002). "Multicolor and electron microscopic imaging of connexin trafficking." Science **296**(5567): 503-507.
- Gambato, C., A. Ghirlando, et al. (2005). "Mitomycin C modulation of corneal wound healing after photorefractive keratectomy in highly myopic eyes." Ophthalmology **112**(2): 208-218; discussion 219.
- Gambichler, T., S. Rotterdam, et al. (2008). "Impact of ultraviolet radiation on the expression of marker proteins of gap and adhesion junctions in human epidermis." Photodermatol Photoimmunol Photomed **24**(6): 318-321.
- Garcia-Dorado, D., A. Rodriguez-Sinovas, et al. (2004). "Gap junction-mediated spread of cell injury and death during myocardial ischemia-reperfusion." Cardiovasc Res **61**(3): 386-401.
- Garinis, G. A., L. M. Uittenboogaard, et al. (2009). "Persistent transcription-blocking DNA lesions trigger somatic growth attenuation associated with longevity." Nat Cell Biol **11**(5): 604-615.
- Garinis, G. A., G. T. van der Horst, et al. (2008). "DNA damage and ageing: new-age ideas for an age-old problem." Nat Cell Biol **10**(11): 1241-1247.
- Garweg, J. G., M. Wegmann-Burns, et al. (2006). "Effects of daunorubicin, mitomycin C, azathioprine and cyclosporin A on human retinal pigmented epithelial, corneal endothelial and conjunctival cell lines." Graefes Arch Clin Exp Ophthalmol **244**(3): 382-389.
- Geroski, D. H., M. Matsuda, et al. (1985). "Pump function of the human corneal endothelium. Effects of age and cornea guttata." Ophthalmology **92**(6): 759-763.
- Ghosheh, F. R., F. A. Cremona, et al. (2008). "Trends in penetrating keratoplasty in the United States 1980-2005." Int Ophthalmol **28**(3): 147-153.
- Giepmans, B. N. and W. H. Moolenaar (1998). "The gap junction protein connexin43 interacts with the second PDZ domain of the zona occludens-1 protein." Curr Biol **8**(16): 931-934.
- Giepmans, B. N., I. Verlaan, et al. (2001). "Gap junction protein connexin-43 interacts directly with microtubules." Curr Biol **11**(17): 1364-1368.
- Glover, D., J. B. Little, et al. (2003). "Low dose ionizing radiation-induced activation of connexin 43 expression." Int J Radiat Biol **79**(12): 955-964.
- Goldberg, G. S., P. D. Lampe, et al. (1999). "Selective transfer of endogenous metabolites through gap junctions composed of different connexins." Nat Cell Biol **1**(7): 457-459.
- Goldberg, G. S., A. P. Moreno, et al. (2002). "Gap junctions between cells expressing connexin 43 or 32 show inverse permselectivity to adenosine and ATP." J Biol Chem **277**(39): 36725-36730.
- Goldsberry, D. H., R. J. Epstein, et al. (2007). "Effect of mitomycin C on the corneal endothelium when used for corneal subepithelial haze prophylaxis following photorefractive keratectomy." J Refract Surg **23**(7): 724-727.
- Gomes, P., S. P. Srinivas, et al. (2006). "Gap junctional intercellular communication in bovine corneal endothelial cells." Exp Eye Res **83**(5): 1225-1237.
- Goodenough, D. A. and D. L. Paul (2003). "Beyond the gap: functions of unpaired connexon channels." Nat Rev Mol Cell Biol **4**(4): 285-294.

- Goodenough, D. A. and D. L. Paul (2009). "Gap junctions." Cold Spring Harb Perspect Biol **1**(1): a002576.
- Gorburnova, V., A. Seluanov, et al. (2007). "Changes in DNA repair during aging." Nucleic Acids Res **35**(22): 7466-7474.
- Goss, J. R., D. Beer Stolz, et al. (2011). "Premature age-related peripheral neuropathy in a mouse model of progeria." Mechanisms of Ageing and Development (**In Press**).
- Goss, J. R., D. B. Stolz, et al. (2011). "Premature aging-related peripheral neuropathy in a mouse model of progeria." Mech Ageing Dev.
- Goyal, J. L., V. A. Rao, et al. (1994). "Oculocutaneous manifestations in xeroderma pigmentosa." Br J Ophthalmol **78**(4): 295-297.
- Gregg, S. Q., A. R. Robinson, et al. (2011). "Physiological consequences of defects in ERCC1-XPF DNA repair endonuclease." DNA Repair (Amst).
- Grillari, J., H. Katinger, et al. (2007). "Contributions of DNA interstrand cross-links to aging of cells and organisms." Nucleic Acids Res **35**(22): 7566-7576.
- Guthoff, R. F., A. Zhivov, et al. (2009). "In vivo confocal microscopy, an inner vision of the cornea - a major review." Clin Experiment Ophthalmol **37**(1): 100-117.
- Haigis, M. C. and B. A. Yankner (2010). "The Aging Stress Response." Mol Cell **40**(October 22, 2010): 12.
- Hanger, D. P., H. L. Byers, et al. (2007). "Novel phosphorylation sites in tau from Alzheimer brain support a role for casein kinase 1 in disease pathogenesis." J Biol Chem **282**(32): 23645-23654.
- Harman, D. (1956). "Aging: a theory based on free radical and radiation chemistry." J Gerontol **11**(3): 298-300.
- Harris, A. L. (2007). "Connexin channel permeability to cytoplasmic molecules." Prog Biophys Mol Biol **94**(1-2): 120-143.
- Hassell, J. R. and D. E. Birk (2010). "The molecular basis of corneal transparency." Exp Eye Res **91**(3): 326-335.
- He, J., A. H. Kakazu, et al. (2011). "Aspirin-Triggered Lipoxin A4 (15-epi-LXA4) Increases the Endothelial Viability of Human Corneas Storage in Optisol-GS." J Ocul Pharmacol Ther.
- Hernandez, V. H., M. Bortolozzi, et al. (2007). "Unitary permeability of gap junction channels to second messengers measured by FRET microscopy." Nat Methods **4**(4): 353-358.
- Hlavin, E. M., M. B. Smeaton, et al. (2010). "Initiation of DNA interstrand cross-link repair in mammalian cells." Environ Mol Mutagen **51**(6): 604-624.
- Huang, R. P., Y. Fan, et al. (1998). "Reversion of the neoplastic phenotype of human glioblastoma cells by connexin 43 (cx43)." Cancer Res **58**(22): 5089-5096.
- Hudde, T., R. M. Comer, et al. (2002). "Modulation of hydrogen peroxide induced injury to corneal endothelium by virus mediated catalase gene transfer." Br J Ophthalmol **86**(9): 1058-1062.
- Hunter, A. W., R. J. Barker, et al. (2005). "Zonula occludens-1 alters connexin43 gap junction size and organization by influencing channel accretion." Mol Biol Cell **16**(12): 5686-5698.
- Hunter, A. W., J. Jourdan, et al. (2003). "Fusion of GFP to the carboxyl terminus of connexin43 increases gap junction size in HeLa cells." Cell Commun Adhes **10**(4-6): 211-214.

- Hutnik, C. M., C. E. Pocrnich, et al. (2008). "The protective effect of functional connexin43 channels on a human epithelial cell line exposed to oxidative stress." Invest Ophthalmol Vis Sci **49**(2): 800-806.
- Ikebe, H., T. Takamatsu, et al. (1986). "Age-dependent changes in nuclear DNA content and cell size of presumably normal human corneal endothelium." Exp Eye Res **43**(2): 251-258.
- Ing, J. J., H. H. Ing, et al. (1998). "Ten-year postoperative results of penetrating keratoplasty." Ophthalmology **105**(10): 1855-1865.
- Inuzuka, H., A. Tseng, et al. (2010). "Phosphorylation by casein kinase I promotes the turnover of the Mdm2 oncoprotein via the SCF(beta-TRCP) ubiquitin ligase." Cancer Cell **18**(2): 147-159.
- Jackson, S. P. and J. Bartek (2009). "The DNA-damage response in human biology and disease." Nature **461**(7267): 1071-1078.
- Jalali, S., S. Boghani, et al. (1994). "Penetrating keratoplasty in xeroderma pigmentosum. Case reports and review of the literature." Cornea **13**(6): 527-533.
- Janssens, S. and J. Tschopp (2006). "Signals from within: the DNA-damage-induced NF-kappaB response." Cell Death Differ **13**(5): 773-784.
- Jaspers, N. G., A. Raams, et al. (2007). "First reported patient with human ERCC1 deficiency has cerebro-oculo-facio-skeletal syndrome with a mild defect in nucleotide excision repair and severe developmental failure." Am J Hum Genet **80**(3): 457-466.
- Jiang, J. X. and S. Gu (2005). "Gap junction- and hemichannel-independent actions of connexins." Biochim Biophys Acta **1711**(2): 208-214.
- Johnson, D. H., W. M. Bourne, et al. (1982). "The ultrastructure of Descemet's membrane. I. Changes with age in normal corneas." Arch Ophthalmol **100**(12): 1942-1947.
- Joyce, N. C. (2003). "Proliferative capacity of the corneal endothelium." Prog Retin Eye Res **22**(3): 359-389.
- Joyce, N. C. (2005). "Cell cycle status in human corneal endothelium." Exp Eye Res **81**(6): 629-638.
- Joyce, N. C. and D. L. Harris (2010). "Decreasing expression of the G1-phase inhibitors, p21Cip1 and p16INK4a, promotes division of corneal endothelial cells from older donors." Mol Vis **16**: 897-906.
- Joyce, N. C., D. L. Harris, et al. (2010). "Age-Related Gene Response of Human Corneal Endothelium to Oxidative Stress and DNA Damage." Invest Ophthalmol Vis Sci.
- Joyce, N. C., B. Meklir, et al. (1990). "In vitro pharmacologic separation of corneal endothelial migration and spreading responses." Invest Ophthalmol Vis Sci **31**(9): 1816-1826.
- Joyce, N. C., C. Zhu, et al. (2008). "Relationship between oxidative stress, DNA damage, and proliferative capacity in human corneal endothelium." Invest Ophthalmol Vis Sci.
- Joyce, N. C., C. C. Zhu, et al. (2009). "Relationship among oxidative stress, DNA damage, and proliferative capacity in human corneal endothelium." Invest Ophthalmol Vis Sci **50**(5): 2116-2122.
- Jun, A. S., S. Chakravarti, et al. (2006). "Aging changes of mouse corneal endothelium and Descemet's membrane." Exp Eye Res **83**(4): 890-896.
- Jurkunas, U. V., M. S. Bitar, et al. (2010). "Evidence of Oxidative Stress in the Pathogenesis of Fuchs Endothelial Corneal Dystrophy." Am J Pathol.

- Jurkunas, U. V., M. S. Bitar, et al. (2010). "Evidence of oxidative stress in the pathogenesis of fuchs endothelial corneal dystrophy." Am J Pathol **177**(5): 2278-2289.
- Jurkunas, U. V., M. S. Bitar, et al. (2008). "Increased clusterin expression in Fuchs' endothelial dystrophy." Invest Ophthalmol Vis Sci **49**(7): 2946-2955.
- Jurkunas, U. V., I. Rawe, et al. (2008). "Decreased expression of peroxiredoxins in Fuchs' endothelial dystrophy." Invest Ophthalmol Vis Sci **49**(7): 2956-2963.
- Kalcheva, N., J. Qu, et al. (2007). "Gap junction remodeling and cardiac arrhythmogenesis in a murine model of oculodentodigital dysplasia." Proc Natl Acad Sci U S A **104**(51): 20512-20516.
- Kalvelyte, A., A. Imbrasaitė, et al. (2003). "Connexins and apoptotic transformation." Biochem Pharmacol **66**(8): 1661-1672.
- Kim, T. I., J. H. Pak, et al. (2004). "Mitomycin C-induced reduction of keratocytes and fibroblasts after photorefractive keratectomy." Invest Ophthalmol Vis Sci **45**(9): 2978-2984.
- Kim, T. I., H. Tchah, et al. (2003). "Apoptosis in keratocytes caused by mitomycin C." Invest Ophthalmol Vis Sci **44**(5): 1912-1917.
- Kjenseth, A., T. Fykerud, et al. (2010). "Regulation of gap junction intercellular communication by the ubiquitin system." Cell Signal **22**(9): 1267-1273.
- Knippschild, U., A. Gocht, et al. (2005). "The casein kinase 1 family: participation in multiple cellular processes in eukaryotes." Cell Signal **17**(6): 675-689.
- Knippschild, U., D. M. Milne, et al. (1997). "p53 is phosphorylated in vitro and in vivo by the delta and epsilon isoforms of casein kinase 1 and enhances the level of casein kinase 1 delta in response to topoisomerase-directed drugs." Oncogene **15**(14): 1727-1736.
- Knippschild, U., S. Wolff, et al. (2005). "The role of the casein kinase 1 (CK1) family in different signaling pathways linked to cancer development." Onkologie **28**(10): 508-514.
- Koh, S. W. (2002). "Ciliary neurotrophic factor released by corneal endothelium surviving oxidative stress ex vivo." Invest Ophthalmol Vis Sci **43**(9): 2887-2896.
- Koh, S. W., J. Celeste, et al. (2008). "Restoration of Functional CNTF Receptor {alpha} Subunit (CNTFR{alpha}) in Corneal Endothelial Cells in Stored Human Donor Corneas by Recombinant CNTFR{alpha}: Connexin-43 Up-regulation." Invest Ophthalmol Vis Sci.
- Koh, S. W., J. Cheng, et al. (2009). "VIP Down-regulates the Inflammatory Potential and Promotes Survival of Dying (Neural Crest-derived) Corneal Endothelial Cells ex vivo: Necrosis to Apoptosis Switch and Up-regulation of Bcl-2 and N-cadherin." J Neurochem.
- Kolozsvari, L., A. Nogradi, et al. (2002). "UV absorbance of the human cornea in the 240- to 400-nm range." Invest Ophthalmol Vis Sci **43**(7): 2165-2168.
- Konomi, K. and N. C. Joyce (2007). "Age and topographical comparison of telomere lengths in human corneal endothelial cells." Mol Vis **13**: 1251-1258.
- Koval, M. (2006). "Pathways and control of connexin oligomerization." Trends Cell Biol **16**(3): 159-166.
- Lacayo, G. O., 3rd and P. A. Majmudar (2005). "How and when to use mitomycin-C in refractive surgery." Curr Opin Ophthalmol **16**(4): 256-259.

- Laird, D. W. (2006). "Life cycle of connexins in health and disease." Biochem J **394**(Pt 3): 527-543.
- Laird, D. W., M. Castillo, et al. (1995). "Gap junction turnover, intracellular trafficking, and phosphorylation of connexin43 in brefeldin A-treated rat mammary tumor cells." J Cell Biol **131**(5): 1193-1203.
- Lampe, P. D., C. D. Cooper, et al. (2006). "Analysis of Connexin43 phosphorylated at S325, S328 and S330 in normoxic and ischemic heart." J Cell Sci **119**(Pt 16): 3435-3442.
- Lampe, P. D. and A. F. Lau (2004). "The effects of connexin phosphorylation on gap junctional communication." Int J Biochem Cell Biol **36**(7): 1171-1186.
- Lane, H. A., J. A. Swale, et al. (2003). "Prophylactic use of mitomycin-C in the management of a buttonholed LASIK flap." J Cataract Refract Surg **29**(2): 390-392.
- Langlois, S., K. N. Cowan, et al. (2008). "Caveolin-1 and -2 interact with connexin43 and regulate gap junctional intercellular communication in keratinocytes." Mol Biol Cell **19**(3): 912-928.
- Langlois, S., A. C. Maher, et al. (2007). "Connexin levels regulate keratinocyte differentiation in the epidermis." J Biol Chem **282**(41): 30171-30180.
- Lauf, U., B. N. Giepmans, et al. (2002). "Dynamic trafficking and delivery of connexons to the plasma membrane and accretion to gap junctions in living cells." Proc Natl Acad Sci U S A **99**(16): 10446-10451.
- Law, C. S., O. A. Candia, et al. (2009). "Inhibitions of chloride transport and gap junction reduce fluid flow across the whole porcine ciliary epithelium." Invest Ophthalmol Vis Sci **50**(3): 1299-1306.
- Lawley, P. D. and D. H. Phillips (1996). "DNA adducts from chemotherapeutic agents." Mutat Res **355**(1-2): 13-40.
- Lawrence, N. J., J. J. Sacco, et al. (2008). "A neurological phenotype in mice with DNA repair gene Ercc1 deficiency." DNA Repair (Amst) **7**(2): 281-291.
- Lee, D. H., H. S. Chung, et al. (2005). "Photorefractive keratectomy with intraoperative mitomycin-C application." J Cataract Refract Surg **31**(12): 2293-2298.
- Lee, W. B., D. S. Jacobs, et al. (2009). "Descemet's stripping endothelial keratoplasty: safety and outcomes: a report by the American Academy of Ophthalmology." Ophthalmology **116**(9): 1818-1830.
- Legerski, R. J. (2010). "Repair of DNA interstrand cross-links during S phase of the mammalian cell cycle." Environ Mol Mutagen **51**(6): 540-551.
- Leithe, E., A. Kjenseth, et al. (2009). "Ubiquitylation of the gap junction protein connexin-43 signals its trafficking from early endosomes to lysosomes in a process mediated by Hrs and Tsg101." J Cell Sci **122**(Pt 21): 3883-3893.
- Levy, S. G., A. C. McCartney, et al. (1995). "Descemet's membrane in the iridocorneal-endothelial syndrome: morphology and composition." Exp Eye Res **61**(3): 323-333.
- Levy, S. G., J. Moss, et al. (1996). "The composition of wide-spaced collagen in normal and diseased Descemet's membrane." Curr Eye Res **15**(1): 45-52.
- Leykauf, K., M. Salek, et al. (2006). "Ubiquitin protein ligase Nedd4 binds to connexin43 by a phosphorylation-modulated process." J Cell Sci **119**(Pt 17): 3634-3642.
- Li, G., H. Yin, et al. (2004). "Casein kinase 1 delta phosphorylates tau and disrupts its binding to microtubules." J Biol Chem **279**(16): 15938-15945.

- Li, H., J. R. Mitchell, et al. (2008). "DNA double-strand breaks: a potential causative factor for mammalian aging?" Mech Ageing Dev **129**(7-8): 416-424.
- Li, S., K. T. Allen, et al. (2011). "Soluble adenylyl cyclase mediates bicarbonate-dependent corneal endothelial cell protection." Am J Physiol Cell Physiol **300**(2): C368-374.
- Liao, Y., K. H. Day, et al. (2001). "Endothelial cell-specific knockout of connexin 43 causes hypotension and bradycardia in mice." Proc Natl Acad Sci U S A **98**(17): 9989-9994.
- Liao, Y., C. P. Regan, et al. (2007). "Smooth muscle-targeted knockout of connexin43 enhances neointimal formation in response to vascular injury." Arterioscler Thromb Vasc Biol **27**(5): 1037-1042.
- Lin, J. H., J. Yang, et al. (2003). "Connexin mediates gap junction-independent resistance to cellular injury." J Neurosci **23**(2): 430-441.
- Little, J. B. (2006). "Cellular radiation effects and the bystander response." Mutat Res **597**(1-2): 113-118.
- Liu, K., M. Kasper, et al. (1997). "Connexin 43 expression in normal and irradiated mouse skin." Radiat Res **147**(4): 437-441.
- Lohler, J., H. Hirner, et al. (2009). "Immunohistochemical characterisation of cell-type specific expression of CK1delta in various tissues of young adult BALB/c mice." PLoS ONE **4**(1): e4174.
- Long, C. J., M. R. Roth, et al. (2000). "Fibroblast growth factor-2 promotes keratan sulfate proteoglycan expression by keratocytes in vitro." J Biol Chem **275**(18): 13918-13923.
- Majmudar, P. A., S. L. Forstot, et al. (2000). "Topical mitomycin-C for subepithelial fibrosis after refractive corneal surgery." Ophthalmology **107**(1): 89-94.
- Matchkov, V. V., H. Gustafsson, et al. (2007). "Interaction between Na⁺/K⁺-pump and Na⁺/Ca²⁺-exchanger modulates intercellular communication." Circ Res **100**(7): 1026-1035.
- Matsuoka, S., B. A. Ballif, et al. (2007). "ATM and ATR substrate analysis reveals extensive protein networks responsive to DNA damage." Science **316**(5828): 1160-1166.
- McDermott, M. L., J. Wang, et al. (1994). "Mitomycin and the human corneal endothelium." Arch Ophthalmol **112**(4): 533-537.
- McElvanney, A. M., W. J. Wooldridge, et al. (1996). "Ophthalmic management of Cockayne's syndrome." Eye (Lond) **10** (Pt 1): 61-64.
- McHugh, P. J., V. J. Spanswick, et al. (2001). "Repair of DNA interstrand crosslinks: molecular mechanisms and clinical relevance." Lancet Oncol **2**(8): 483-490.
- McKenna, D. J., M. Gallus, et al. (2003). "Modification of the alkaline Comet assay to allow simultaneous evaluation of mitomycin C-induced DNA cross-link damage and repair of specific DNA sequences in RT4 cells." DNA Repair (Amst) **2**(8): 879-890.
- McKenzie, J. A., K. Riento, et al. (2006). "Casein kinase I epsilon associates with and phosphorylates the tight junction protein occludin." FEBS Lett **580**(9): 2388-2394.
- McWhir, J., J. Selfridge, et al. (1993). "Mice with DNA repair gene (ERCC-1) deficiency have elevated levels of p53, liver nuclear abnormalities and die before weaning." Nat Genet **5**(3): 217-224.

- Mese, G., G. Richard, et al. (2007). "Gap junctions: basic structure and function." J Invest Dermatol **127**(11): 2516-2524.
- Mietz, H., S. Roters, et al. (2005). "Bullous keratopathy as a complication of trabeculectomy with mitomycin C." Graefes Arch Clin Exp Ophthalmol **243**(12): 1284-1287.
- Milne, D. M., P. Looby, et al. (2001). "Catalytic activity of protein kinase CK1 delta (casein kinase 1delta) is essential for its normal subcellular localization." Exp Cell Res **263**(1): 43-54.
- Mimura, T. and N. C. Joyce (2006). "Replication competence and senescence in central and peripheral human corneal endothelium." Invest Ophthalmol Vis Sci **47**(4): 1387-1396.
- Mohammadpour, M., M. Jabbarvand, et al. (2007). "Focal corneal decompensation after filtering surgery with mitomycin C." Cornea **26**(10): 1285-1287.
- Moller, P., M. Lohr, et al. (2010). "Aging and oxidatively damaged nuclear DNA in animal organs." Free Radic Biol Med **48**(10): 1275-1285.
- Morales, A. J., D. Zadok, et al. (2006). "Intraoperative mitomycin and corneal endothelium after photorefractive keratectomy." Am J Ophthalmol **142**(3): 400-404.
- Murray, J. I., M. L. Whitfield, et al. (2004). "Diverse and specific gene expression responses to stresses in cultured human cells." Mol Biol Cell **15**(5): 2361-2374.
- Musa, F. U., P. Ratajczak, et al. (2008). "Ocular manifestations in oculodentodigital dysplasia resulting from a heterozygous missense mutation (L113P) in GJA1 (connexin 43)." Eye.
- Musil, L. S., B. A. Cunningham, et al. (1990). "Differential phosphorylation of the gap junction protein connexin43 in junctional communication-competent and -deficient cell lines." J Cell Biol **111**(5 Pt 1): 2077-2088.
- Musil, L. S. and D. A. Goodenough (1991). "Biochemical analysis of connexin43 intracellular transport, phosphorylation, and assembly into gap junctional plaques." J Cell Biol **115**(5): 1357-1374.
- Nakano, E. M., H. S. Bains, et al. (2007). "Comparison of laser epithelial keratomileusis with and without mitomycin C for wavefront customized surface ablations." J Refract Surg **23**(9 Suppl): S1021-1028.
- Nakase, T., S. Fushiki, et al. (2003). "Astrocytic gap junctions composed of connexin 43 reduce apoptotic neuronal damage in cerebral ischemia." Stroke **34**(8): 1987-1993.
- Nassiri, N., S. Farahangiz, et al. (2008). "Corneal endothelial cell injury induced by mitomycin-C in photorefractive keratectomy: nonrandomized controlled trial." J Cataract Refract Surg **34**(6): 902-908.
- Nickel, B. M., B. H. DeFranco, et al. (2008). "Clathrin and Cx43 gap junction plaque endocytosis." Biochem Biophys Res Commun **374**(4): 679-682.
- Niedernhofer, L. J. (2008). "Tissue-specific accelerated aging in nucleotide excision repair deficiency." Mech Ageing Dev **129**(7-8): 408-415.
- Niedernhofer, L. J., J. S. Daniels, et al. (2003). "Malondialdehyde, a product of lipid peroxidation, is mutagenic in human cells." J Biol Chem **278**(33): 31426-31433.
- Niedernhofer, L. J., G. A. Garinis, et al. (2006). "A new progeroid syndrome reveals that genotoxic stress suppresses the somatotroph axis." Nature **444**(7122): 1038-1043.

- Niedernhofer, L. J., H. Odijk, et al. (2004). "The structure-specific endonuclease Ercc1-Xpf is required to resolve DNA interstrand cross-link-induced double-strand breaks." Mol Cell Biol **24**(13): 5776-5787.
- Niedernhofer, L. J. and P. D. Robbins (2008). "Signaling mechanisms involved in the response to genotoxic stress and regulating lifespan." Int J Biochem Cell Biol **40**(2): 176-180.
- Noll, D. M., T. M. Mason, et al. (2006). "Formation and repair of interstrand cross-links in DNA." Chem Rev **106**(2): 277-301.
- Nospikel, T. (2007). "DNA repair in differentiated cells: some new answers to old questions." Neuroscience **145**(4): 1213-1221.
- Nospikel, T. and P. C. Hanawalt (2002). "DNA repair in terminally differentiated cells." DNA Repair (Amst) **1**(1): 59-75.
- Novakova, Z., S. Hubackova, et al. (2010). "Cytokine expression and signaling in drug-induced cellular senescence." Oncogene **29**(2): 273-284.
- Olbina, G. and W. Eckhart (2003). "Mutations in the second extracellular region of connexin 43 prevent localization to the plasma membrane, but do not affect its ability to suppress cell growth." Mol Cancer Res **1**(9): 690-700.
- Parikh, C. H. and H. F. Edelhauser (2003). "Ocular surgical pharmacology: corneal endothelial safety and toxicity." Curr Opin Ophthalmol **14**(4): 178-185.
- Paulson, A. F., P. D. Lampe, et al. (2000). "Cyclic AMP and LDL trigger a rapid enhancement in gap junction assembly through a stimulation of connexin trafficking." J Cell Sci **113** (Pt 17): 3037-3049.
- Paznekas, W. A., S. A. Boyadjev, et al. (2003). "Connexin 43 (GJA1) mutations cause the pleiotropic phenotype of oculodentodigital dysplasia." Am J Hum Genet **72**(2): 408-418.
- Pfister, R. R. (2004). "Permanent corneal edema resulting from the treatment of PTK corneal haze with mitomycin: a case report." Cornea **23**(7): 744-747.
- Piehl, M., C. Lehmann, et al. (2007). "Internalization of large double-membrane intercellular vesicles by a clathrin-dependent endocytic process." Mol Biol Cell **18**(2): 337-347.
- Price, M. O. and F. W. Price (2007). "Descemet's stripping endothelial keratoplasty." Curr Opin Ophthalmol **18**(4): 290-294.
- Price, M. O. and F. W. Price, Jr. (2008). "Endothelial cell loss after descemet stripping with endothelial keratoplasty influencing factors and 2-year trend." Ophthalmology **115**(5): 857-865.
- Prise, K. M. and J. M. O'Sullivan (2009). "Radiation-induced bystander signalling in cancer therapy." Nat Rev Cancer **9**(5): 351-360.
- Qi, J., L. Chi, et al. (2011). "Gap junctions in IL-1 {beta}-mediated cell survival response to strain." J Appl Physiol.
- Qin, H., Q. Shao, et al. (2002). "Retroviral delivery of connexin genes to human breast tumor cells inhibits in vivo tumor growth by a mechanism that is independent of significant gap junctional intercellular communication." J Biol Chem **277**(32): 29132-29138.
- Ramachandran, S., L. H. Xie, et al. (2007). "A novel role for connexin hemichannel in oxidative stress and smoking-induced cell injury." PLoS ONE **2**(1): e712.

- Reaume, A. G., P. A. de Sousa, et al. (1995). "Cardiac malformation in neonatal mice lacking connexin43." Science **267**(5205): 1831-1834.
- Rehany, U., Y. Ishii, et al. (2000). "Ultrastructural changes in corneas of diabetic patients: an electron-microscopy study." Cornea **19**(4): 534-538.
- Reiling, J. H. and D. M. Sabatini (2006). "Stress and mTOR signaling." Oncogene **25**(48): 6373-6383.
- Remo, B. F., J. Qu, et al. (2011). "Phosphatase-Resistant Gap Junctions Inhibit Pathological Remodeling and Prevent Arrhythmias." Circ Res.
- Rhett, J. M., J. Jourdan, et al. (2011). "Connexin43 Connexon to Gap Junction Transition Is Regulated by Zonula Occludens-1." Mol Biol Cell.
- Rodier, F., J. P. Coppe, et al. (2009). "Persistent DNA damage signalling triggers senescence-associated inflammatory cytokine secretion." Nat Cell Biol **11**(8): 973-979.
- Roh, D. S., A. L. Cook, et al. (2008). "DNA Cross-linking, Double-strand Breaks and Apoptosis in Corneal Endothelial Cells After a Single Exposure to Mitomycin-C." Invest Ophthalmol Vis Sci.
- Roh, D. S., A. L. Cook, et al. (2008). "DNA cross-linking, double-strand breaks, and apoptosis in corneal endothelial cells after a single exposure to mitomycin C." Invest Ophthalmol Vis Sci **49**(11): 4837-4843.
- Roh, D. S. and J. L. Funderburgh (2011). "Rapid Changes in Connexin-43 in Response to Genotoxic Stress Stabilize Cell-Cell Communication in Corneal Endothelium." Invest Ophthalmol Vis Sci **52**(8): 5174-5182.
- Romanello, M., L. Moro, et al. (2001). "Effects of cAMP on intercellular coupling and osteoblast differentiation." Biochem Biophys Res Commun **282**(5): 1138-1144.
- Rosenblatt, J., M. C. Raff, et al. (2001). "An epithelial cell destined for apoptosis signals its neighbors to extrude it by an actin- and myosin-dependent mechanism." Curr Biol **11**(23): 1847-1857.
- Roszkowska, A. M., C. G. Tringali, et al. (1999). "Corneal endothelium evaluation in type I and type II diabetes mellitus." Ophthalmologica **213**(4): 258-261.
- Saez, J. C., V. M. Berthoud, et al. (2003). "Plasma membrane channels formed by connexins: their regulation and functions." Physiol Rev **83**(4): 1359-1400.
- Sakaguchi, K., S. Saito, et al. (2000). "Damage-mediated phosphorylation of human p53 threonine 18 through a cascade mediated by a casein 1-like kinase. Effect on Mdm2 binding." J Biol Chem **275**(13): 9278-9283.
- Salvi, S. M., S. Akhtar, et al. (2006). "Ageing changes in the eye." Postgrad Med J **82**(971): 581-587.
- Sarkar, S., A. A. Davies, et al. (2006). "DNA interstrand crosslink repair during G1 involves nucleotide excision repair and DNA polymerase zeta." EMBO J **25**(6): 1285-1294.
- Schelonka, L. P., D. Siegel, et al. (2000). "Immunohistochemical localization of NQO1 in epithelial dysplasia and neoplasia and in donor eyes." Invest Ophthalmol Vis Sci **41**(7): 1617-1622.
- Schumacher, B., I. van der Pluijm, et al. (2008). "Delayed and accelerated aging share common longevity assurance mechanisms." PLoS Genet **4**(8): e1000161.
- Schwab, C., A. J. DeMaggio, et al. (2000). "Casein kinase 1 delta is associated with pathological accumulation of tau in several neurodegenerative diseases." Neurobiol Aging **21**(4): 503-510.

- Sedelnikova, O. A., I. Horikawa, et al. (2004). "Senescing human cells and ageing mice accumulate DNA lesions with unreparable double-strand breaks." Nat Cell Biol **6**(2): 168-170.
- Sedelnikova, O. A., D. R. Pilch, et al. (2003). "Histone H2AX in DNA damage and repair." Cancer Biol Ther **2**(3): 233-235.
- Sedelnikova, O. A., C. E. Redon, et al. (2010). "Role of oxidatively induced DNA lesions in human pathogenesis." Mutat Res **704**(1-3): 152-159.
- Segretain, D. and M. M. Falk (2004). "Regulation of connexin biosynthesis, assembly, gap junction formation, and removal." Biochim Biophys Acta **1662**(1-2): 3-21.
- Segretain, D., C. Fiorini, et al. (2004). "A proposed role for ZO-1 in targeting connexin 43 gap junctions to the endocytic pathway." Biochimie **86**(4-5): 241-244.
- Senoo, T. and N. C. Joyce (2000). "Cell cycle kinetics in corneal endothelium from old and young donors." Invest Ophthalmol Vis Sci **41**(3): 660-667.
- Setala, K. (1980). "Response of human corneal endothelial cells to increased intraocular pressure." Acta Ophthalmol Suppl(144): 1-38.
- Shaw, R. M., A. J. Fay, et al. (2007). "Microtubule plus-end-tracking proteins target gap junctions directly from the cell interior to adherens junctions." Cell **128**(3): 547-560.
- Sihota, R., T. Sharma, et al. (1998). "Intraoperative mitomycin C and the corneal endothelium." Acta Ophthalmol Scand **76**(1): 80-82.
- Simek, J., J. Churko, et al. (2009). "Cx43 has distinct mobility within plasma-membrane domains, indicative of progressive formation of gap-junction plaques." J Cell Sci **122**(Pt 4): 554-562.
- Smolin, G., C. S. Foster, et al. (2005). Smolin and Thoft's The cornea : scientific foundations and clinical practice. Philadelphia, Lippincott Williams & Wilkins.
- Solan, J. L. and P. D. Lampe (2007). "Key connexin 43 phosphorylation events regulate the gap junction life cycle." J Membr Biol **217**(1-3): 35-41.
- Solan, J. L. and P. D. Lampe (2009). "Connexin43 phosphorylation: structural changes and biological effects." Biochem J **419**(2): 261-272.
- Song, J. S., J. H. Kim, et al. (2006). "Concentrations of mitomycin C in rabbit corneal tissue and aqueous humor after topical administration." Cornea **25**(10 Suppl 1): S20-23.
- Song, J. S., J. H. Kim, et al. (2007). "Mitomycin-C concentration in cornea and aqueous humor and apoptosis in the stroma after topical mitomycin-C application: effects of mitomycin-C application time and concentration." Cornea **26**(4): 461-467.
- Song, Z., Y. Wang, et al. (2008). "Expression of senescence-related genes in human corneal endothelial cells." Mol Vis **14**: 161-170.
- Sosinsky, G. E., J. L. Solan, et al. (2007). "The C-terminus of connexin43 adopts different conformations in the Golgi and gap junction as detected with structure-specific antibodies." Biochem J **408**(3): 375-385.
- Sridharan, S., R. Brehm, et al. (2007). "Role of connexin 43 in Sertoli cells of testis." Ann N Y Acad Sci **1120**: 131-143.

- Srinivas, S. P. (2010). "Dynamic regulation of barrier integrity of the corneal endothelium." Optom Vis Sci **87**(4): E239-254.
- Storchova, Z. and D. Pellman (2004). "From polyploidy to aneuploidy, genome instability and cancer." Nat Rev Mol Cell Biol **5**(1): 45-54.
- Takahashi, H. (2005). "Free radical development in phacoemulsification cataract surgery." J Nippon Med Sch **72**(1): 4-12.
- Talamo, J. H., S. Gollamudi, et al. (1991). "Modulation of corneal wound healing after excimer laser keratomileusis using topical mitomycin C and steroids." Arch Ophthalmol **109**(8): 1141-1146.
- Tekpli, X., E. Rivedal, et al. "The B[a]P-increased intercellular communication via translocation of connexin-43 into gap junctions reduces apoptosis." Toxicol Appl Pharmacol **242**(2): 231-240.
- Thornton, I., A. Puri, et al. (2007). "Low-dose mitomycin C as a prophylaxis for corneal haze in myopic surface ablation." Am J Ophthalmol **144**(5): 673-681.
- Tognetto, D., P. Cecchini, et al. (2004). "Survey of ophthalmic viscosurgical devices." Curr Opin Ophthalmol **15**(1): 29-32.
- Tomasz, M. (1995). "Mitomycin C: small, fast and deadly (but very selective)." Chem Biol **2**(9): 575-579.
- Torres, R. M., J. Merayo-Llodes, et al. (2006). "Presence of mitomycin-C in the anterior chamber after photorefractive keratectomy." J Cataract Refract Surg **32**(1): 67-71.
- van der Pluijm, I., G. A. Garinis, et al. (2007). "Impaired genome maintenance suppresses the growth hormone--insulin-like growth factor 1 axis in mice with Cockayne syndrome." PLoS Biol **5**(1): e2.
- VanSlyke, J. K. and L. S. Musil (2005). "Cytosolic stress reduces degradation of connexin43 internalized from the cell surface and enhances gap junction formation and function." Mol Biol Cell **16**(11): 5247-5257.
- Vo, N., H. Y. Seo, et al. (2010). "Accelerated aging of intervertebral discs in a mouse model of progeria." J Orthop Res **28**(12): 1600-1607.
- Wang, C., D. Jurk, et al. (2009). "DNA damage response and cellular senescence in tissues of aging mice." Aging Cell **8**(3): 311-323.
- Wang, D., N. V. Vo, et al. (2011). "Bupivacaine decreases cell viability and matrix protein synthesis in an intervertebral disc organ model system." Spine J **11**(2): 139-146.
- Watsky, M. A., M. D. McCartney, et al. (1990). "Corneal endothelial junctions and the effect of ouabain." Invest Ophthalmol Vis Sci **31**(5): 933-941.
- Weeda, G., I. Donker, et al. (1997). "Disruption of mouse ERCC1 results in a novel repair syndrome with growth failure, nuclear abnormalities and senescence." Curr Biol **7**(6): 427-439.
- Williams, K. K. and M. A. Watsky (2004). "Bicarbonate promotes dye coupling in the epithelium and endothelium of the rabbit cornea." Curr Eye Res **28**(2): 109-120.
- Wilson, M. R., T. W. Close, et al. (2000). "Cell population dynamics (apoptosis, mitosis, and cell-cell communication) during disruption of homeostasis." Exp Cell Res **254**(2): 257-268.
- Workman, C. T., H. C. Mak, et al. (2006). "A systems approach to mapping DNA damage response pathways." Science **312**(5776): 1054-1059.

- Wu, K. Y., S. J. Hong, et al. (1999). "Toxic effects of mitomycin-C on cultured corneal keratocytes and endothelial cells." J Ocul Pharmacol Ther **15**(5): 401-411.
- Yamaguchi, K., H. Okabe, et al. (1991). "Corneal perforation in a patient with Cockayne's syndrome." Cornea **10**(1): 79-80.
- Yan, W., L. Spruce, et al. (2007). "Intracellular trafficking of a polymorphism in the COOH terminus of the alpha-subunit of the human epithelial sodium channel is modulated by casein kinase 1." Am J Physiol Renal Physiol **293**(3): F868-876.
- Yang, J., Y. Yu, et al. (2003). "Protein kinases and their involvement in the cellular responses to genotoxic stress." Mutat Res **543**(1): 31-58.
- Yu, S. and M. G. Roth (2002). "Casein kinase I regulates membrane binding by ARF GAP1." Mol Biol Cell **13**(8): 2559-2570.
- Zhang, C., W. R. Bell, et al. (2006). "Immunohistochemistry and electron microscopy of early-onset fuchs corneal dystrophy in three cases with the same L450W COL8A2 mutation." Trans Am Ophthalmol Soc **104**: 85-97.